ENGINEERING A LIBRARY OF ANISOTROPIC BUILDING BLOCKS FOR DNA-PROGRAMMED COLLOIDAL SELF-ASSEMBLY

James T. McGinley, III

A DISSERTATION

in

Chemical and Biomolecular Engineering

Presented to the Faculties of the University of Pennsylvania in Partial Fulfillment of the Requirements for the Degree of Doctor of Philosophy

2015

Supervisor of Dissertation

Dr. John C. Crocker

Professor, Chemical and Biomolecular Engineering

Graduate Group Chairperson

Dr. Raymond J. Gorte

Russel Pearce and Elizabeth Crimian Heuer Professor, Chemical and Biomolecular Engineering

Dissertation Committee:

Dr. Talid R. Sinno, Professor, Chemical and Biomolecular Engineering

Dr. Daniel Hammer, Alfred G. and Meta A. Ennis Professor, Chemical and Biomolecular Engineering

Dr. So-Jung Park, Adjunct Associate Professor, Chemistry

ENGINEERING A LIBRARY OF ANISOTROPIC BUILDING BLOCKS FOR

DNA-PROGRAMMED COLLOIDAL SELF-ASSEMBLY

COPYRIGHT

2015

James Thomas McGinley, III

Acknowledgments

I would like to thank my advisor, John Crocker, for his guidance and support over the past five years. He has been a wonderful mentor, and his passion for scientific research has been a huge inspiration. He provided me with invaluable insights into not only science, but also politics, the economy and life. I am truly grateful for the education and new perspectives that I have gained under his mentorship.

I would also like to thank Dr. So-Jung Park, whose technical advice regarding ligase made this work possible, Dr. Talid Sinno and Ian Jenkins, who have proven to be exceptional collaborators that have helped to advance this work in meaningful ways, and Dr. Dan Hammer and Eric Wang, who have provided a great deal of technical assistance regarding sample preparation. I would further like to thank Dr Valeria Milam at Georgia Tech and Dr. Vinny Manoharan at Harvard for useful technical conversations. The Yodh Group, and in particular Zoey Davidson, Tim Still, and Matthew Lohr, are thanked for their help with the confocal microscope.

I also greatly appreciate the friendship, collaborations, and support from the people in the Crocker Lab over the years. In particular, I would like to thank Dr.

Ben Rogers for training me when I arrived in the Crocker Lab, and for the additional advice he has provided over the years, and Marie Casey, whose research laid much of the groundwork for my own. I would also like to thank Dr. Zaki Estephan, Dr. Steven Henry, and Dr. Tae Soup Shim, who have been a pleasure to work with, and have provided a great deal of technical expertise. I am also grateful for the support of Jennifer Hwang, Tianyu Liu, Gregory Cordina-McSweeney, Christopher Porter, Sashikumar Ramamirtham, Ramnath Easwar, and Yue Xu. I would like to give a special thanks to Yifan Wang, who has been a great friend, an exceptional collaborator, and wonderful lab mate over the past several years.

Finally, I would like to thank my family for their love and support. To my parents, Jim and Helen McGinley, and my sister and her husband, Caitlin and Peter Balawajder, for loving and supporting me not only throughout the past five years, but also throughout my life. To my wonderful partner, Paul Ginart, for his love and support, and for frequently helping me to take a step back from the trees to see the forest.

ABSTRACT

ENGINEERING A LIBRARY OF ANISOTROPIC BUILDING BLOCKS FOR DNA-PROGRAMMED COLLOIDAL SELF-ASSEMBLY

James T. McGinley, III

Dr. John C. Crocker

Programmable DNA interactions are an effective and versatile tool in the field of colloidal directed self-assembly. Colloidal systems are programmed by manipulating a variety of tunable parameters, such as particle sizes and DNA interaction strengths, and can self-assemble into a large and growing variety of colloidal crystal and gel structures. Since isotropically-interacting spherical particles generally form close-packed structures, the production and use of building blocks with anisotropic interactions, such as polyhedral particles, colloidal clusters, and patchy colloids, has been a rich research area in recent years.

This work represents a true expansion of the capabilities of DNA-directed colloidal assemblies, and presents scalable and facile processes for the high-yield generation of stable colloidal clusters and patchy particles with targeted symmetries. We have developed, in Colloidal Crystal Templating and Reprogrammable DNA Interactions, highly tunable tools for the synthesis of such anisotropic building blocks for DNA-directed assembly applications. Notably, these processes are scalable both in batch size and in the size of the resulting building blocks due to the

three-dimensional nature of the templates. More notably, these systems are highly tunable and expandable. The templates are only limited by the ever-expanding library of colloidal crystals generated using DNA interactions. The tunability of DNA interactions is virtually unlimited due to DNA's ability to be reprogrammed and edited by enzymes. Finally, the constituent particles are not limited to polystyrene and gold, but can be of any material that can be synthesized into colloids on the micro- and nano-scales and subsequently functionalized with DNA.

Contents

Acknowledgments **iii**

Abstract **v**

List of Tables **xii**

List of Figures **xiii**

1 Introduction **1**

1.1 Self-Assembling Systems 1

1.2 DNA-Directed Self-Assembly 2

1.3 Expanding the variety of realizable structures 6

1.3.1 Reprogrammable DNA Interactions 7

1.3.2 Anisotropic Building Blocks 8

1.4 Thesis Overview 10

References 12

2 System Design, Synthesis, and Characterization **18**

2.1 DNA Design 20

2.2 DNA Design Validation using Gel Tms and a Thermodynamic Model 21

2.3 Synthesizing DNA-Coated Microspheres 22

2.4 Colloidal Crystallization 22

2.5 Purification by Sedimentation Velocity 23

2.6 Imaging and Characterization 24

2.6.1 Confocal Imaging 25

2.6.2 Confocal Image Analysis 26

2.6.3 SEM Imaging 26

2.6.4 APTES-Treated Positively Charged Glass 27

2.6.5 Methanol Washing 28

2.6.6 Ethane Vitrification 29

2.6.7 Sample Mounting for SEM 30

References 31

3 Assembling Colloidal Clusters Using Crystalline Templates and Reprogrammable DNA Interactions 33

3.1 Abstract 34

3.2 Introduction 34

3.3 Materials and Methods 38

3.3.1 Particle Preparation and Conjugation 38

3.3.2 T_m Analyses 39

3.3.3 FCC Crystal Formation 39
3.3.4 BCC Crystal Formation 40
3.3.5 Cluster Formation from FCC crystals 41
3.3.6 Cluster Formation from BCC crystals 42
3.3.7 Imaging Crystals and Clusters 42
3.3.8 Cluster Simulation and Mode Analysis 43
3.4 Results and Discussion 45
3.4.1 DNA Design Approach and Findings 45
3.4.2 FCC System 48
3.4.3 BCC System 50
3.4.4 Co-crystallization of Host/Impurity Crystals 51
3.4.5 Cluster Formation and Transformation 57
3.4.6 '1+12' Cluster Results 60
3.4.7 '1+8' Cluster Results 65
3.5 Conclusions 66
References 68

4 Crystal Templated Colloidal Clusters Exhibit Directional DNA Interactions 72

4.1 Abstract 72
4.2 Introduction 74
4.3 Materials and Methods 77

4.3.1 Particle Preparation 77
4.3.2 Cluster Formation 78
4.3.3 Purification 78
4.3.4 Confocal Microscopy 79
4.3.5 SEM Imaging and Cluster Analysis 79
4.4 Results and Discussion 81
4.4.1 DNA Design for Ligatable System 81
4.4.2 Colloidal Crystals as Cluster Templates 84
4.4.3 Clusters Display Directional Interactions 91
4.5 Conclusions 95
References 96

5 Generation of Patchy Particles *via* Point-of-Contact Templating 101
5.1 Abstract 101
5.2 Introduction 102
5.3 Materials and Methods 104
5.3.1 Particle Synthesis 104
5.3.2 Homogeneous Colloidal Crystallization 106
5.3.3 Extending Bridges using Ligation 106
5.3.4 Purification by Particle Size *via* Sedimentation Velocity . . . 107
5.3.5 Patch Hybridization with Gold Nanoparticles 107
5.3.6 SEM Sample Preparation 108

5.4 Results and Discussion 109

5.4.1 DNA Design and Validation 109

5.4.2 Patchy Particles from Binary Crystals and Gels 112

5.4.3 Patch Size Estimation and Control 113

5.5 Conclusions 117

References 119

6 Conclusions and Future Directions 122

6.1 Conclusions 123

6.2 Future Directions 125

References 126

List of Tables

3.1 B Kickoff Strand for Modulating $A - B$ Melting Temperatures at 150mM NaCl, assuming 1000 DNA strands per B particle 52

3.2 PP' Sedimentation System: Cluster Statistics 56

3.3 AB' Sedimentation System: Cluster Statistics 57

3.4 ABB' BCC System: Cluster Statistics 61

List of Figures

1.1 Hydrodynamic Radii and Interaction Range 5

1.2 Tunable Parameters for Binary System. 6

2.1 Traditional DNA Design Method 19

3.1 Schematic for Colloidal Crystal Tempting of '1+12 Clusters using Competitive DNA Strands 36

3.2 DNA Strand Architecture for Reprogrammable Palindromic System 45

3.3 DNA Strand Architecture for Reprogrammable Binary System . . . 46

3.4 Impurity Particle Incorporation into FCC and BCC Host Crystals . 53

3.5 '1+12' Clusters Templated from Sedimented Host Crystals using 150mM NaCl and Palindromic Sequences 55

3.6 '1+12' and '1+10' Clusters Templated from Sedimented Host Crystals using 300mM NaCl and Binary Sequences 58

3.7 '1+8' Clusters formed from BCC Crystals 64

3.8 Diagram of Cluster Formations Resulting from the Reprogrammed FCC and BCC Systems 67

4.1 Schematic for Colloidal Crystal Tempting of '1+4' Clusters using Ligatable DNA Strands 76

4.2 DNA Strand Architecture for Ligatable Binary Sustem 82

4.3 SEM Images of Clusters of Cuboctahedra, Triangular Orthobicupola, and Icosahedra from Sedimented Host Crystals 85

4.4 Density Gradient Fractionation of Icosahedral Cluster System . . . 87

4.5 SEM Images of Pure Tetrahedral, Octahedral, and Icosahedral Colloidal Clusters from Sedimented Crystal Template 89

4.6 Heat-Map of Particle-Cluster Interaction Strength, Illustrating Directional Binding Potential 92

4.7 Second Order Clusters from Icosahedral Seeds, Demonstrating Directional Bonding 93

5.1 Schematic for Patchy Particle Generation *via* Point-of-Contact Templating 105

5.2 DNA Architecture for Binary Patchy System 111

5.3 Crystallization of Binary System of Two Sizes Using Patchy DNA Design 112

5.4 Purification of Patchy Particle Systems 114

5.5 Schematic for Understanding Patch Size and Control 115

5.6 SEM Images of Purified Patchy Particles Hybridized with Complimentary Gold Nanoparticles 118

Chapter 1

Introduction

1.1 Self-Assembling Systems

The spontaneous generation of ordered structures from smaller building blocks, also known as Self-Assembly, has been a prominent research focus in various fields within science and engineering for decades. Self-assembly is a robust process which, when well-understood and adequately controlled, has the potential to be revolutionary. Currently, self-assembling melts of diblock copolymers are being used to drastically enhance the resolution of surface printing and modification, and yield resolutions more than four times greater than traditional photoresist topography and chemical patterning [1, 2]. A self-assembling system of biomolecules has also been used to generate mechanically active drug delivery capsules for use in targeted drug delivery applications [3].

Self-assembly occurs frequently in nature, both through living organisms and through geological and other natural processes. In either case, self-assembly only arises when proper conditions are met. Viral capsids, complex proteins, and other intricate three-dimensional cellular structures are routinely and robustly synthesized in a cellular environment on short timescales. This is a fascinating ability, and the ultimate goal of the field of self-assembly is to emulate biology's ability to reproducibly generate highly complex three-dimensional structures from the 'bottom-up' in an efficient manner. Bottom-up assembly offers a good many advantages over the more traditional 'top-down' assembly and manufacturing processes, which generally rely on tools like microfabrication, lithography, and two-dimensional assembly lines. Bottom-up assembly would allow us to eschew those limitations, and to spontaneously generate highly ordered three-dimensional structures and patterns without outside intervention in a cheap, scalable, and robust way.

The ultimate goal of this field is to be able to *direct* the self-assembly of materials. By controlling all variables involved in self-assembly, we will be able to define previously inaccessible structures, and build them from the bottom up, reliably and reproducibly.

1.2 DNA-Directed Self-Assembly

Deoxyribonucleic Acid (DNA) offers a convenient means of directing these assemblies. DNA strands are comprised of combinations of four bases which self-assemble

and reversibly interact with one another in very specific and thermodynamically understood ways *via* Watson-Crick base-pairings [4]. By carefully designing DNA sequences with targeted interaction energies, we have a high level of control over the assembly of DNA-based systems. DNA interactions are so specific and controllable, in fact, that DNA has been used to assemble three-dimensional building blocks, mechanically active boxes, and even DNA origami [5–7]. While DNA is a versatile and powerful molecule, its uses in materials science are limited by its mechanical properties. One could not assemble a viable microchip out of DNA, for example.

It is for this reason that DNA-coated nanoparticles and polymer spheres have been a large research focus within the field of directed assembly. By functionalizing specifically designed DNA strands to the surface of gold nanoparticles or polystyrene microspheres, we can drive the assembly of these particles *via* DNA interactions.

The Mirkin Group, at Northwestern University, found success in generating nine distinct crystal structures using DNA-coated gold nanoparticles in 2011 [8, 9], and generated a list of six design rules which govern the final crystal structure. While the crystals developed using this system are impressive, the particles within these crystals are packed fairly close together (based on hydrodynamic radii), since spheres generally form close-packed structures.

Oleg Gang's research group at Brookhaven National Laboratory synthesized an open body-centered-cubic structure using DNA-directed assembly of gold nanoparticles in 2008 [10]. In this work, particles occupy only around four percent of the

unit cell volume. This is achieved by using exceptionally long DNA strands in relation to the particle size, such that the hydrodynamic radius is much greater than the particle radius. If we include the hydrodynamic radius instead of the particle radius, however, the volume fraction of this crystal is comparable to those of the Mirkin Group described previously, as well as those crystals formed from colloidal microspheres, whose hydrodynamic radii are at most 10% greater than the particle radii. A graphical explanation is provided in Figure 1.1.

The production of crystals using micron-scale colloidal particles is more challenging, with most structures forming amorphous assemblies despite the fact that their minimum energy structures should be crystalline [11]. Despite this, the first DNA-directed colloidal crystallization was performed in the Crocker Group in 2005 using such a system [12–14]. Furthermore, in 2012, the group synthesized the first DNA-directed colloidal crystal structure to undergo a phase-transition from one crystal structure into another [15], demonstrating that the DNA bonds linking the particles within the crystal are dynamic, and allow for structural transformations.

The systems outlined above generate a wide variety of interesting crystal structures, with the structure of the resulting crystals determined by several tunable parameters. The parameters thus far explored have been limited to the size ratio of the hydrodynamic radii of component particles, the molar ratio of the component particles, the interaction energies between the component particles, and the temperature conditions where assembly takes place, as shown in Figure 1.2.

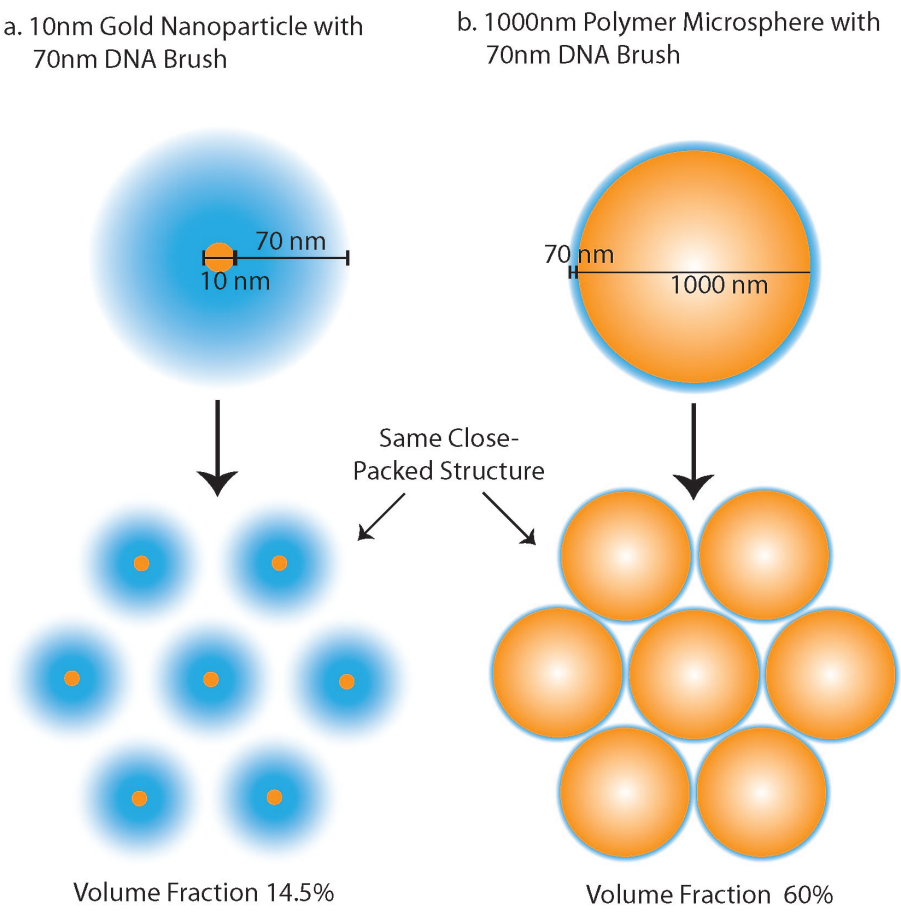

Figure 1.1: The current method for obtaining open structures is to increase the hydrodynamic radius relative to the radius of the core particle. A 10 nm gold nanoparticle with a 70 nm DNA brush (a) can form a close-packed crystal with a particle volume-fraction of 14.5%, while the total volume fraction including the DNA brushes is close to 74%. A 1000 nm polymer microsphere with a 70 nm DNA brush, however, forms a close packed crystal with a particle volume fraction of 60%, while, again, the total volume fraction including the DNA brush is 74%.

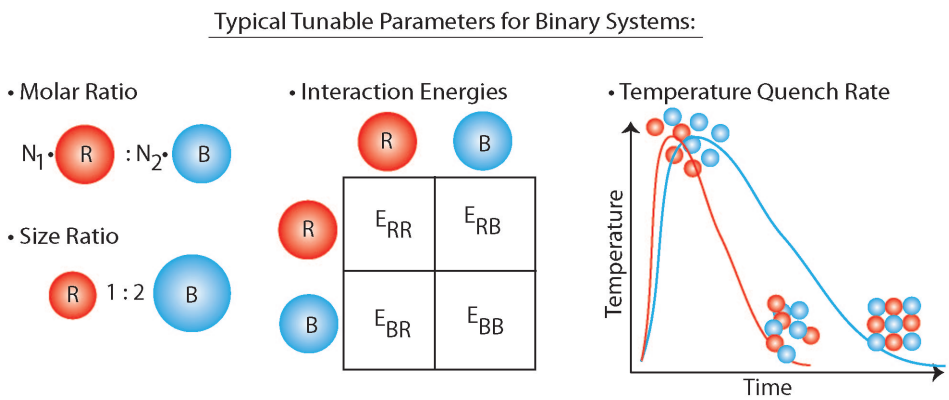

Figure 1.2: Tunable Parameters for Binary System.

While the diversity of crystals formed using these methods is great, it does appear to be limited to close-packed or nearly close-packed crystal structures, all of which have analogs in naturally formed binary opals or molecular crystals. To expand the variety of attainable structures, more tunable parameters must be introduced. This thesis will focus on adding Reprogrammable DNA Interactions and Anisotropic Interactions as viable tunable parameters.

1.3 Expanding the variety of realizable structures

Several new tools will be explored throughout this thesis pertaining to the introduction of these new tunable parameters. Reprogrammable DNA Interactions will be implemented *via* two means: competitive DNA interactions and enzymatic modification. The development of anisotropic building blocks will require the use of these Reprogrammable DNA Interactions, and will also require the implementa-

tion of Colloidal Crystal Templating, which will ensure that the building blocks are reliably synthesized with targeted symmetries.

1.3.1 Reprogrammable DNA Interactions

DNA is an exceptionally versatile molecule for directed self-assembly not only because of its highly specific, reversible, and thermodynamically understood interactions, but also because DNA interactions can be easily modulated. DNA strands can compete with one another at room temperature, and their structure and interactions can be modified by a large number of enzymes.

The first tool within Reprogrammable DNA Interactions that will be explored is competitive DNA interactions. Valeria Milam's research group at Georgia Tech has shown that competing strands of DNA can effectively drive bridge-melting at room temperature [16–18]. It was found, through her work as well as through work in the Crocker Lab [19], that adding non-tethered, soluble DNA strands to an aggregated binary system of DNA-coated colloids in which the interactions between the soluble strand and one of the system's two particle species is greater in magnitude than the interactions between the original two particle species, the system will melt as the Particle-Particle bonds are displaced by the soluble strand-Particle bonds.

The impact of incorporating such interactions is more clearly seen in recent work in the Manoharan Group, where W. Benjamin Rogers has further utilized such competitive interactions, in a more elegant manner, to design a system which both

exhibits reentrant melting, and can transition between two crystal structures [20].

The second tool within Reprogrammable DNA Interactions which will be explored is the enzymatic modification of DNA-colloid systems. Several enzymes have been shown to be effective at modifying such systems, such as T4 DNA Ligase, which is explored in this thesis, as well as restriction enzymes, which are not. Chad Mirkin's group and others have demonstrated that T4 DNA Ligase is effective at forging covalent bonds between two DNA strands in DNA-colloid systems [21, 22]. The Keating Group at Penn State and the Bates group at the University of Liverpool have shown that other enzymes, like restriction enzymes, are reliably active in DNA-colloid systems [23–25] as well. These enzymes have been used both to forge covalent bridges between colloidal particles, and to destroy bridges between particles.

1.3.2 Anisotropic Building Blocks

The inclusion of anisotropic building blocks into DNA-directed self-assembling systems can drastically augment the number and type of structures that can be generated. Simulations have shown that shape anisotropy can determine a system's structure, not by the nature of the shapes themselves, but rather *via* directional entropic interactions *between* shapes [26–30]. As such, polyhedral particles [31–39], rigid clusters of spheres [19, 40–44], and patchy particles [45–48] have been generated in an attempt to realize this additional tunable parameter.

Few groups have studied DNA-coated polyhedral particles. A noteworthy exception is the recent work by Oleg Gang's group. Polyhedral nanoparticles (cubes and octahedra) were functionalized with DNA strands and were interacted with complementary spheres to drive crystalline assemblies with long-range order [26]. This marks the first time that large well-ordered three-dimensional crystal structures have been grown using a combination of directional and DNA-induced interactions. This work further validates the utility in exploring shape-induced directional interactions, though polyhedral particles will not be a focus in this thesis.

This work will focus on the development of scalable processes for the generation of rigid colloidal clusters and patchy particles for use as anisotropic building blocks. These processes require Reprogrammable DNA Interactions as outlined above, as well as three-dimensional Colloidal Crystal Templates, which are highly controllable and much more scalable than two-dimensional templates typically used in particle fabrication.

First, we will look at the generation of rigid colloidal clusters. Experimentally generating colloidal clusters, in particular, has been a major focus within the research community. The Pine Group has utilized both depletion interactions and emulsion-confinement as a means of generating rigid clusters of colloids [40–42]. The clusters are stable and versatile, and can be modified and used in many ways; in one case, they were transformed into patchy particles with distinct patches of DNA on their surfaces. Unfortunately, these methods lack in their ability to tar-

get a specified structure, and they require complex protocols. Nicholas Schade in the Manoharan Group, however, took a different approach, and formed clusters by varying the size ratios of DNA-coated particles in solution to target clusters with tetrahedral symmetry [44]. By using colloidal crystals as templates, however, we show in this work that we are able to easily target a wide range of specific cluster symmetries and generate high yields of uniformly-coated colloidal clusters with an exceptionally straightforward and scalable protocol.

Next we will focus on the generation of patchy particles. While simulations have shown that patchy particles can vastly increase the number and type of structures generated [49–55], and phase diagrams of such systems have also been created [52, 56–58], no experimental realizations of crystals formed using patchy DNA-coated particles have been published, though particles with hydrophobic patches were assembled into a colloidal kagome lattice by the Granick group in 2011 [59]. Nonetheless, groups have been working to engineer methods of patchy particle production [39, 45, 47, 48, 60–62]. The method presented in this thesis utilizes colloidal crystals and gels as templates, and generates high yields of purified patchy particles with symmetries that are defined by the host template.

1.4 Thesis Overview

In Chapter Two, we explain the design, synthesis, and optimization of the various self-assembling systems of DNA-coated colloidal microspheres. The chap-

ter will delve into DNA design, functionalization of colloidal microspheres with biomolecules, and the creation of colloidal crystals. Various general protocols pertaining to the manipulation, analysis, and characterization of such systems are included, with more detailed Materials and Methods sections relegated to their relevant chapters. In Chapter Three we will demonstrate the feasibility of reprogrammable DNA interactions for making colloidal clusters. The challenges addressed include designing and validating a system of competitive DNA interactions, incorporating impurity particles into a host crystal, and generating colloidal clusters containing a targeted number of particles. Chapter Four expands on the work done in Chapter Three, illustrating a means of forging *stable* colloidal clusters with targeted symmetries, and demonstrate their directional binding. The challenges addressed include expanding the number of cluster symmetries obtainable from a single host crystal, incorporating a DNA-reactive enzyme to form stable bonds between particles, and purifying and imaging the resulting structures. The clusters generated in this chapter are also used to demonstrate that DNA-coated colloidal clusters exhibit directional bonding, paving the way for their use in further assemblies. In Chapter Five we go over a preliminary protocol for the generation of patchy colloidal particles, which will also hopefully be used as anisotropic building blocks in future assemblies. Chapter Six summarizes the conclusions of this work, and its implications in the field of directed self-assembly. We then conclude with potential new directions for the lab's research.

References

[1] Mark P. Stoykovich, Marcus Müller, Sang Ouk Kim, Harun H. Solak, Erik W. Edwards, Juan J. de Pablo, and Paul F. Nealey. Directed assembly of block copolymer blends into nonregular device-oriented structures. *Science*, 308(5727):1442–1446, 2005.

[2] Ricardo Ruiz, Huiman Kang, François A. Detcheverry, Elizabeth Dobisz, Dan S. Kercher, Thomas R. Albrecht, Juan J. de Pablo, and Paul F. Nealey. Density multiplication and improved lithography by directed block copolymer assembly. *Science*, 321(5891):936–939, 2008.

[3] Shawn M Douglas, Ido Bachelet, and George M Church. A logic-gated nanorobot for targeted transport of molecular payloads. *Science*, 335(6070):831–834, 2012.

[4] J SantaLucia and D Hicks. The thermodynamics of DNA structural motifs. *Annual Review of Biophysics and Biomolecular Structure*, 33:415–440, 2004.

[5] John P. Sadowski, Colby R. Calvert, David Yu Zhang, Niles A. Pierce, and Peng Yin. Developmental self-assembly of a dna tetrahedron. *ACS Nano*, 8(4):3251–3259, 2014. PMID: 24720462.

[6] Paul W. K. Rothemund. Folding dna to create nanoscale shapes and patterns. *Nature*, 440(7082):297–302, 03 2006.

[7] Ebbe S. Andersen, Mingdong Dong, Morten M. Nielsen, Kasper Jahn, Ramesh Subramani, Wael Mamdouh, Monika M. Golas, Bjoern Sander, Holger Stark, Cristiano L. P. Oliveira, Jan Skov Pedersen, Victoria Birkedal, Flemming Besenbacher, Kurt V. Gothelf, and Jorgen Kjems. Self-assembly of a nanoscale dna box with a controllable lid. *Nature*, 459(7243):73–76, 05 2009.

[8] Robert J. Macfarlane, Byeongdu Lee, Matthew R. Jones, Nadine Harris, George C. Schatz, and Chad A. Mirkin. Nanoparticle superlattice engineering with dna. *Science*, 334(6053):204–208, 2011.

[9] Sung Yong Park, Abigail K. R. Lytton-Jean, Byeongdu Lee, Steven Weigand, George C. Schatz, and Chad A. Mirkin. Dna-programmable nanoparticle crystallization. *Nature*, 451(7178):553–556, 01 2008.

[10] Dmytro Nykypanchuk, Mathew M. Maye, Daniel van der Lelie, and Oleg Gang. Dna-guided crystallization of colloidal nanoparticles. *Nature*, 451(7178):549–552, 01 2008.

[11] Lorenzo Di Michele and Erika Eiser. Developments in understanding and controlling self assembly of dna-functionalized colloids. *Phys. Chem. Chem. Phys.*, 15:3115–3129, 2013.

[12] Paul L. Biancaniello, Anthony J. Kim, and John C. Crocker. Colloidal interactions and self-assembly using dna hybridization. *Phys. Rev. Lett.*, 94:058302, Feb 2005.

[13] Anthony J. Kim, Paul L. Biancaniello, and John C. Crocker. Engineering dna-mediated colloidal crystallization. *Langmuir*, 22(5):1991–2001, 2006.

[14] Anthony J. Kim, Raynaldo Scarlett, Paul L. Biancaniello, Talid Sinno, and John C. Crocker. Probing interfacial equilibration in microsphere crystals formed by dna-directed assembly. *Nat Mater*, 8(1):52–55, 01 2009.

[15] Marie T. Casey, Raynaldo T. Scarlett, W. Benjamin Rogers, Ian Jenkins, Talid Sinno, and John C. Crocker. Driving diffusionless transformations in colloidal crystals using DNA handshaking. *Nature Communications*, 3, November 2012.

[16] Bryan A. Baker and Valeria T. Milam. Dna density-dependent assembly behavior of colloidal micelles. *Langmuir*, 26(12):9818–9826, 2010. PMID: 20349914.

[17] Christopher K. Tison and Valeria T. Milam. Reversing dna-mediated adhesion at a fixed temperature. *Langmuir*, 23(19):9728–9736, 2007.

[18] Christopher Kirby Tison and Valeria Tohver Milam. Programming the kinetics and extent of colloidal disassembly using a dna trigger. *Soft Matter*, 6:4446–4453, 2010.

[19] James T. McGinley, Ian Jenkins, Talid Sinno, and John C. Crocker. Assembling colloidal clusters using crystalline templates and reprogrammable DNA interactions. *Soft Matter*, 9(38):9119–9128, 2013.

[20] W. Benjamin Rogers and Vinothan N. Manoharan. Programming colloidal phase transitions with DNA strand displacement. *SCIENCE*, 347(6222):639–642, FEB 6 2015.

[21] Xiaoyang Xu, Nathaniel L. Rosi, Yuhuang Wang, Fengwei Huo, and Chad A. Mirkin. Asymmetric functionalization of gold nanoparticles with oligonucleotides. *Journal of the American Chemical Society*, 128(29):9286–9287, JUL 26 2006.

[22] Antonios G. Kanaras, Zhenxin Wang, Andrew D. Bates, Richard Cosstick, and Mathias Brust. Towards multistep nanostructure synthesis: Programmed enzymatic self-assembly of dna/gold systems. *Angewandte Chemie International Edition*, 42(2):191–194, 2003.

[23] AntoniosG. Kanaras, Zhenxin Wang, Mathias Brust, Richard Cosstick, and AndrewD. Bates. Enzymatic disassembly of dna–gold nanostructures. *Small*, 3(4):590–594, 2007.

[24] AntoniosG. Kanaras, Zhenxin Wang, Irshad Hussain, Mathias Brust, Richard Cosstick, and Andrew D. Bates. Site-specific ligation of dna-modified gold nanoparticles activated by the restriction enzyme styi. *Small*, 3(1):67–70, 2007.

[25] Sheila R. Nicewarner Peña, Surabhi Raina, Glenn P. Goodrich, Nina V. Fedoroff, and Christine D. Keating. Hybridization and enzymatic extension of au nanoparticle-bound oligonucleotides. *Journal of the American Chemical Society*, 124(25):7314–7323, 2002. PMID: 12071740.

[26] Fang Lu, Kevin G. Yager, Yugang Zhang, Huolin Xin, and Oleg Gang. Superlattices assembled through shape-induced directional binding. *Nat Commun*, 6, 04 2015.

[27] Greg van Anders, N. Khalid Ahmed, Ross Smith, Michael Engel, and Sharon C. Glotzer. Entropically patchy particles: Engineering valence through shape entropy. *ACS Nano*, 8(1):931–940, 2014. PMID: 24359081.

[28] Greg van Anders, Daphne Klotsa, N. Khalid Ahmed, Michael Engel, and Sharon C. Glotzer. Understanding shape entropy through local dense packing. *Proceedings of the National Academy of Sciences*, 111(45):E4812–E4821, 11 2014.

[29] Pablo F Damasceno, Michael Engel, and Sharon C Glotzer. Predictive self-assembly of polyhedra into complex structures. *Science*, 337(6093):453–457, Jul 2012.

[30] Sharon C. Glotzer and Michael J. Solomon. Anisotropy of building blocks and their assembly into complex structures. *Nat Mater*, 6(7):557–562, 08 2007.

[31] Cristina Paun, Olga V. Safonova, Jakub Szlachetko, Paula M. Abdala, Maarten Nachtegaal, Jacinto Sa, Evgeny Kleymenov, Antonio Cervellino, Frank Krumeich, and Jeroen A. van Bokhoven. Polyhedral ceo2 nanoparticles: Size-dependent geometrical and electronic structure. *The Journal of Physical Chemistry C*, 116(13):7312–7317, 2012.

[32] Zhong Lin Wang and Xiangdong Feng. Polyhedral shapes of ceo2 nanoparticles. *The Journal of Physical Chemistry B*, 107(49):13563–13566, 2003.

[33] Xingchen Ye, Joshua E. Collins, Yijin Kang, Jun Chen, Daniel T. N. Chen, Arjun G. Yodh, and Christopher B. Murray. Morphologically controlled synthesis of colloidal upconversion nanophosphors and their shape-directed self-assembly. *Proceedings of the National Academy of Sciences*, 2010.

[34] Tie Wang, Xirui Wang, Derek LaMontagne, Zhongliang Wang, Zhongwu Wang, and Y. Charles Cao. Shape-controlled synthesis of colloidal superparticles from nanocubes. *Journal of the American Chemical Society*, 134(44):18225–18228, 2012.

[35] Weigang Lu, Qingsheng Liu, Zhaoyong Sun, Jibao He, Chidi Ezeolu, and Jiye Fang. Super crystal structures of octahedral c-in2o3 nanocrystals. *Journal of the American Chemical Society*, 130(22):6983–6991, 2008.

[36] Shuifen Xie, Xi Zhou, Xiguang Han, Qin Kuang, Mingshang Jin, Yaqi Jiang, Zhaoxiong Xie, and Lansun Zheng. Supercrystals from crystallization of octahedral mno nanocrystals. *The Journal of Physical Chemistry C*, 113(44):19107–19111, 2009.

[37] Weon-kyu Koh, Sangameshwar R. Saudari, Aaron T. Fafarman, Cherie R. Kagan, and Christopher B. Murray. Thiocyanate-capped pbs nanocubes: Ambipolar transport enables quantum dot based circuits on a flexible substrate. *Nano Letters*, 11(11):4764–4767, 2011.

[38] Laura Rossi, Stefano Sacanna, William T. M. Irvine, Paul M. Chaikin, David J. Pine, and Albert P. Philipse. Cubic crystals from cubic colloids. *Soft Matter*, 7:4139–4142, 2011.

[39] Stefano Sacanna and David J. Pine. Shape-anisotropic colloids: Building blocks for complex assemblies. *Current Opinion in Colloid and Interface Science*, 16(2):96 – 105, 2011.

[40] Natalie Arkus, Vinothan N. Manoharan, and Michael P. Brenner. Minimal energy clusters of hard spheres with short range attractions. *Phys. Rev. Lett.*, 103:118303, Sep 2009.

[41] Vinothan N. Manoharan, Mark T. Elsesser, and David J. Pine. Dense packing and symmetry in small clusters of microspheres. *Science*, 301(5632):483–487, 2003.

[42] Rebecca W. Perry, Guangnan Meng, Thomas G. Dimiduk, Jerome Fung, and Vinothan N. Manoharan. Real-space studies of the structure and dynamics of self-assembled colloidal clusters. *Faraday Discuss.*, 159:211–234, 2012.

[43] Carolyn L. Phillips, Eric Jankowski, Michelle Marval, and Sharon C. Glotzer. Self-assembled clusters of spheres related to spherical codes. *Physical Review E*, 86(4, 1), OCT 15 2012.

[44] Nicholas B. Schade, Miranda C. Holmes-Cerfon, Elizabeth R. Chen, Dina Aronzon, Jesse W. Collins, Jonathan A. Fan, Federico Capasso, and Vinothan N.

Manoharan. Tetrahedral Colloidal Clusters from Random Parking of Bidisperse Spheres. *Physical Review Letters*, 110(14), APR 4 2013.

[45] Lang Feng, Rémi Dreyfus, Ruojie Sha, Nadrian C. Seeman, and Paul M. Chaikin. Dna patchy particles. *Advanced Materials*, 25(20):2779–2783, 2013.

[46] Flavio Romano and Francesco Sciortino. Colloidal self-assembly: Patchy from the bottom up. *Nat Mater*, 10(3):171–173, 03 2011.

[47] Yufeng Wang, Andrew D. Hollingsworth, Si Kyung Yang, Sonal Patel, David J. Pine, and Marcus Weck. Patchy particle self-assembly via metal coordination. *Journal of the American Chemical Society*, 135(38):14064–14067, 2013.

[48] Yufeng Wang, Yu Wang, Dana R. Breed, Vinothan N. Manoharan, Lang Feng, Andrew D. Hollingsworth, Marcus Weck, and David J. Pine. Colloids with valence and specific directional bonding. *Nature*, 491(7422):51–55, 11 2012.

[49] Cristiano De Michele, Piero Tartaglia, and Francesco Sciortino. Slow dynamics in a primitive tetrahedral network model. *The Journal of Chemical Physics*, 125(20):–, 2006.

[50] Nicoletta Gnan, Daniel de las Heras, José Maria Tavares, Margarida M. Telo da Gama, and Francesco Sciortino. Properties of patchy colloidal particles close to a surface: A monte carlo and density functional study. *The Journal of Chemical Physics*, 137(8):–, 2012.

[51] Flavio Romano and Francesco Sciortino. Patterning symmetry in the rational design of colloidal crystals. *Nat Commun*, 3:975, 07 2012.

[52] Flavio Romano, Eduardo Sanz, and Francesco Sciortino. Phase diagram of a tetrahedral patchy particle model for different interaction ranges. *The Journal of Chemical Physics*, 132(18):–, 2010.

[53] Lorenzo Rovigatti, Daniel de las Heras, José Maria Tavares, Margarida M. Telo da Gama, and Francesco Sciortino. Computing the phase diagram of binary mixtures: A patchy particle case study. *The Journal of Chemical Physics*, 138(16):–, 2013.

[54] John Russo, Piero Tartaglia, and Francesco Sciortino. Reversible gels of patchy particles: Role of the valence. *The Journal of Chemical Physics*, 131(1):–, 2009.

[55] Frank Smallenburg and Francesco Sciortino. Liquids more stable than crystals in particles with limited valence and flexible bonds. *Nat Phys*, 9(9):554–558, 09 2013.

[56] Oleg A. Vasilyev, Boris A. Klumov, and Alexei V. Tkachenko. Precursors of order in aggregates of patchy particles. *Phys. Rev. E*, 88:012302, Jul 2013.

[57] Eric Jankowski and Sharon C. Glotzer. Calculation of partition functions for the self-assembly of patchy particles. *The Journal of Physical Chemistry B*, 115(48):14321–14326, 2011. PMID: 22004443.

[58] G. Munao, D. Costa, F. Sciortino, and C. Caccamo. Simulation and theory of a model for tetrahedral colloidal particles. *Journal of Chemical Physics*, 134(19), May 21 2011.

[59] Qian Chen, Sung Chul Bae, and Steve Granick. Directed self-assembly of a colloidal kagome lattice. *Nature*, 469(7330):381–384, 01 2011.

[60] Stefano Sacanna, David J. Pine, and Gi-Ra Yi. Engineering shape: the novel geometries of colloidal self-assembly. *Soft Matter*, 9:8096–8106, 2013.

[61] Stefano Sacanna, Mark Korpics, Kelvin Rodriguez, Laura ColÃn-MelÃ©ndez, Seung-Hyun Kim, David J. Pine, and Gi-Ra Yi. Shaping colloids for self-assembly. *Nat Commun*, 4:1688, 04 2013.

[62] S. Sacanna, W. T. M. Irvine, P. M. Chaikin, and D. J. Pine. Lock and key colloids. *Nature*, 464(7288):575–578, 03 2010.

Chapter 2

System Design, Synthesis, and Characterization

In this chapter, we present the general protocols and analysis techniques utilized throughout Chapters Three through Five. First, the design, analysis, and validation of DNA architectures is described. Then, two means of synthesizing DNA-labeled colloidal particles are described. The use of these particles in the formation of colloidal crystals using both homogenous nucleation and sedimentation follows. Finally, the various means of purifying, imaging, analyzing these systems are presented. This section is intended to be more general, with the specific protocols being found in their respective chapters.

	A	T	C	G
A	AAA ~~AAT~~ AAC AAG	ATA ~~ATT~~ ATC ~~ATG~~	ACA ACT ACC ACG	AGA AGT AGC AGG
T	TAA TAT TAC TAG	TTA TTT TTC TTG	~~TCA~~ TCT TCC TCG	~~TGA~~ TGT TGC TGG
C	CAA ~~CAT~~ CAC CAG	CTA CTT CTC CTG	CCA CCT CCC CCG	CGA CGT CGC CGG
G	GAA GAT GAC GAG	GTA GTT GTC GTG	GCA GCT GCC GCG	GGA GGT GGC GGG

Strand A Design: 5′ - CATTA . . . - 3′

Strand A Complement: 3′ - GTAAT . . . - 5′ → 5′ - . . . TAATG - 3′

Figure 2.1: Method for designing DNA sequences developed by Nadrian Seeman. DNA sequences designed using this method are generally devoid of unwanted interactions such as hairpins, and preferentially bind to their complement. Each three-base sequence listed above is used a maximum of one time to minimize the presence of unwanted secondary structures.

2.1 DNA Design

The colloidal systems described in this work rely on relatively complex DNA architectures. In general, a simple design technique developed by Nadrian Seeman, shown in Figure 5.2, is utilized in the generation of DNA sequences for binary systems, and works well when the targeted interaction regimes ranging from eight to twenty bases. The technique works by defining all possible 64 three-base combinations, known as 'codons.' First, a codon is arbitrarily chosen from the list, and that codon and it's reverse-complement (shown at the bottom-right of Figure 5.2) are crossed off of the list. The sequence is then grown by a single base, by choosing a codon whose first two bases are equal to the last two of the previous codon. Both this codon and its reverse compliment are then removed from the list. In the example provided here, the original codon chosen is CAT, so CAT and ATG are crossed off of the list. The second codon chosen is ATT, growing the sequence by a single T base to CATT. ATT and AAT are then crossed off of the list as well. The sequence is grown in this manner until the desired number of bases has been reached, or until you run out of available codons. The AAA, TTT, CCC, and GGG sequences should be avoided if possible. Because the reverse codons are removed, the sequences designed using this method have minimal unwanted interactions, and strongly favor hybridization with their complements.

After this sequence is designed, a T-spacer is added to the 5' end of each the design strand and its complement, where a T spacer is a string of T bases 40-90 bases

long. The entire sequence is then analyzed using IDTDNA.com's OligoAnalyzer tool, and the sequence is screened for hairpins, other unwanted interactions, and for a reasonable Gibbs free energy (which varies by application, but is usually between -9 and -12 kcal/mol).

2.2 DNA Design Validation using Gel Tms and a Thermodynamic Model

Melting Temperature analyses of aggregates are performed by mixing colloidal solutions of various interacting particle species at a given salt concentration. Their melting temperatures are estimated by enclosing samples in microscopy chambers formed of two coverslips sealed with vacuum grease, and viewing it on an inverted Leica DM IRB microscope as the temperature is slowly increased at a rate of less than 1 degree per minute via an objective heating unit (Bioptechs). This analysis typically starts 5 degrees below the expected T_m (which is estimated as described below), and concludes when the aggregates are mostly a dynamic cloud of weakly interacting particles, with a few small dynamic clusters remaining. Melting temperatures are reproducible to better than 0.5 degrees.

Using the known thermodynamic quantities associated with the interacting DNA sequences [1, 2], a published model [3] was modified and used to estimate the melting temperature of particle aggregates using a nominal DNA grafting density of between

1000 and 2000 strands/particle (depending on the system we are assessing). This ability to predict melting temperatures a priori is key to designing the complex DNA architectures we require.

2.3 Synthesizing DNA-Coated Microspheres

DNA-coated polymer microspheres of varying sizes were synthesized using a previously reported technique [3–9]. Carboxylate-modified polystyrene microspheres of varying sizes were obtained from Seradyn Inc. DNA strands, obtained from IDT DNA, were then covalently coupled to Pluronic F108, obtained from BASF. The DNAylated Pluronic was then physically grafted to the surfaces of the microspheres by a swelling/deswelling technique previously developed in this lab [8]. Particles were dyed with green Bodipy(R) Dye [4,4-difluoro-1,3,5,7,8-pentamethyl-4-bora-3a,4a-diaza-s-indacene] or Red Bodipy(R) [4,4-Difluoro-5-(2-Thienyl)-4-Bora-3a,4a-Diaza-s-Indacene-3-Dodecanoic Acid] during the swelling/deswelling step. Bodipy Dyes were obtained from Invitrogen, and were used in confocal imaging of the clusters.

2.4 Colloidal Crystallization

Crystals are formed by homogeneous nucleation at 20% total particle volume fraction in 150mM pH=8 1xTE buffer. 5 μl samples are sealed in 300 μl microcentrifuge

tubes, brought to 70°C and mixed vigorously, and immediately submerged in a water bath in an insulated cooler. The initial temperature of the bath is 50°C and it cools to room temperature at a rate of roughly 0.3 degrees per hour.

In other experiments, crystals are formed by simple sedimentation in a bench-top centrifuge. Particles are prepared at 1% volume fraction in pH=8 1xTE buffer without added NaCl salt (turning off the DNA interactions) and centrifuged in a low speed bench-top centrifuge at room temperature overnight. Salt is then added in five stages to a final concentration of between 100 and 300 mM, to turn the DNA interactions on.

2.5 Purification by Sedimentation Velocity

Purification was performed in either an 8 mL 3-9% w/w gradient, or in an 8 mL 3-6% w/w of Ficoll 400 (obtained from Sigma) in DI water, made using an Amersham Biosciences SG 15 Gradient Maker. We have tried out several solutes in our density gradients. Ficoll 400 is exclusively used in this thesis, though it is a bit expensive and in some cases induces depletion interactions. Dextran products of various molecular weights work well, and the smaller-sized Dextran products reduce the strength of depletion interactions during separation. Methylcellulose was also tested, but does not work well. It provided great separations, but had low solubility and residual Methylcellulose polymer is extremely difficult to remove from samples after the separation takes place. Other groups have had success with glycerol and sucrose,

though these do not provide stable enough gradients for our purposes.

The first step is to choose a polymer from above, and make two solutions with different densities. Make sure the viscosity is sufficiently low so that it can flow through the gradient maker (SG 15 Gradient Maker, 15ml total Volume, in our case). The mixtures will vary based on your solute, but for Ficoll gradients in particular, we make one solution of high density Ficoll solutions in DI water at either 9% w/w or 6% w/w, and a low density solution at either 3% w/w or 1% w/w. Be sure to de-gas the mixtures, to improve the resulting gradient stability. The solutions are added to the gradient maker, which is used according to the manufacturer's instructions, and empties into a washed and dried glass centrifuge tube in the form of a linear density gradient.

A 10^{-4} volume fraction solution of clusters was made by diluting the ligated system with deionized water. 400 μL of this solution was then placed atop the density gradient. Centrifugation at 3150 RCF for 25-75 minutes (depending on the size of the clusters) separates clusters into distinct purified bands. [10]. Each band is removed separately.

2.6 Imaging and Characterization

In assessing the previously described systems, three main means of imaging were utilized: White-Light Microscopy, Confocal Microscopy, and Scanning Electron Microscopy (SEM). Confocal microscopy and SEM are explained below, as well as the

analysis techniques and programs that were used to assess the data.

2.6.1 Confocal Imaging

Non-ligated clusters and crystals were diluted with 1xTE buffer at pH=8 with a concentration of 150mM NaCl for crystals and 500mM NaCl for clusters, to ensure strong binding and to reduce the risk of melting clusters under confocal laser scanning. DNAylated particles rapidly and irreversibly bind to the surface of untreated glass coverslips, a feature which we use to immobilize clusters for confocal microscopy. Ligated clusters and crystals can be reliably imaged outside of aqueous environments, minimizing differences between the refractive indices of the particles and the solution, and hence vastly improving image quality. Glycerol has been used effectively as a mounting solution in this work, though various other index-matched mounting solutions will work as well.

After sample preparation, high resolution imaging of the fluorescently dyed particles was performed on an inverted Leica DM-IRB microscope with a 100x oil immersion lens equipped with a VTEye confocal, by Visitech. Z stack scans were taken of the samples, averaging 25 frames per slice to reduce noise. The red and green slices are then merged to form a single image showing both the green- and red-dyed particles, after manually correcting for minor optical offsets, validated by control runs performed with beads dyed with both the red and green Bodipy(R) dyes.

2.6.2 Confocal Image Analysis

Due to the small size of the 381 nm particles used in confocal images, automated centroiding and analysis is not feasible. Therefore, in order to determine the structures of the clusters that were assessed using this method, manual centroiding of the constituent spheres was necessary. By going through the Z-stack captures of clusters, the centroids of each constituent particle can be determined. The centroids are then used to render the three dimensional structure using either MATLAB or POVray. The rendered images are then easily studied to determine their structure. Images of crystals have too many particles, and are generally a bit too fuzzy, to reliably assess via manual centroiding. Therefore, in the case of crystals, the particle spacings and angles between particles are determined and used to ascertain which crystal structure has been synthesized.

2.6.3 SEM Imaging

SEM Images were obtained using a JEOL 7500F HRSEM. Clusters are typically first purified using the above methods, and are then prepared and dried using either Methanol Drying or Ethane Vitrification (both protocols are outlined below). After the sample has been dried, it is then sputter-coated with a 10nm layer of Au-Pd, and copper tape is used to attach the metal coating to an aluminum SEM stub in order to prevent charging issues during imaging. For some samples, a second sputter-coating , with the sample sitting at a 45° angle was necessary. Even with

the care taken in preparation, approximately 50% of the clusters imaged were broken in some manner, though in most cases a starting structure could be determined. If a starting structure could not be determined, the cluster was excluded from the analysis.

2.6.4 APTES-Treated Positively Charged Glass

Various protocols exist for the treatment of glass with APTES. This protocol was provided by Dr. Tae Soup Shim, and works extremely well. In order to complete this protocol, APTES (3-aminopropyltrimethoxy silane), glass cover slips or slides, Piranha solution, Acetic Acid, Ethanol, and a reliable oven are required. First, Prepare a 1wt% APTES in 1mM acetic acid solution. Second, prepare the slide glasses and Piranha solution (3:1 concentrated sulfuric acid to 30% hydrogen peroxide solution). Then, soak the glass slides in Piranha solution for 15 min and then, very carefully, wash with water. Next, soak the glass slides in 1wt% APTES in 1mM acetic acid solution for 30 min for silanization and then wash with ethanol. The silanized glass slides must then be baked in a 130°C oven for 20 min. Finally, store the resulting slides in ethanol, and be sure to dry the slides prior to use for LbL coating using compressed air. Be sure to follow all safety protocols, particularly when dealing with Piranha solution, and make sure to have a suitable means of storing the waste.

2.6.5 Methanol Washing

Methanol washing is a facile method for drying fragile colloidal samples prior to SEM sample preparation. In order to prepare a sample using this method, a fume hood, vacuum dessicator filled with dessicant, and a beaker for waste are required. Also needed are APTES-treated positively charged cover slips, a dilute cluster or sample solution, a washing solution, and anhydrous methanol (10 mL).

First, adsorb the negatively charged clusters to the surface of the positively charged glass from the above APTES treatment protocol. A dilute solution of clusters is used (virtually clear), and a large drop is placed on the surface of the treated glass. Wait 20 or so minutes (depending on the sizes and densities of the clusters) for them to sediment and stick, then gently wash the droplet with approximately 10mL of washing solution from a pipet (continuously wash the glass, gently). For ligated systems, the washing solution should be DI water, and for transiently hybridized systems which are not ligated, a solution of 150mM Ammonium Acetate or NaCl, followed by a quick wash with 5 mL of Ethanol, can be used effectively. Then, very quickly take 10mL of anhydrous methanol, and repeat the above step, washing the sample with methanol using a pipet tip (catching the waste in a beaker). Then, tip the glass slide to have all the methanol run off of it, forming a thin layer of methanol, and I rapidly place the sample in the vacuum dessicator. The dessicator used in this thesis is attached to a weak vacuum nozzle in a fume hood to create a slight negative pressure, so that no water can get into the system. When dry, your

sample is ready for SEM prep.

The clusters imaged using this method appear to be slightly squished, and have been a little deformed by the drying process. However, the structures are largely representative of the starting structures, as has been validated by comparing images taken from samples prepared using this method to samples prepared using the more complicated Ethane Vitrification method, outlined below.

2.6.6 Ethane Vitrification

Ethane vitrification is a highly reliable way to completely freeze and preserve the structure of the fragile colloidal clusters. In order to vitrify a sample in ethane, liquid ethane, an ethane plunger or plunging apparatus, and a freeze dryer or lyophilizer are required. Ideally the temperature in the freeze-dryer should be below the T_g of water, $-80°$C, but we have had reasonable results at $-40°$C (Above the T_g of water, the vitrified water will begin to reassemble into crystalline ice, which could tear the sample up). Also needed are APTES-treated positively charged cover slips, a dilute cluster (or other sample) solution, preferably with ligated DNA bridges, and 10 mL of DI Water or other washing solution.

First, adsorb the negatively charged particles or clusters to the surface of the positively charged glass from the above APTES treatment protocol. A dilute solution of clusters is used (virtually clear), and a large drop is placed on the surface of the treated glass. Wait 20 or so minutes (depending on the sizes and densities

of the clusters) for them to sediment and stick, then gently wash the droplet with approximately 10mL of washing solution from a pipet (continuously wash the glass, gently). For ligated systems, the washing solution should be DI water (For transiently hybridized systems which are not ligated, this process is not advisable, but a solution of 150mM NaCl or Ammonium Acetate could potentially be used effectively.). Try to ensure that only a thin film of water remains on the glass surface, then, rapidly plunge the sample into liquid ethane. After vitrification, the sample can be stored in liquid nitrogen until ready to freeze-dry. The vitrified sample is placed in the prepared freeze dryer / lyophilizer, and the water then completely sublimate from the sample over time. When dry, the sample is ready for SEM prep.

2.6.7 Sample Mounting for SEM

Take an SEM stub, and cover the surface with double-sided carbon tape. Place the bottom of the glass sample onto the taped surface, and gently tap it down until it is securely stuck. The sample and stub are then placed into a sputtering machine to coat the sample with metal (Iridium, or a Gold Palladium blend both work well), though the protocol for this depends on the machine. After the sample is prepared, a strip of copper-tape is placed connecting the surface of the metal-coated sample to the surface of the metal SEM stub (on which it is sitting) to ensure conductivity. If this step is avoided, charging issues will result from a buildup of electrons on the surface of the sample, and the images will be of poor quality. If charging issues are

present even after using the copper tape, re-coat the taped sample at a 45 degree angle to ensure that a seamless metal coating exists between the surface of your sample to the metal stub. Consult with the SEM operators for the specific systems you will be working with, as some larger systems will require special treatment.

References

[1] John SantaLucia, Hatim T. Allawi, and P. Ananda Seneviratne. Improved nearest-neighbor parameters for predicting dna duplex stability. *Biochemistry*, 35(11):3555–3562, 1996.

[2] J SantaLucia and D Hicks. The thermodynamics of DNA structural motifs. *Annual Review of Biophysics and Biomolecular Structure*, 33:415–440, 2004.

[3] W. Benjamin Rogers and John C. Crocker. Direct measurements of DNA-mediated colloidal interactions and their quantitative modeling. *Proceedings of the National Academy of Sciences of the United States of America*, 108(38):15687–15692, SEP 20 2011.

[4] Paul L. Biancaniello, Anthony J. Kim, and John C. Crocker. Colloidal interactions and self-assembly using dna hybridization. *Phys. Rev. Lett.*, 94:058302, Feb 2005.

[5] Marie T. Casey, Raynaldo T. Scarlett, W. Benjamin Rogers, Ian Jenkins, Talid Sinno, and John C. Crocker. Driving diffusionless transformations in colloidal crystals using DNA handshaking. *Nature Communications*, 3, November 2012.

[6] James T. McGinley, Ian Jenkins, Talid Sinno, and John C. Crocker. Assembling colloidal clusters using crystalline templates and reprogrammable DNA interactions. *Soft Matter*, 9(38):9119–9128, 2013.

[7] W. Benjamin Rogers, Talid Sinno, and John C. Crocker. Kinetics and non-exponential binding of DNA-coated colloids. *Soft Matter*, 9(28):6412–6417, 2013.

[8] A.J. Kim, V.N. Manoharan, and J.C. Crocker. Swelling-based method for preparing stable, functionalized polymer colloids. *Journal of the American Chemical Society*, 127(6):1592–1593, 2005.

[9] Anthony J. Kim, Paul L. Biancaniello, and John C. Crocker. Engineering dna-mediated colloidal crystallization. *Langmuir*, 22(5):1991–2001, 2006.

[10] Guangnan Meng, Natalie Arkus, Michael P. Brenner, and Vinothan N. Manoharan. The Free-Energy Landscape of Clusters of Attractive Hard Spheres. *Science*, 327(5965):560–563, January 29 2010.

Chapter 3

Assembling Colloidal Clusters Using Crystalline Templates and Reprogrammable DNA Interactions

James T. McGinley, Ian Jenkins, Talid Sinno, and John C. Crocker. "Assembling colloidal clusters using crystalline templates and reprogrammable DNA interactions." *Soft Matter*, **9**(38):9119-9128, 2013. - Reproduced by permission of The Royal Society of Chemistry.

3.1 Abstract

Transient bridges of DNA have been used to direct the self assembly of microscopic spherical particles into a variety of crystal structures. Here, by selectively reprogramming the strength of the DNA interactions within such crystals we form colloidal clusters with well-defined valence and symmetry at high yield. We first form 'host' crystals containing a small proportion of 'impurity' particles bearing a unique DNA sequence, and then add soluble DNA strands that cause the host crystal to melt while preserving the nearest neighbor bonds around each impurity particle. This yields clusters with cubical and cuboctahedral symmetry from host crystals having BCC and FCC structures, respectively. Annealing of these clusters leads them to transform into lower free energy, but still highly symmetric forms, sometimes accompanied by the ejection of particles. The interactions between such clusters in principle could be further reprogrammed to allow hierarchical assembly processes.

3.2 Introduction

Small clusters of colloidal particles provide both building blocks for the directed self-assembly of a greater diversity of structures than feasible with spherical particles as well as model systems with rich behavior is determined by statistical mechanics within a modestly sized configuration space. The fundamental barrier to forming

clusters by self-assembly is that the same attractive interactions that drive cluster assembly will in general also drive the formation of larger assemblies such as colloidal gels or crystals. In one approach, the assembly of clusters is limited by directional bonding, binding kinetics or limited bond valency [1, 2], while in the other approach, only a finite number of particles with spherically symmetric interactions are present in a microvolume (e.g. an emulsion droplet or microfabricated cavity) [2–7]. The various methods in use vary greatly in their scalability, both in terms of sample size and particle size, the ordering of the resulting assemblies and the fractional yield of clusters having a desired structure.

Here we demonstrate a new approach to the formation of colloidal clusters, based upon the formation of 'host' colloidal crystals containing an 'impurity' particle species, followed by the selective dissociation of all particle bonds except those associated with the impurity species. This causes the crystal to melt, freeing the host particles as well as small clusters each with an impurity particle at their center, as in Fig 3.1. Our cluster formation approach relies on the specificity and tunabilty afforded by DNA-mediated particle interactions [8–10]. Attractive particle interactions driven by transient bridges of DNA have been previously shown to drive the formation of multicomponent crystals having a range of different symmetries [11–18], to allow the substitutional co-crystallization of an 'impurity' species in a 'host' lattice [19], and to be 'reprogrammable' by the addition of new DNA strands that complex or compete with the strands on the particles [20–22]. We combine

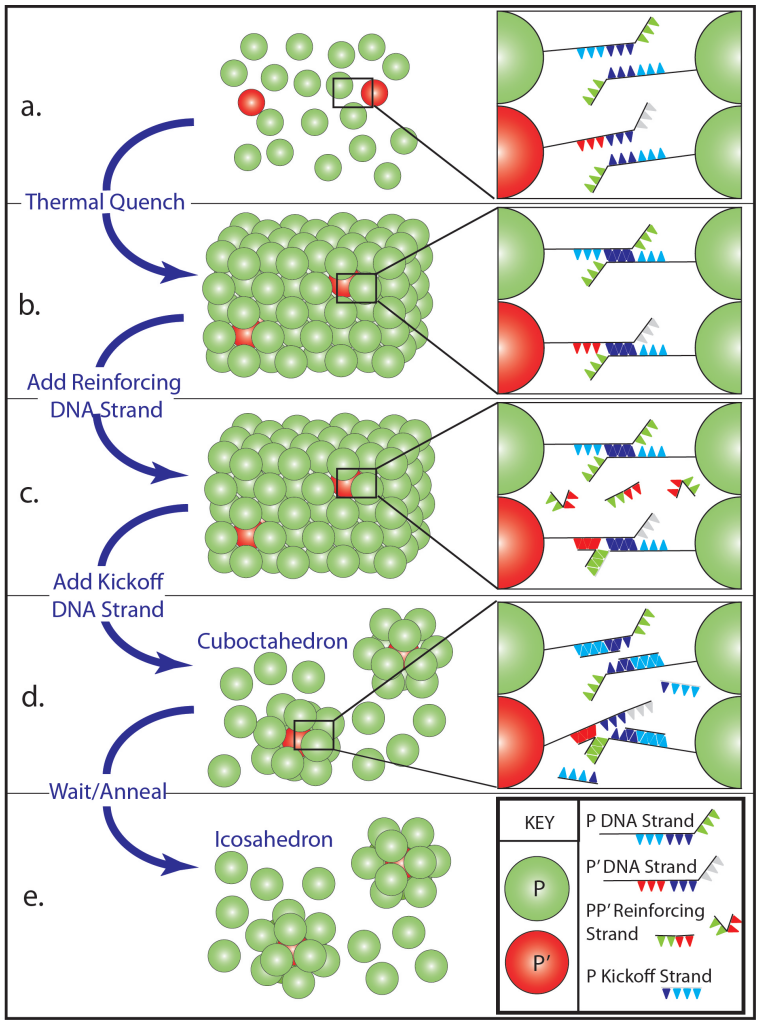

Figure 3.1: A system of two particle species (P,P') is thermally quenched (a) to form large crystals with an FCC structure due to identically attractive $P-P$, $P'-P'$, and $P-P'$ interactions (b). A pair of DNA strands are sequentially added (c,d) which compete with the $P-P$ bonds. Assuming "impurity" $P'-P'$ bonds are rare, the corresponding $P-P$ bond melting temperature T_m drops below room temperature, releasing "$1+12$ clusters" formed of single P' particles and their 12 P neighbors (d). While the clusters are initially cuboctahedra, annealing of these clusters reproducibly transforms them to icosahedra (e).

these various capabilities in two different experimental systems, one of which forms BCC crystals and yields cubical clusters, and another which forms FCC crystals and cuboctahedral clusters. As neither of these cluster symmetries are the lowest free energy structure and the DNA interactions are dynamic, these clusters transform into skew cubes and icosahedra, respectively. We modulate the rate of transformation by adding salt, which has the effect of slowing particle rearrangements by slowing the kinetics of the DNA bridges holding the particles together.

The clusters formed by our crystal templating approach consist of a central impurity particle surrounded by n identical host particles, which we will generically term '$1 + n$' clusters. Note that while the outer particles in these clusters have a strong attraction to the central particle, they are not attracted to each other, as was the case in some previous studies [5–7], but instead merely have a short ranged repulsion with each other. In this way, our clusters are a physical realization of a classical packing problem in applied mathematics, called the Tammes or spherical code problem. The minimum free energy Tammes clusters have been computed for different n values [23], and neither the cube nor the cuboctahedron correspond to the $n = 8$ or $n = 12$ clusters, which are rather the 'skew cube' (square anti-prism) and the icosahedron. This situation leads to two intriguing questions which we answer here. Does crystal templating provide a route for forming highly symmetric clusters having non-minimum free energy? Do the structural rearrangements allowed by DNA handshaking allow the clusters to transform into their lowest free energy

forms?

3.3 Materials and Methods

3.3.1 Particle Preparation and Conjugation

Caboxylate modified polystyrene spheres of 381nm diameter [12] were purchased from Seradyn Inc, and were physically grafted with DNA strands, purchased from IDT DNA, using a technique we have previously reported based on covalent coupling to a triblock copolymer, Pluronic F108 [8, 12, 14, 19, 24]. Five types of particles, each bearing DNA strand having unique sequences, were prepared. Three of these particles, types A, B, and B', form two-component BCC lattices when crystallized. The last two, P and P', form one component FCC crystals. Under our nominal reaction conditions [8, 12, 24], DNA yields of 1000±150 strands per particle are obtained. The particles of A and P' were dyed with green Bodipy(R) Dye [4,4-difluoro-1,3,5,7,8-pentamethyl-4-bora-3a,4a-diaza-s-indacene], those of B' and P were dyed with Red Bodipy(R) [4,4-Difluoro-5-(2-Thienyl)-4-Bora-3a,4a-Diaza-s-Indacene-3-Dodecanoic Acid], and B particles were left undyed. Bodipy Dyes were obtained from Invitrogen, and were used in confocal imaging of the crystals and clusters. The dyes, when used at low concentrations, have no detectable effect on the melting temperature of DNA driven particle aggregation [12] .

3.3.2 T_m Analyses

Melting Temperature analyses of aggregates were performed by mixing colloidal solutions of various interacting particle species with modifying strands in 150mM NaCl 1xTE buffer (10 mM Tris + 1mM EDTA) at pH=8. Their melting temperatures are estimated by simply enclosing samples in microscopy chambers formed of two coverslips sealed with silicone vacuum grease, and viewing it on an inverted Leica DM IRB microscope as the temperature is slowly increased at a rate of less than 1 degree per minute via an objective heating unit (Bioptechs). This analysis typically starts 5 degrees below the expected T_m, and concludes when the aggregates are mostly a dynamic cloud of weakly interacting particles, with a few small dynamic clusters remaining. Melting temperatures are reproducible to better than 0.5 degrees. Using the known thermodynamic quantities associated with the interacting DNA sequences [25, 26], a recently published model [8] was modified and used to estimate the melting temperature of particle aggregates using a nominal DNA grafting density of 1000 strands/particle. This ability to predict melting temperatures a priori is key to designing the complex DNA architectures we require.

3.3.3 FCC Crystal Formation

The one component FCC crystals are formed by P and P' particles, which is accomplished by using a palindromic DNA sequence. This sequence is identical for both P and P', with reaction energies of $\Delta G = -8.92\frac{kcal}{mol}$, as determined by the

nearest-neighbor model [26]. Crystals of P with P' impurities are formed by homogeneous nucleation at 20% total particle volume fraction in 150mM pH=8 1xTE buffer. 5 μl samples are sealed in 300 μl microcentrifuge tubes and submerged in a water bath in an insulated cooler. The initial temperature of the bath is 50°C and cools to room temperature at a rate of 0.3 degrees per hour. In other experiments, either P and P' *or* A and B' particles are prepared at 1% volume fraction in pH=8 1xTE buffer without added NaCl salt (turning off the DNA interactions) and centrifuged in a low speed benchtop centrifuge at room temperature overnight. Salt is then added in five stages to a final concentration of 150 mM, to turn the DNA interactions back on. In the PP' case, the result is solid colloidal crystals that can be imaged, or melted into clusters using added DNA strands (described below). For the AB' system, the resulting crystalline pellet is not crosslinked by DNA, and can be gently resuspended, releasing the clusters within.

3.3.4 BCC Crystal Formation

Two component BCC/CsCl crystals are formed of A particles that interact selectively with B and B' particles. The B and B' particles were designed to interact with A with the same reaction energy ($\Delta G = -6.33\frac{kcal}{mol}$). The melting temperatures of AB and AB' aggregates are matched by using a modulating strand in the solution during crystallization. BCC/CsCl crystals of A, B and B' impurities are formed by homogeneous nucleation at a 20% total particle volume fraction in

150mM pH=8 1xTE buffer (10 mM Tris + 1mM EDTA). 5 μl samples are sealed in 300 μl microcentrifuge tubes and submerged in a water bath in an insulated cooler. The initial temperature of the bath is 50°C and cools to room temperature at a rate of 0.3 degrees per hour.

3.3.5 Cluster Formation from FCC crystals

A strand called the $P' - P$ Reinforcer, which has an energy of reaction of $\Delta G = -7.20\frac{kcal}{mol}$ with strand P' and an energy of $\Delta G = -5.89\frac{kcal}{mol}$ with P, is added to the solution to link together and reinforce all $P - P'$ bonds. It is added to the system at a stoichiometric ratio with all P and P' strands in the system, and the system is quenched overnight from between 23 and 29 degrees celsius, which removes any negative effects of the reinforcer's 23°C hairpin, and yet is not hot enough to anneal the crystal structure. This ensures a near complete hybridization reaction. A P Kickoff strand ($\Delta G = -11.597\frac{kcal}{mol}$) is then added in excess, which eliminates all $P - P$ bonds, and weakens all $P' - P'$ and $P' - P$ bonds. The $P' - P'$ bonds should be relatively rare, and $P' - P$ bonds, since they were reinforced, only weaken to a T_m of roughly 33°C, so they remain intact. These clusters can be further strengthened by the addition of additional NaCl, if necessary.

3.3.6 Cluster Formation from BCC crystals

A strand called B' Protector is introduced into the crystallized system in slight excess of the total number of B' strands present, assuming 1000 DNA strands per bead. The energy governing the reaction ($\Delta G = -8.58\frac{kcal}{mol}$) is experimentally shown to be sufficient to ensure that the reaction approaches completion relatively fast. Just to be sure, the system is left to sit for at least 30 minutes. A strand of B Kickoff ($\Delta G = -13.17\frac{kcal}{mol}$) is then added in excess of the total number of B strands in the solution. This excess ensures a near instant and complete reaction, that destroys all $A-B$ bonds, and leaves only the protected $A-B'$ bonds unaffected. Therefore, based on the structure of the BCC system, each well-incorporated B' particle will be left with eight A particles still attached, thus producing $1+8$ clusters.

3.3.7 Imaging Crystals and Clusters

Clusters and crystals were diluted with 1xTE buffer at pH=8 with a concentration of 150mM NaCl for crystals and 500mM NaCl for clusters, to ensure strong binding and to reduce the risk of melting clusters under confocal laser scanning. We find that DNAylated particles rapidly and irreversibly bind to the surface of untreated glass coverslips, a feature which we use to immobilize clusters for confocal microscopy. Typically, we find clusters with 3 or more particle adhered to the glass. We conjecture that this configuration results from internal rearrangements within the cluster after the first particle adheres, and that particle-glass contacts

are permanent (i.e. they do not roll).

High resolution imaging of the fluorescently dyed particles was performed on an inverted Leica DM-IRB microscope with a 100x oil immersion lens equipped with a VTEye confocal, by Visitech. Z stack scans were taken of the samples, averaging 25 frames per slice to reduce noise. The red and green slices are then merged to form a single image showing both the green- and red-dyed particles, after manually correcting for minor optical offsets, validated by control runs performed with beads dyed with both the red and green Bodipy(R) dyes.

3.3.8 Cluster Simulation and Mode Analysis

Langevin Dynamics (LD) simulations were performed within the NVT ensemble using the LAMMPS software package [27]. A time step of 10^{-12}s and a damping time of 10^{-5}s were used. The damping time, which corresponds to under-damped conditions (vibrational timescale is $\sim 10^{-9}$-10^{-7}s), was chosen so that the cluster relaxation occurred in reasonable simulation time. Notably, we do not expect the dynamics of the simulation to quantitatively match those of the experiment. The binding and rolling kinetics of DNA linked particles are currently poorly understood, but are likely to be orders of magnitude slower than predicted by Brownian motion due to the slow hybridization kinetics of the DNA bridges well below their melting temperature. Our goal is merely to determine the physical plausibility of different transformation mechanisms, and at most to consider the relative ratio of rates for

different processes to occur.

For all runs the system was initiated with 13 particles placed in a cuboctahedron configuration. Particle interactions were modeled according to the DNA mediated potential derived in ref. [[8]]. The centerhalo particle interactions were attractive, with a maximum well-depth of $10k_BT$. Interactions between halo particles were purely repulsive. Simulations were performed in which varying numbers of particles were held fixed. In the first type of constrained simulation a set of three particles from a single triangular face of the cuboctahedron were kept fixed, while in the second type a set of four particles from a single square face of the cuboctahedron were kept fixed. Simulations were also performed with no constrained particles. The particle energies were monitored and a particle ejection event was recorded each time a particle exhibited zero energy.

Vibrational mode analysis of cluster configurations was performed using lattice dynamics within the quasi-harmonic approximation [28, 29] to identify 'soft' modes along which transformations may occur. In lattice dynamics, the dynamical matrix of second derivatives of the interaction potential is evaluated about a given particle configuration. Eigenvalues and eigenvectors of the dynamical matrix were computed using the Eigen package [http://eigen.tuxfamily.org]. These eigenvalues and eigenvectors correspond to the vibrational frequencies and modes, respectively, of a fictitious undamped replica of the (overdamped) physical system.

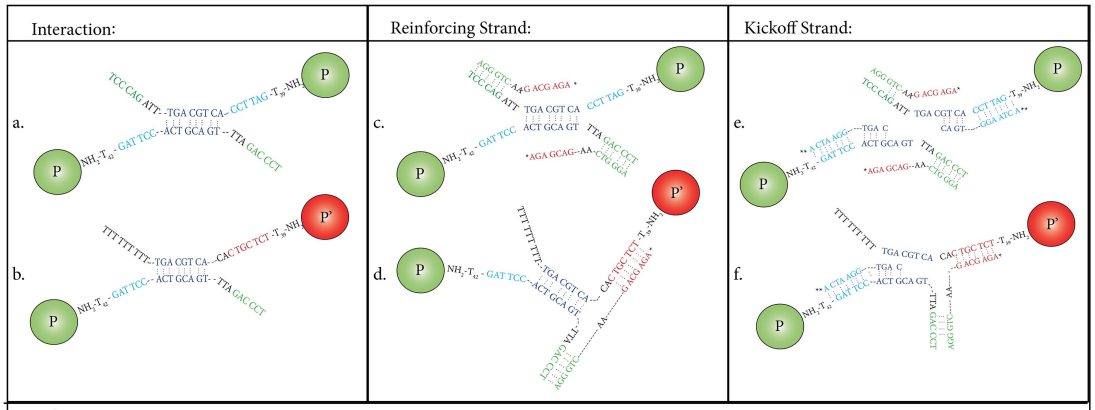

Melting Temperature Data:

	Strands Present	Nominal T_m (°C)	Measured T_m (°C)
a.	P, P	36	35
b.	P, P′	36	N/A
c.	P, P, PP′-Reinforcer*	36	29
d.	P, P′, PP′ Reinforcer*	>36	41.8
e.	P, P, PP′ Reinforcer*, P Kickoff**	< 20	< 20
f.	P, P′, PP′ Reinforcer*, P Kickoff**	>RT	33

Bonds Not Shown:

	Strands Present	Nominal T_m (°C)	Measured T_m (°C)
g.	P′, P′	36	34
h.	P′, P′, PP′-Reinforcer*	36	35
i.	P′, P′, PP′ Reinforcer*, P Kickoff**	<36	34

Figure 3.2: DNA strand architectures and Particle Melting Temperatures for the $P-P'$ system. Melting temperatures, both nominal and experimentally measured, for $P-P$ (a,c,e) and $P-P'$ (b,d,f) particle bonds with relevant competing strands are provided in the corresponding table, as are the three bonds, (g,h,i), not illustrated, from $P'-P'$ particle and competing strand interactions.

3.4 Results and Discussion

3.4.1 DNA Design Approach and Findings

The successful production of clusters required the development of several new DNA tools. First, systems of particles and interactions that yielded FCC and BCC crystals were expanded by the addition of a new impurity particle species whose DNA strands bore the same DNA sequence in their 'interaction' domain as one of the host species, but which contained a different, unique DNA sequence in an adjacent 'recognition' domain. To ensure that the impurity species co-crystallizes as a stoichiometric substitution, it is crucial that its interaction strength correspond very

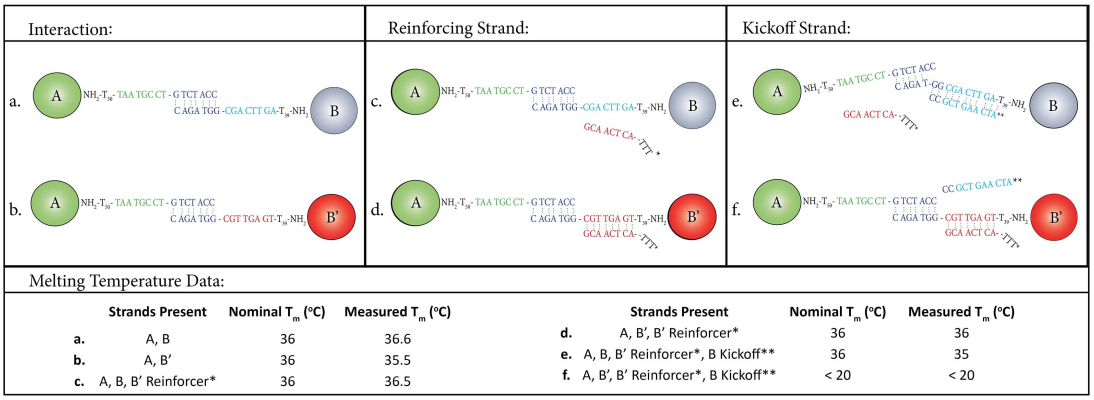

	Strands Present	Nominal T_m (°C)	Measured T_m (°C)
a.	A, B	36	36.6
b.	A, B′	36	35.5
c.	A, B, B′ Reinforcer*	36	36.5
d.	A, B′, B′ Reinforcer*	36	36
e.	A, B, B′ Reinforcer*, B Kickoff**	36	35
f.	A, B′, B′ Reinforcer*, B Kickoff**	< 20	< 20

Figure 3.3: DNA strand architectures and Particle Melting Temperatures for the $A - B - B'$ system. Melting temperatures, both nominal and experimentally measured, for $A{-}B$ (a,c,e) and $A{-}B'$ (b,d,f) particle bonds with relevant competing strands are provided in the corresponding table.

closely to the host particles that it replaces [30]. This was achieved by the addition of a small amount of a 'modulating' strand which complexes with DNA strands on either the host or impurity particle, slightly reducing its interaction strength without modifying that of the other particles significantly. Once crystallized, the system is melted by adding DNA 'kickoff' strands that hybridize with the host particles' spacer DNA sequences but which also extend into the interaction domain, destabilizing the DNA bridges between host particles. If needed, additional 'reinforcing' strands can be added to selectively strengthen the intracluster bonds by hybridizing across the appropriate particle bridges.

We first describe our DNA sequence design approach. To avoid sequences having undesirable hybridization or hairpin formation, the sequences were constructed manually using a trial and error procedure that strives to avoid any complementary or repetitive sequences three bases or longer in length. All of the DNA sequences

generated were screened individually to be free of stable hairpins and against each other for unintentional hybridization at relevant temperatures using standard tools based on the nearest neighbor model [25, 26] for DNA thermodynamics. For situations involving bridge formation between particle-grafted DNA strands, the spatial distribution of interacting DNA strands around the particles must be explicitly taken into account when computing the bridge thermodynamics and melting temperature. We rely upon a recently published model [8] for such bridge formation to compute the effective melting temperature of the particle-bridge-particle complexes. During the design phase, these models assume a nominal DNA grafting density of 1000 DNA molecules per microparticle, typical for our bioconjugation protocol (see Materials and Methods). In general the overlap length of designed complexes were made long enough to be stable at room temperature, corresponding to a melting temperature $> 32°$C. The DNA sequence design for reinforcing strands and kickoffs was done by ensuring that there were sufficient ΔG differences to quickly drive desired reactions to completion. By assuming that all soluble strands were in excess and completely reacted, the number of remaining reactive bridges and their overlap domains were used to estimate a nominal meting temperature T_m.

To validate our DNA sequence design and sample preparation processes, we formed colloidal gels of different particle and soluble strand combinations, and experimentally determined the temperatures at which they melted. Such melting temperatures are readily measured and closely correspond to the temperature at

which colloidal crystals form from the same samples. In general, the predicted and measured melting temperatures, reported below, are in excellent systematic agreement with roughly ±1.6°C random error, consistent with the expected uncertainty of the NNM [26] and 15% batch to batch variations in DNA density on the particles.

3.4.2 FCC System

The simplest possible system is one containing a single particle species, where each particle is attracted to every other particle. Such self interacting particles, species P, require an interaction domain having a palindromic DNA sequence, Fig. 2a. Spacer domains consisting of 39 and 42 base long poly-dT for P' and P, respectively, provide a comparatively long-ranged interaction. We find that our 380 nm diameter particles readily nucleate and grow large crystals near the bridge melting temperature, 36°C. The resulting crystals have a face centered cubic (FCC) structure, with a low density of stacking faults, resembling crystals formed by other short-ranged attractive interactions such as the depletion interaction [31, 32].

To enable cluster formation, we first introduce a second species, P', whose DNA strands bear the same palindromic interaction domain and identical length spacer domain, but which differ from the P particles DNA in regions flanking the interaction domain. Because of the identical interaction domain, the two species can readily complex with each other as well, Fig. 2b; the similar interaction free energy should allow both species to co-crystallize; details of that process are provided in

the next section.

To form clusters, we clearly need to form a P host lattice with a low density of impurity P' particles as substitutions. We then need to reprogram the interaction matrix of these two particle species such that $P - P$ bonds melt at room temperature, while the $P - P'$ bonds remain stable. Since any added DNA strand that competitively binds the $P - P$ interaction domain will also bind the $P - P'$ interaction domain, it is necessary to first add a reinforcing strand to selectively stabilize the $P - P'$ bonds. A 15 bp strand that binds facing recognition domains of the P and P' particles forms a highly stable complex, Fig. 1d. While the same reinforcement strand will also complex with $P - P$ bridges, Fig. 1c, it does not physically link the two particles together.

Melting experiments with co-aggregated PP' gels reveals complex formation associated with the reinforcing strand. The reinforcing strands form hairpins at temperatures $< 23°$C, so strands and particle assemblies must be incubated together near or just above that temperature overnight to allow complex formation. Moreover, an unidentified interaction associated with the reinforcing strands, appears to slightly weaken the host lattice, reducing its melting temperature, but only to a still acceptable 29°C when the reinforcing strands are added 1:1 mole ratio to their target strands. Higher concentrations of the reinforcing strands, that would melt the host crystal at room temperature, were avoided.

Once the crystals (or gels) have been reinforced, the host $P - P$ bonds can be

weakened with a kick-off strand, Fig. 2e,f, that hybridizes with the free recognition domain on the P particles, and extends into the interaction domain displacing the strand from the other particle. While this process also occurs in $P-P'$ bridge complexes, the reinforcing strands maintains the particle connection, up to its melting temperature of 33°C.

3.4.3 BCC System

To create clusters having a different network of nearest neighbors, we direct the assembly of particles having a different symmetry, body centered cubic (BCC). As in a recent paper [12], here we create a binary suspension of two particle species, A and B whose interaction matrix is such that only $A-B$ bridges are thermodynamically favored. Specifically, such a binary system forms a CsCl-type superlattice of BCC, with A and B particles in alternating locations. We designed the A and B DNA sequences to bear complimentary interaction domain sequences on the end of long poly-dT spacers, and the strands on both the A and B particles have unique recognition domains adjacent to their interaction domains, Fig. 3a.

As before, to form clusters we add an impurity species, B' which contains the same spacer and interaction domain as the B particles, allowing it to cocrystallize as a substitution for B, but which has a distinct recognition domain, Fig. 3b. To ensure that the interaction free energy of the $A-B$ and $A-B'$ bridges are identical, we also keep two bases adjacent to the interaction domain identical in the two sequences.

To reprogram the interaction matrix of this ABB' system, we can add a kickoff strand that hybridizes to the B recognition domain as well as part of the adjacent interaction domain, destabilizing any $A - B$ bonds, Fig. 3d.

In practice, since four bases of the kickoff strands are necessarily complementary to the B' particle strand as well (since they share an interaction and buffer domain), kickoff strands also weaken $A - B'$ bonds, reducing the melting temperature by 2°C at the required concentration. To avoid this effect, we add a reinforcing strand, Fig. 3c, which hybridizes with the B' recognition and buffer domains after the crystals have been formed, but before the kickoff strands are added.

3.4.4 Co-crystallization of Host/Impurity Crystals

To reproducibly yield a large number of well ordered clusters, we seek to form crystals in which the impurity species are stoichiometrically and randomly substituted through the crystal interior [19]. It is straightforward to make the physical characteristics of the impurity particles, such as size and mass density be identical to the host lattice particles. Ensuring that the DNA interactions of the impurity particles closely match those of the particles they substitute is more difficult. Beyond using the same interaction domain sequence, and spacer length, it is also important that the particle be prepared with nearly identical number of DNA strands per particle. In practice, DNA-labeling of the polystyrene particles introduces a run-to-run surface density variation of about 15%, leading to typical differences in the particles

Table 3.1: B Kickoff Strand for Modulating $A - B$ Melting Temperatures at 150mM NaCl, assuming 1000 DNA strands per B particle

Moles Kickoff/Moles B Strands	Model T_m / °C	Measured T_m / °C
0.00	35	35
0.09	34.5	34
0.17	34	33
0.52	30.5	30.5
0.87	< 20	< 20

melting temperatures of ∼2°C. Since crystal nucleation and growth typically occur over a range of a few degree Centigrade [12], such large variations in DNA density could easily lead to nearly complete exclusion of the impurity species from the growing crystals, as in Figure 3.4a. Achieving effective co-crystallization is thus a non-trivial technical challenge to realize the crystal templating approach. We used multiple strategies to drive effective co-crystallization in our different DNA-particle systems.

FCC crystals were formed by homogeneous nucleation from a 20% volume fraction suspension during a slow thermal quench, as described in Materials and Methods. The stoichiometry was chosen to be 399:1 $P : P'$ particles, to minimize the number of times two P' particles were next nearest neighbors, which form 'conjoined' and defective clusters. Multiple bioconjugation trials were executed, resulting in P and P' samples whose melting temperatures differed by only 1°C, corresponding to an approximate 0.5°C difference between $P - P$ and $P - P'$ bond melting. This

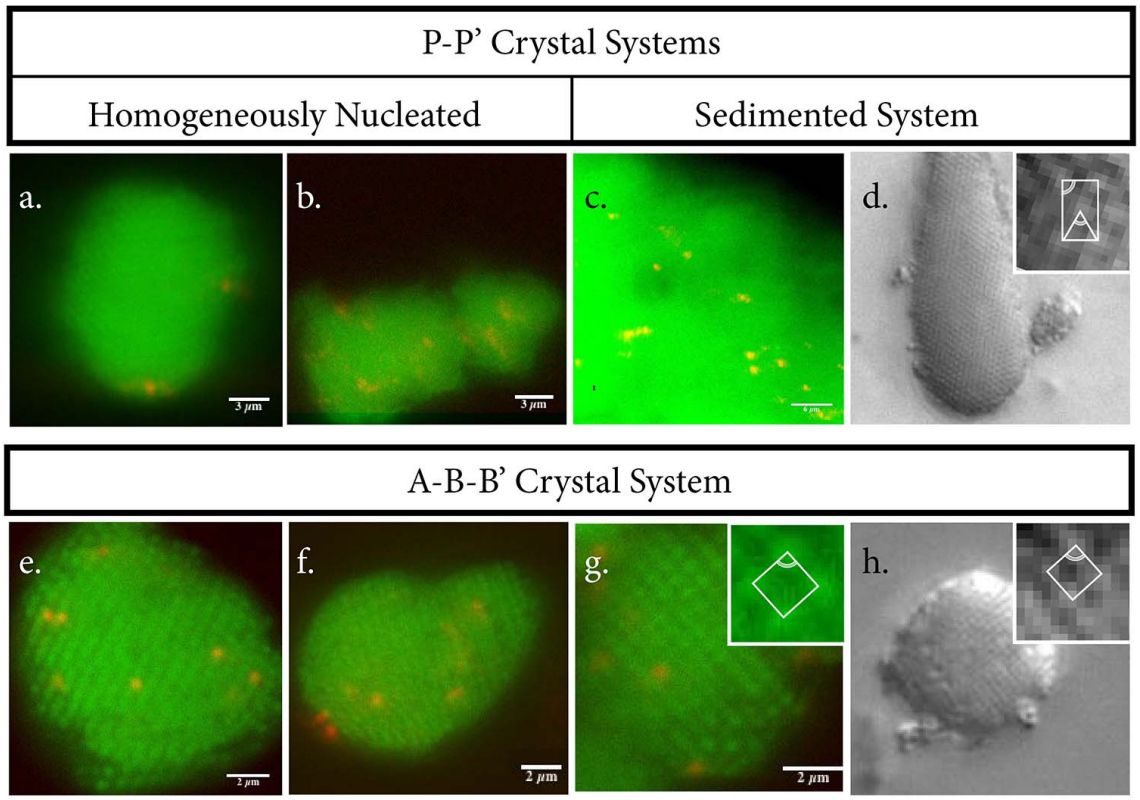

Figure 3.4: Red impurity species were effectively incorporated into host crystals, in green. PP' close-packed crystals were formed *via* two methods: homogeneous nucleation with a temperature difference of $0.5°C$, in which some crystals were highly segregated (a) while others exhibited exceptional incorporation(b), and sedimentation, which provides a well incorporated sample(c) within a close-packed crystal lattice (d). ABB' crystals were formed with an approximate temperature difference of $0.5°C$ *via* homogeneous nucleation, with well incorporated impurities (a-c) within a well-defined BCC lattice structure (c-d). Focus scans of the crystals in panels (a,b,c,e) are available as Supplementary Movies 1-4, respectively, found here.

system yields crystals, shown in Figure 3.4a,b displaying various degrees of co-crystallization. In a small number of crystals, it appears that the impurity particles are concentrated near the exterior of the crystal, as if they only could be incorporated during the later stages of growth, Figure 3.4a. While other crystals in the same sample show excellent incorporation, Figure 3.4b, the excess of surface segregated particles in homogeneously nucleated FCC crystals would introduce an undesirable number of defective clusters.

A simple and effective method of circumventing the segregation issue is to completely eliminate all DNA interactions during crystallization, and to drive crystal formation by other means, such as sedimentation. In this experiment, a mixture of P and P' particles, with the ratio used above, is first prepared in a buffer with no added salt, which effectively turns off all attractive DNA interactions at room temperature. Due to the small size of our particles, sedimentation is performed in a low-speed benchtop centrifuge overnight, forming a dense pellet of particles. The salt concentration in the supernatant is then increased from 0mM to 150mM NaCl in multiple addition steps consisting of gentle pipette mixing and further centrifugation, turning on all attractive interactions and stabilizing the assembled structure at room temperature. The resultant pellet has large crystalline domains having a close packed structure, which can be broken apart manually and visualized by microscopy, Figure 3.4c,d. As expected, the impurity particles are well dispersed.

Co-crystallizing impurity species into the BCC crystal forming system is rela-

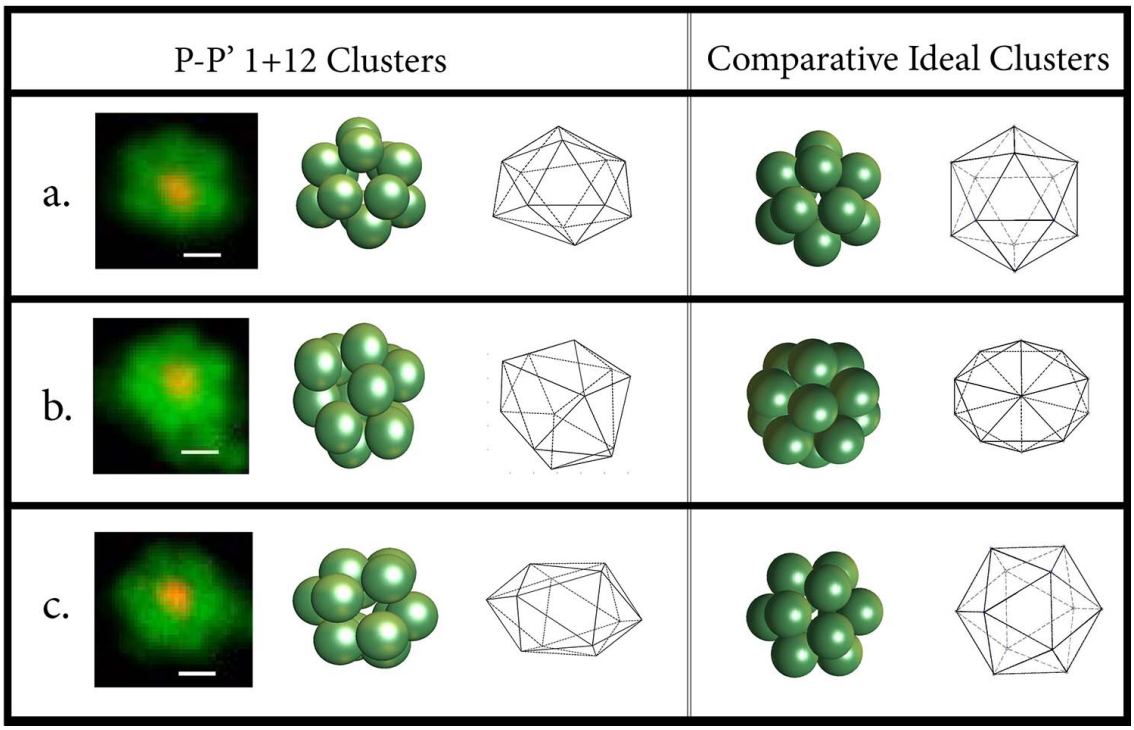

Figure 3.5: Representative Clusters formed *via* PP' Sedimentation. The clusters are shown as bound to the glass by the prevalent three-particle equilateral triangle (a,c), and by a single particle vertex (b). Scale bars correspond to 0.5μm. A focus scan of the cluster in (a) is available as Supplementary Movie 5, found here.

tively straightforward. The same kickoff strand that is used to melt the AB crystals can be used to modulate the strength of the AB interaction until it matches that of AB', compensating any differences that would otherwise be present due to differing numbers of DNA strands on the B and B' particles. Kickoff strands are simply added in stoichiometric amounts to effectively nullify the interactions of a certain fraction of DNA strands on the surface of the B particles. (Such an approach is not feasible in the more complex palindromic system that forms FCC crystals). Table 3.1 shows the associated AB melting temperature shifts as a function of the fraction of silenced DNA strands.

Table 3.2: PP' Sedimentation System: Cluster Statistics. Note: non-'1+12' clusters were not extensively sampled, and may be underrepresented in total.

Valence:		$1+11$	$1+12$	$2+n$
Number of Clusters		1	12	1
Percentage of Clusters		7%	86%	7%
Symmetry:	Number of Icosahedra:	12		
	Number of disordered:	0		

By using modulating strands, the difference in melting temperature between AB and AB' was reduced to < 0.5°C, and BCC crystals formed by homogeneous nucleation at 20% total particle volume fraction, during a slow thermal quench, see Materials and Methods for details. To avoid conjoined clusters, a low proportion of impurity was used, namely a 1:1 ratio of $A : (B + B')$ and a 1:199 ratio of $B' : B$. The resulting crystals, shown in Figure 3.4e-h, show excellent impurity incorporation. Control experiments were performed without modulating strands, using particles whose AB and AB' melting temperatures differed by about 2°C. The resulting crystals, not shown, displayed a high degree of segregation, with all the impurity particles binding the crystals' surfaces. Were the B' more weakly interacting than the B particles, this would make intuitive sense, as they would only bind the host crystals at the end of the crystal growth cycle when the temperature was lowest. In the control experiments, however, the B' particles were the more strongly interacting. We conjecture that each B' gathers a disordered halo of A particles around it which is neither able to nucleate AB crystals nor effectively

Table 3.3: AB' Sedimentation System: Cluster Statistics

Valence:	1+7	1+8	1+9	1+10	1+11	1+12	2+n
Number of Clusters	1	1	2	8	1	15	1
Percentage of Clusters	3%	3%	7%	28%	3%	52%	3%
Symmetry:			Num. Icosohedra			15	
			Num. Tammes n=10	4			
			Num. disordered	4			

incorporate into growing AB crystals.

3.4.5 Cluster Formation and Transformation

Once the samples have been co-crystallized, reinforcing and kickoff strands can be added to melt the crystals while releasing the clusters embedded within them. By allowing the samples stand for a few minutes, the clusters preferentially settle to the bottom of their container, providing a crude enrichment of clusters relative to the excess of host particles. These samples are then loaded into microscopy chambers for confocal imaging, which takes advantage of the fact that DNA-coated particles readily stick to untreated glass, immobilizing the clusters for imaging, details of which are provided in Materials and Methods. Clusters are prepared immediately before imaging, and pipetted gently to minimize the effects of applied shear during handling. Confocal images of clusters are collected randomly to allow the estimation of yields of different n values and cluster symmetries.

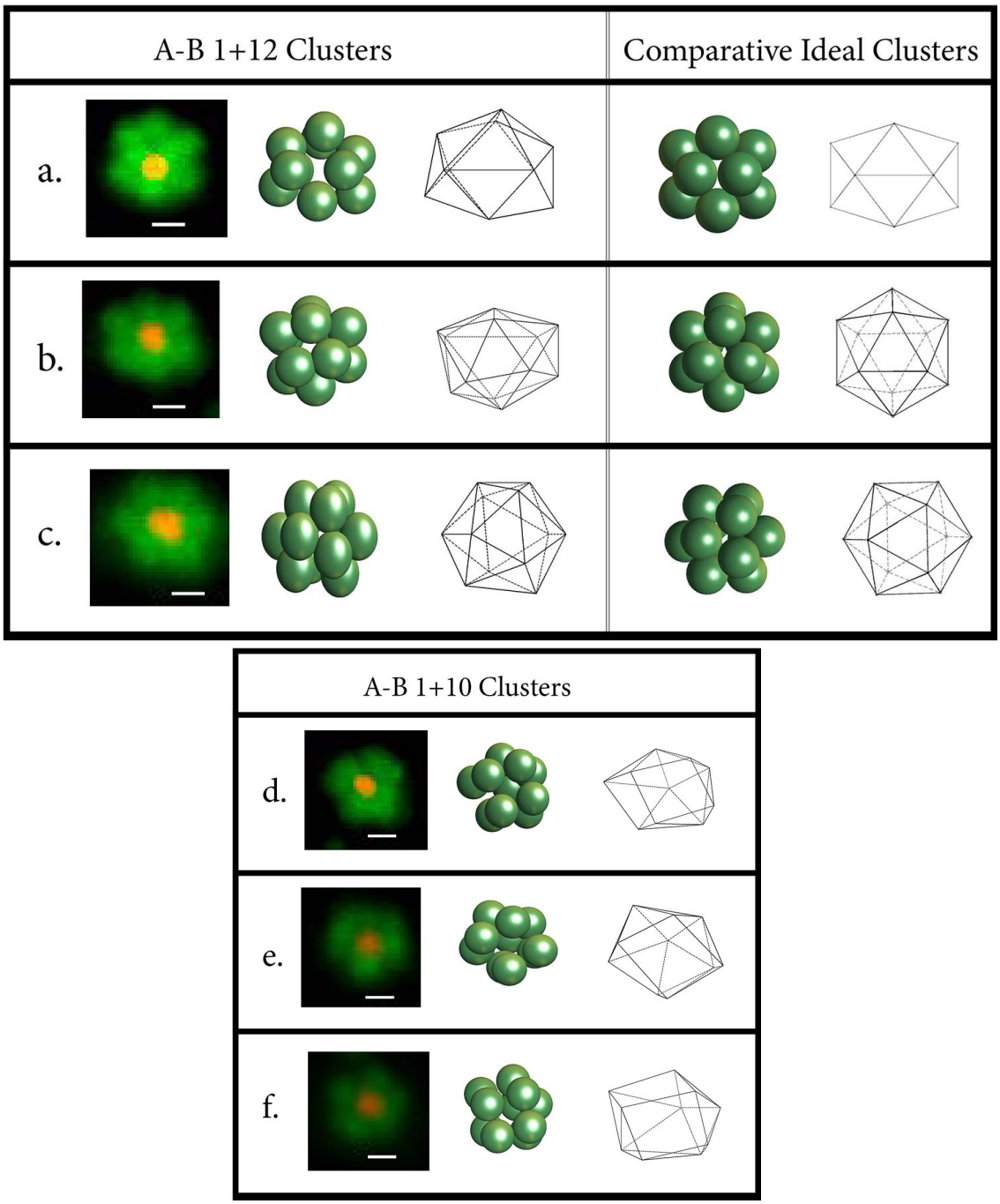

Figure 3.6: Representative Clusters formed *via* AB' Sedimentation. The clusters shown are $1+12$ icosahedral clusters bound by an edge (a) or by a triangular faces (b,c). Three $1+10$ clusters (d-f) display a square face, comparable to a face of cuboctahedral clusters, beyond which are six particles in a pentagonal pyramid, i.e. a Tammes n=10 cluster. Scale bars correspond to 0.5μm. Focus scans of the clusters in (a,d) are available as Supplementary Movies 6,7, respectively , found here.

After confocal image acquisition, the three-dimensional locations of the host/halo particles in each cluster are determined by manual centroiding, and the resulting xyz values are used to create solid and wireframe renderings of the cluster structure. Any cluster whose valency was unclear were not analyzed further. While we expect the clusters released from our two crystal structures to be predominantly of the $1 + 8$ and $1 + 12$ types, impurity atoms near the crystal surfaces or in disordered regions could be expected to have a different n ranging up to the maximum possible value of $n = 12$. Clusters containing more than one impurity particle, e.g. $2 + n$ clusters, will be counted in what follows to determine our cluster yields, but we will not consider their structures nor free energies here.

Notably, most of the clusters we observe have a form other than that expected from the local coordination in the host crystal. The observed states correspond to lower energy structures, leading us to conclude that clusters can structurally transform without the particles becoming unbound, presumably requiring the sliding or rolling of DNA-linked particle contacts. While the kinetics of such processes are not well understood, we conjecture that relative particle motion is possible in our system due to dynamic 'handshaking' of the DNA bridge complexes. The same DNA dynamics allows the clusters to slowly 'evaporate' by particle dissociation—the clusters are only metastable at low particle volume fraction. We expect that the rates of transformation, rolling and evaporation will all depend strongly on the difference between the observation temperature and the melting temperature

of the DNA bridging complexes. To slow evaporation and transformation as much as possible, we can add salt to increase the DNA bridge melting temperature, and minimize heating effects during imaging.

3.4.6 '1+12' Cluster Results

Clusters of the $1 + 12$ type, formed from sedimentation using the PP' system, predominantly produced well ordered icosahedral clusters, shown in Figure 3.5. While the other two cluster systems were randomly sampled, we were selective while imaging the PP' results, so the proportion of $1 + 12$ clusters is artificially inflated. As detailed in Table 3.2, roughly 85% of all imaged clusters formed in this system were icosahedra, with all of the exceptions being $1 + 11$ or $2 + n$ clusters. That is, all twelve of the $1 + 12$ clusters formed were icosahedra. The natural conclusion is that the cuboctohedral clusters released from the crystal rapidly transformed into the corresponding minimum free energy $n = 12$ Tammes cluster. A similar process, icosahedral twinning, is well known in atomic clusters [33].

Langevin Dynamics (LD) simulations of initially cuboctohedral $1 + 12$ clusters using realistic DNA potentials showed rapid transformation to icosahedra. A vibrational mode spectrum analysis shows the close packed cuboctohedron clusters to have predominantly rigid modes with a single soft mode. This soft mode corresponds to the simultaneous transformation of the clusters six square faces into sheared and bent parallelograms. Continuation along this pathway results in each

Table 3.4: ABB' BCC System: Cluster Statistics

Valence:	1+6	1+7	1+8	1+9	2+n
Number of Clusters	6	8	23	2	2
Percentage of Clusters	15%	20%	56%	5%	5%
Symmetry:		Number of Cubes:	13		
		Number of Skew Cubes:	5		
		Number of Gyrobifastigia:	2		
		Number of disordered:	3		

square face transforming into two triangular faces in the resulting icosahedron. Simple estimates of free solid angle suggest that the free energy difference between the cuboctahedron and icosahedron is tens of k_BT, due to the much higher configurational entropy of the floppy $1 + 12$ icosahedron (Tammes n=12) relative to the nearly rigid cuboctahedron. (The short range repulsions between the halo spheres contribute some enthalpy change to this free energy difference). In the 22 dimensional configuration space of 12 spheres pinned to a spherical surface (excluding rigid halo rotations), the cuboctahedron corresponds to single unstable saddlepoint which is an energy maximum along the cluster's single soft mode eigenvector, and a parabolic energy minimum in the other 21 directions. The zero eigenfrequency of the soft mode is due to the system energy being a quartic function of position along the transformation pathway.

To observe the pre-transformation cuboctohedral clusters, we sought to slow

the rate of transformation. Unfortunately, simply adding salt is not feasible for the complex PP' system, as increasing the salt also stabilizes undesirable DNA complexes that cause P particle aggregation. For this reason, we formed close-packed FCC crystals by centrifuging a suspension of A and B' particles in the ratio 399:1 at low salt, so no attractions would be present. When salt is added to the system, the only bonds which are present are $A - B'$ bonds. Unlike the PP' pellets, the AB' pellets are easily redispersed by gentle agitation, releasing the cuboctohedral clusters. This system allows enough salt to be added to raise the DNA bond melting temperature well above room temperature.

Upon confocal imaging, the more stable $1 + 12$ clusters released at high salt show a more complex result, Figure 3.6, with both icosahedral clusters as before and an unexpectedly high yield of $1 + 10$ clusters; statistics reported in Table 3.3. Neglecting various other outcomes, icosahedra now represent roughly two thirds (15/23) of the clusters, with 1+10 clusters providing one third (8/23), statistically inconsistent with the preceding PP' experiment that showed no $1 + 10$ clusters. This result is unexpected—in the PP' clusters the halo particles are less tightly bound and would be expected to 'evaporate' faster, yet we find far more missing halo particles from the more stable clusters.

We hypothesize that the unexpected outcome for stabilized 1+12 clusters results from frustrated transformation after binding to the glass coverslip. Specifically, if cuboctahedral clusters bind to the glass, they can do so by a vertex, an edge, or

via triangular or square faces. When only 1, 2 or 3 particles are pinned by surface binding, the other halo particles in the cluster can still rearrange via the previously described pathway, and the result is a complete icosahedron tethered to the glass. If a square face is pinned to the glass, however, then this relaxation pathway is blocked, trapping the cluster in a high free energy configuration. In this case, the most favourable mechanism for relaxation would be to eject particles until a low free energy structure that contains a square face is obtained. The first Tammes cluster with a square face is the $n = 10$ cluster that consists of a square of four spheres joined to a pentagonal pyramid (C_{2v} symmetry). Remarkably, four out of the eight $1 + 10$ clusters we observe correspond exactly to the $n = 10$ Tammes cluster, with their single square faces stuck to the glass, Figure 3.6d-f.

This frustrated transformation mechanism was replicated in simulation, where cuboctohedral clusters with a square face pinned repeatably ejected two particles and relaxed to an n=10 Tammes cluster. The rate for ejecting the first particle was roughly 50 times greater than the same process for an unpinned icosahedral cluster. The corresponding rate to eject two particles was roughly 6 times faster than for the icosahedron. In another simulation, cubocotohedra with pinned triangular faces readily relaxed to icosahedra without ejecting particles.

Additional evidence for this complex sequence of $1 + 12$ cluster transformations can be found by analyzing the separation of particles pinned to the glass. If the cluster binds the glass prior to transforming, the particle on the glass should be close

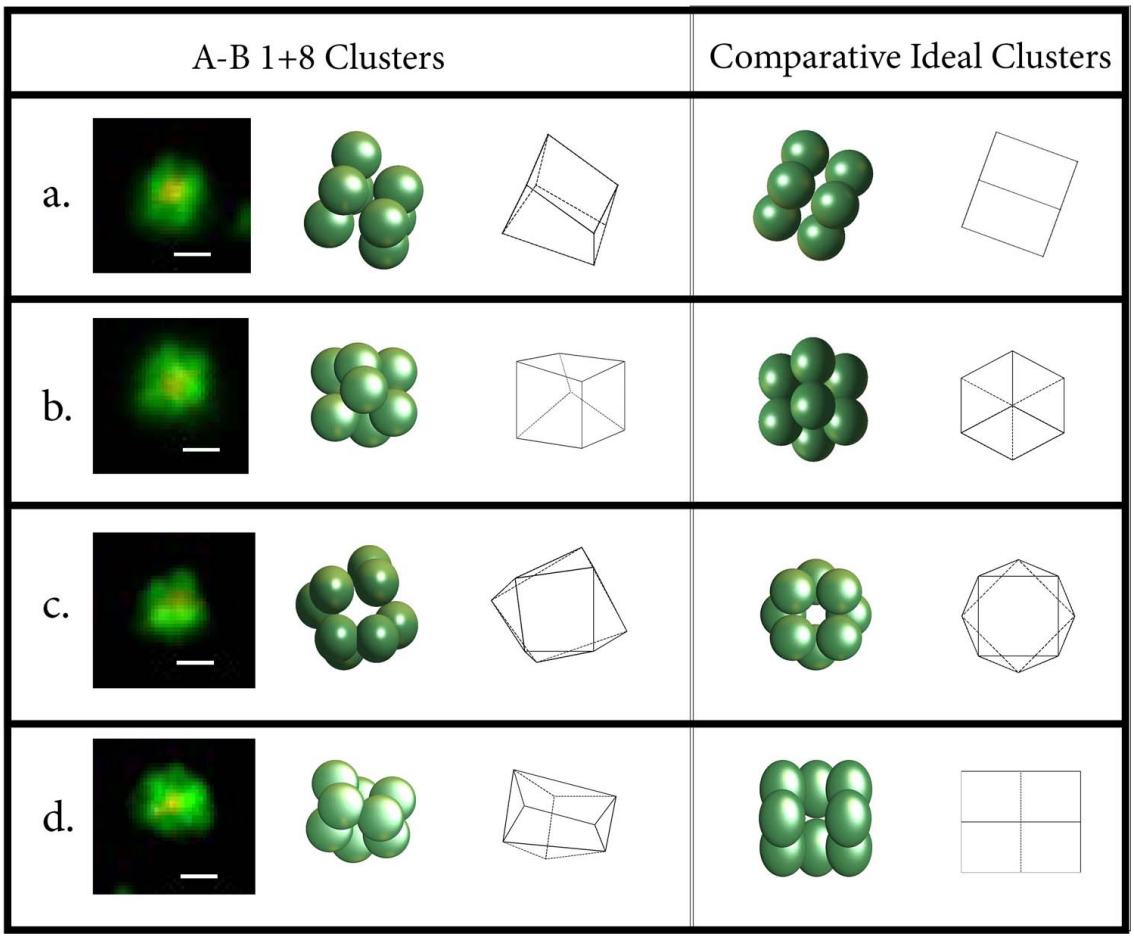

Figure 3.7: Representative clusters formed *via* BCC $A-B-B'$ crystals. Clusters shown are an edge-bound cube (a), a vertex-bound cube (b), a face-bound skew cube (c) and a gyrobifastigium (d). Scale bars correspond to 0.5μm. Focus scans of the clusters in (b,c) are available as Supplementary Movies 8,9, respectively[2].

packed. If the transformation occurs prior to glass binding, the particles should be separated by roughly 5% of a particle diameter (the spacing in a Tammes $n = 12$ icosahedron). A expected, the faster transforming PP' clusters show a significantly larger spacing between their adhered particles than the corresponding particles in AB' clusters, see Supplementary Figure 1, found here, for details.

3.4.7 '1+8' Cluster Results

Clusters released from homogeneously nucleated BCC/CsCl crystals showed a high incidence of $1 + 8$ clusters, >60% of non-conjoined clusters, statistics in Table 3.4. Most of the remaining clusters were $1 + 7$ and $1 + 6$ types presumably formed at crystal interfaces or in disordered regions. Two $1 + 9$ clusters suggest that halo particles can be inserted after cluster release, made plausible by the strong $A - B'$ attractive interactions in these systems and the large free solid angle available in low 'valence' clusters.

As with the $1 + 12$ clusters, we find that our initially cubical clusters relax towards lower free energy states over the duration of the experiment. Unlike the cubotohedral case, however, the free energy driving between the cube and skew cube is much lower, due to the fact that both have a large amount of free solid angle and correspondingly high configurational entropy. This greater configurational freedom suggests that the transformation has a more 'diffusive' character with the halo particles rolling diffusively over the center particle.

Of the 23 $1 + 8$ clusters examined, 13/23 maintained a roughly cubical orientation, and 5/23 resembled skew cubes, correspond to the Tammes $n = 8$ cluster. Of the remaining 5/23 $1 + 8$ clusters two have a gyrobifastigium structure (D_{2d} symmetry), and the remainder were disordered. It seems likely that the free energy difference between these these structures are rather small, and the barriers low enough to allow the clusters to interconvert among different morphologies. The ob-

servation of fewer skew cubes than cubes suggests that the transformation has not reached equilibrium at the time of observation presumably due to the low free energy driving. None of the skew cubes observed showed triangular faces stuck to the glass, suggesting that they transformed after deposition on the glass. Based on the degree of deformation, we estimate that the particles roll diffusively their own diameter in order 1000 seconds, indicating a diffusivity roughly 4 orders of magnitude slower than the particles free Brownian diffusivity. Reexamination of the clusters several hours later showed a significant amount of halo particle evaporation.

3.5 Conclusions

We have demonstrated the use of colloidal crystal templates and reprogrammable DNA interactions to form colloidal clusters with a variety of predictable structures. The symmetries of the clusters as formed, the cube or cuboctohedron, are determined by the nearest neighbor network within the host crystal, and are not the lowest free energy form for the released cluster. Clusters tend to evolve toward their minimum free energy Tammes clusters after annealing, so as to maximize the configurational entropy of the cluster's halo particles, while they are constrained to be bound to a core particle. We have demonstrated the formation of three such Tammes solution clusters, for n=8,10,12, as well as other forms via pathways summarized in Figure 8. For the icosahedral (n=12) case, the yield is exceptionally high.

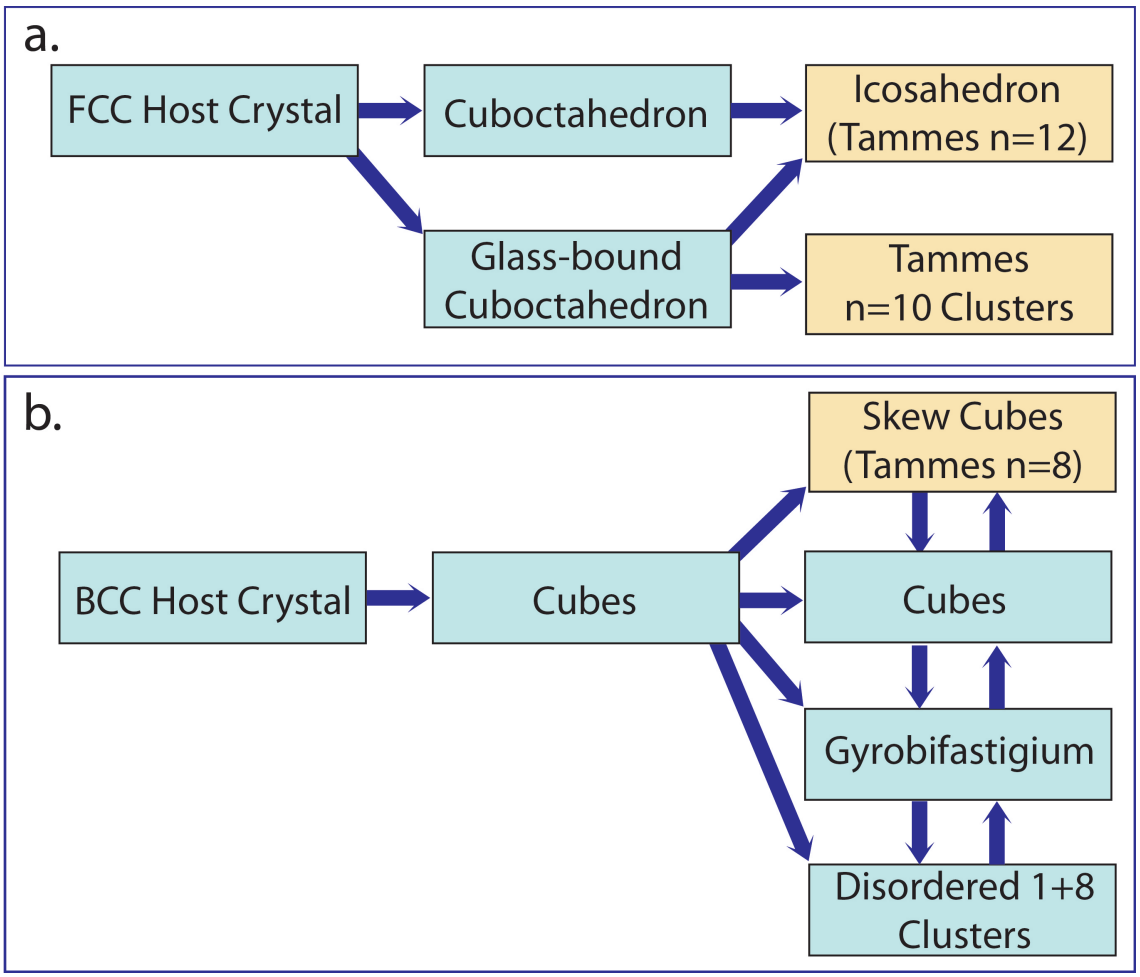

Figure 3.8: Diagram of cluster formations from the FCC systems (a), and BCC system (b). In the FCC system (a), cuboctahedral clusters are released from the host crystals, and rapidly transform into icosahedron. If the transformation is slowed by increasing the DNA interaction strength through salt addition, some cuboctahedra adhere to the coverslip glass. From there, if it is bound by 1,2, or 3 particles, it transforms easily into an icosahedron. However, if it is bound by 4 on its square face, it ejects two particles and transforms into a Tammes n=10 cluster. In the BCC system (b), cubical clusters are released from the host crystals. These cubes then slowly transform into other n=8 structures, though we believe they transform from one state to another readily due to low free energy barriers between states.

In future work, we will use covalent crosslinking to stabilize both the as formed and annealed polyhedral forms. We further anticipate that other crystal structures and different-sized binary suspensions will allow the extension of this work to other cluster symmetries at similarly high yield. We note that our process is readily scalable, and works with colloidal crystals formed by means other than DNA-directed assembly. Because the number of halo particles is set by the crystal symmetry, rather than Poisson statistics, our process results in very high yield into the expected halo particle valency. This in turn should facilitate the separation and purification of desirable clusters from mixtures containing other valancy (or free host particles). As previously illustrated in multiple experiments [34–38] and simulations [39] with non-spherical colloids, we expect cross-linked stable clusters with well defined symmetry to form interesting assemblies at a second hierarchical level, with potential applications for photonic metamaterials [40].

References

[1] Kun-Ta Wu, Lang Feng, Ruojie Sha, Rémi Dreyfus, Alexander Y. Grosberg, Nadrian C. Seeman, and Paul M. Chaikin. Polygamous particles. *Proceedings of the National Academy of Sciences*, 109(46):18731–18736, 2012.

[2] Yufeng Wang, Yu Wang, Dana R. Breed, Vinothan N. Manoharan, Lang Feng, Andrew D. Hollingsworth, Marcus Weck, and David J. Pine. Colloids with valence and specific directional bonding. *Nature*, 491(7422):51–55, 11 2012.

[3] Vinothan N. Manoharan, Mark T. Elsesser, and David J. Pine. Dense packing and symmetry in small clusters of microspheres. *Science*, 301(5632):483–487, 2003.

[4] Rebecca W. Perry, Guangnan Meng, Thomas G. Dimiduk, Jerome Fung, and Vinothan N. Manoharan. Real-space studies of the structure and dynamics of self-assembled colloidal clusters. *Faraday Discuss.*, 159:211–234, 2012.

[5] Guangnan Meng, Natalie Arkus, Michael P. Brenner, and Vinothan N. Manoharan. The free-energy landscape of clusters of attractive hard spheres. *Science*, 327(5965):560–563, 2010.

[6] N. Arkus, V. Manoharan, and M. Brenner. Deriving finite sphere packings. *SIAM Journal on Discrete Mathematics*, 25(4):1860–1901, 2011.

[7] Natalie Arkus, Vinothan N. Manoharan, and Michael P. Brenner. Minimal energy clusters of hard spheres with short range attractions. *Phys. Rev. Lett.*, 103:118303, Sep 2009.

[8] W. Benjamin Rogers and John C. Crocker. Direct measurements of DNA-mediated colloidal interactions and their quantitative modeling. *Proceedings of the National Academy of Sciences of the United States of America*, 108(38):15687–15692, SEP 20 2011.

[9] Mirjam E. Leunissen and Daan Frenkel. Numerical study of dna-functionalized microparticles and nanoparticles: Explicit pair potentials and their implications for phase behavior. *The Journal of Chemical Physics*, 134(8):084702, 2011.

[10] Bianca M. Mladek, Julia Fornleitner, Francisco J. Martinez-Veracoechea, Alexandre Dawid, and Daan Frenkel. Quantitative prediction of the phase diagram of dna-functionalized nanosized colloids. *Phys. Rev. Lett.*, 108:268301, Jun 2012.

[11] Robert J. Macfarlane, Byeongdu Lee, Matthew R. Jones, Nadine Harris, George C. Schatz, and Chad A. Mirkin. Nanoparticle superlattice engineering with dna. *Science*, 334(6053):204–208, 2011.

[12] Marie T. Casey, Raynaldo T. Scarlett, W. Benjamin Rogers, Ian Jenkins, Talid Sinno, and John C. Crocker. Driving diffusionless transformations in colloidal crystals using dna handshaking. *Nat Commun*, 3:1209, 11 2012.

[13] Paul L. Biancaniello, Anthony J. Kim, and John C. Crocker. Colloidal interactions and self-assembly using dna hybridization. *Phys. Rev. Lett.*, 94:058302, Feb 2005.

[14] Anthony J. Kim, Paul L. Biancaniello, and John C. Crocker. Engineering dna-mediated colloidal crystallization. *Langmuir*, 22(5):1991–2001, 2006.

[15] Sung Yong Park, Abigail K. R. Lytton-Jean, Byeongdu Lee, Steven Weigand, George C. Schatz, and Chad A. Mirkin. Dna-programmable nanoparticle crystallization. *Nature*, 451(7178):553–556, 01 2008.

[16] Dmytro Nykypanchuk, Mathew M. Maye, Daniel van der Lelie, and Oleg Gang. Dna-guided crystallization of colloidal nanoparticles. *Nature*, 451(7178):549–552, 01 2008.

[17] Raynaldo T. Scarlett, Marie T. Ung, John C. Crocker, and Talid Sinno. A mechanistic view of binary colloidal superlattice formation using dna-directed interactions. *Soft Matter*, 7:1912–1925, 2011.

[18] Mathew M. Maye, Mudalige Thilak Kumara, Dmytro Nykypanchuk, William B. Sherman, and Oleg Gang. Switching binary states of nanoparticle superlattices and dimer clusters by dna strands. *Nat Nano*, 5(2):116–120, 02 2010.

[19] Anthony J. Kim, Raynaldo Scarlett, Paul L. Biancaniello, Talid Sinno, and John C. Crocker. Probing interfacial equilibration in microsphere crystals formed by dna-directed assembly. *Nat Mater*, 8(1):52–55, 01 2009.

[20] Bryan A. Baker and Valeria T. Milam. Dna density-dependent assembly behavior of colloidal micelles. *Langmuir*, 26(12):9818–9826, 2010. PMID: 20349914.

[21] Christopher Kirby Tison and Valeria Tohver Milam. Programming the kinetics and extent of colloidal disassembly using a dna trigger. *Soft Matter*, 6:4446–4453, 2010.

[22] Christopher K. Tison and Valeria T. Milam. Reversing dna-mediated adhesion at a fixed temperature. *Langmuir*, 23(19):9728–9736, 2007.

[23] Carolyn L. Phillips, Eric Jankowski, Michelle Marval, and Sharon C. Glotzer. Self-assembled clusters of spheres related to spherical codes. *Phys. Rev. E*, 86:041124, Oct 2012.

[24] A.J. Kim, V.N. Manoharan, and J.C. Crocker. Swelling-based method for preparing stable, functionalized polymer colloids. *Journal of the American Chemical Society*, 127(6):1592–1593, 2005.

[25] John SantaLucia, Hatim T. Allawi, and P. Ananda Seneviratne. Improved nearest-neighbor parameters for predicting dna duplex stability. *Biochemistry*, 35(11):3555–3562, 1996.

[26] John SantaLucia and Donald Hicks. The thermodynamics of dna structural motifs. *Annual Review of Biophysics and Biomolecular Structure*, 33(1):415–440, 2004. PMID: 15139820.

[27] S Plimpton. Fast Parallel Algorithms for Short-range Molecular-dynamics. *Journal of Computational Physics*, 117(1):1–19, MAR 1 1995.

[28] J. F. Lutsko, D. Wolf, and S. Yip. Molecular dynamics calculation of free energy. *The Journal of Chemical Physics*, 88(10):6525–6528, 1988.

[29] William G. Hoover, Alan C. Hindmarsh, and Brad Lee Holian. Number dependence of small-crystal thermodynamic properties. i. *The Journal of Chemical Physics*, 57(5):1980–1985, 1972.

[30] Sahand Hormoz and Michael P. Brenner. Design principles for self-assembly with short-range interactions. *Proceedings of the National Academy of Sciences*, 2011.

[31] A. D. Dinsmore, A. G. Yodh, and D. J. Pine. Phase diagrams of nearly-hard-sphere binary colloids. *Phys. Rev. E*, 52:4045–4057, Oct 1995.

[32] E. K. Hobbie and M. J. Holter. Depletion-force kinetics in confined colloidal mixtures. *The Journal of Chemical Physics*, 108(6):2618–2621, 1998.

[33] L. L. Boyer and J. Q. Broughton. Statics and dynamics of icosahedrally twinned and single-crystal fcc clusters. *Phys. Rev. B*, 42:11461–11468, Dec 1990.

[34] Matthew R. Jones, Robert J. Macfarlane, Byeongdu Lee, Jian Zhang, Kaylie L. Young, Andrew J. Senesi, and Chad A. Mirkin. Dna-nanoparticle superlattices formed from anisotropic building blocks. *Nat Mater*, 9(11):913–917, 11 2010.

[35] Laura Rossi, Stefano Sacanna, William T. M. Irvine, Paul M. Chaikin, David J. Pine, and Albert P. Philipse. Cubic crystals from cubic colloids. *Soft Matter*, 7:4139–4142, 2011.

[36] Adeline Perro, Etienne Duguet, Olivier Lambert, Jean-Christophe Taveau, Elodie Bourgeat-Lami, and Serge Ravaine. A chemical synthetic route towards "colloidal molecules". *Angewandte Chemie International Edition*, 48(2):361–365, 2009.

[37] Amir Haji-Akbari, Michael Engel, Aaron S. Keys, Xiaoyu Zheng, Rolfe G. Petschek, Peter Palffy-Muhoray, and Sharon C. Glotzer. Disordered, quasicrystalline and crystalline phases of densely packed tetrahedra. *Nature*, 462(7274):773–777, 12 2009.

[38] Tie Wang, Xirui Wang, Derek LaMontagne, Zhongliang Wang, Zhongwu Wang, and Y. Charles Cao. Shape-controlled synthesis of colloidal superparticles from nanocubes. *Journal of the American Chemical Society*, 134(44):18225–18228, 2012.

[39] Pablo F. Damasceno, Michael Engel, and Sharon C. Glotzer. Predictive self-assembly of polyhedra into complex structures. *Science*, 337(6093):453–457, 2012.

[40] Sharon C. Glotzer and Michael J. Solomon. Anisotropy of building blocks and their assembly into complex structures. *Nat Mater*, 6(7):557–562, 08 2007.

Chapter 4

Crystal Templated Colloidal Clusters Exhibit Directional DNA Interactions

James T. McGinley, Yifan Wang, Ian Jenkins, Talid Sinno, and John C. Crocker. "Crystal Templated Colloidal Clusters Exhibit Directional DNA Interactions." Reproduced with permission from *ACS Nano*, submitted for publication. Unpublished work copyright 2015, American Chemical Society.

4.1 Abstract

Spherical colloids covered with grafted DNA have been used in the directed self-assembly of a number of distinct crystal and gel structures. Simulation suggests

that the use of anisotropic building blocks greatly augments the variety of potential colloidal assemblies that can be formed. Here, we form five distinct symmetries of colloidal clusters from DNA-functionalized spheres using a single type of colloidal crystal as a template. The crystals are formed by simple sedimentation of a binary mixture containing a majority 'host' species that forms close-packed crystals with the minority 'impurity' species occupying substitutional or interstitial defect sites. After the DNA strands between the two species are hybridized and enzymatically ligated, the results are colloidal clusters, one for each impurity particle, with a symmetry determined by the nearest neighbors in the original crystal template. By adjusting the size ratio of the two spheres and the timing of the ligation, we are able to generate clusters having the symmetry of tetrahedra, octahedra, cuboctahedra, triangular orthobicupola, and icosahedra, which can be readily separated from defective clusters and leftover spheres by centrifugation. We further demonstrate that these clusters, which are uniformly covered in DNA strands, display directional binding with spheres bearing complementary DNA strands, acting in a manner similar to patchy particles or proteins having multiple binding sites. The scalable nature of the fabrication process, along with the reprogrammability and directional nature of their resulting DNA interactions, makes these clusters suitable building blocks for use in further rounds of directed self-assembly.

4.2 Introduction

Transient bridges of DNA have been shown to be a versatile and effective driver of colloidal assembly. In particular, uniformly-labeled spherical particles have been used in the assembly of a variety of crystal structures [1–6]. Numerical simulations [7–12] predict that utilizing anisotropic building blocks, or ones that display direction bonding, would enable the generation of a larger variety of structures. Experimental methods for manufacturing building blocks have focused on patchy particles [13–16], non-spherical particles [17–24], and colloidal clusters [21, 25–33]. To date, however, reports using these building blocks to assemble large ordered structures, with a few notable exceptions [23, 34], remain scarce. Of particular importance are the variety of morphologies that a given method can produce, their directional interactions, the scalability of the process by which they are generated (both in terms of particle size and sample volume) as well as the ease with which defective particles can be removed by purification.

In this paper, we present a scalable, high-yield process for generating purified, stable clusters consisting of DNA-labeled colloidal spheres in specific symmetric arrangements, which display directional bonding characteristics. We use close-packed colloidal crystals formed simply by sedimentation to template clusters having five distinct symmetries. The crystals are formed from two particle species, with a majority 'host' species forming the crystal, and the minor 'impurity' species present as defects. After crystallization, permanent DNA bridges between the two species

are formed by enzymatic ligation, and the crystals are then melted and diluted by agitation. This process results in clusters consisting of a single impurity particle surrounded by n host particles, which we refer to as $1+n$ clusters. For same-sized host and impurity particles, the impurity particles form substitutional defects in the close-packed lattice, yielding 1+12 clusters. These are found to have three distinct configurations: cuboctahedra, triangular orthobicupola, and icosahedra, depending on the symmetry of the surrounding crystal and degree of cluster annealing. For host and impurity particles with size ratios of approximately 4:1 and 2:1, the impurity particles are present as interstitial defects occupying either the tetrahedral and octahedral interstitial sites, respectively, and form tetrahedral (1+4) and octahedral (1+6) cluster building blocks. Due to ligation, the clusters are stable, and can be reliably separated *via* sedimentation velocity in a density gradient. Relevant for future self-assembly experiments, we demonstrate that our clusters, despite being uniformly covered with DNA strands, display directional interactions during the binding of spheres containing complementary DNA strands. Specifically, we are able to reliably bind 20 spheres to specific sites on icosahedral clusters, hierarchically forming a well-ordered super-cluster. In principle, by expanding the number of crystal templates being used to include the wide variety of DNA-particle crystal structures formed in the literature [2, 6, 35], this process can be used to generate an enormous library of microscopic building blocks for future directed self-assembly processes.

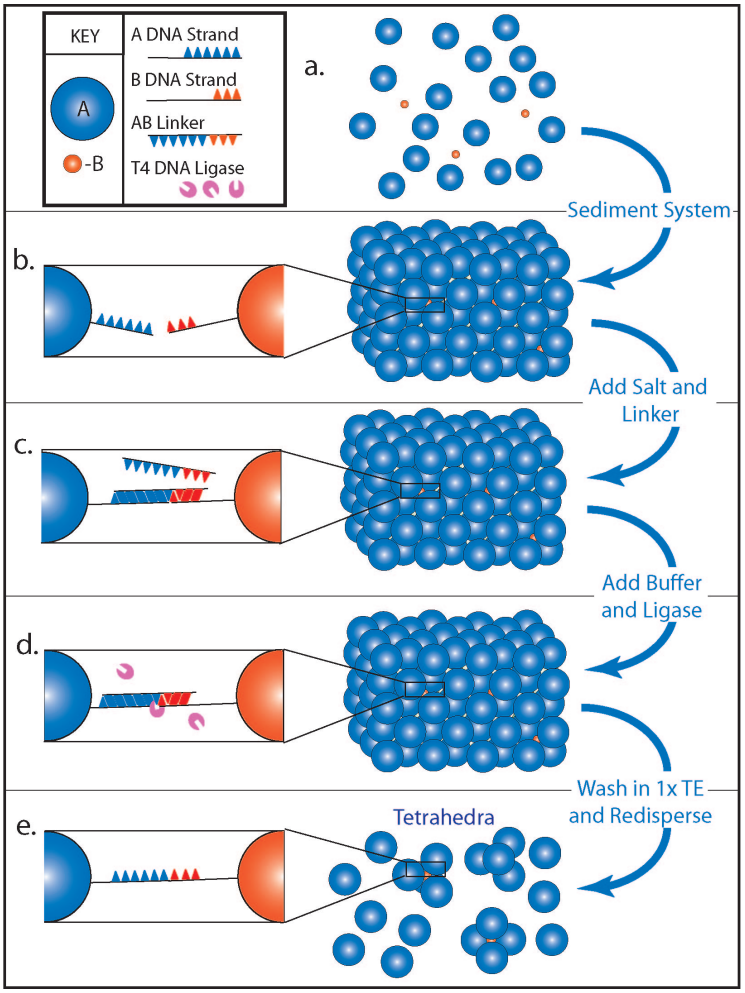

Figure 4.1: A system of two DNAylated particle species (A,B) is sedimented (a) to form large crystals with close-packed structures and interstitial impurities (b). A DNA linking strand is then added with salt (c) which links A particles to B. A ligase buffer and T4 DNA Ligase are then added to the system (d), which covalently link A-type DNA to B-type DNA, forming a single bridge between the particles. After redispersing and diluting the system, the only remaining bonds are A-B bonds, and their symmetry is defined by the crystalline template (e). These resulting clusters are stable, and can be further purified using a density gradient.

4.3 Materials and Methods

4.3.1 Particle Preparation

DNA-coated polymer microspheres of varying sizes were synthesized using a previously reported technique [3, 35–40]. Carboxylate-modified polystyrene microspheres of varying sizes were obtained from Seradyn Inc. DNA strands, obtained from IDT DNA, were then covalently coupled to Pluronic F108, obtained from BASF. The DNAylated Pluronic was then physically grafted to the surfaces of the microspheres by a swelling/deswelling technique previously developed in this lab [39]. Six types of particles were created for this paper, using four different sizes (381 nm, 291 nm, 200 nm and 106 nm), and two different DNA strand designs (A-type and B-type). Particles with sizes of $381nm$ and $291nm$ were grafted with A-type DNA, and were dyed with green Bodipy(R) Dye [4,4-difluoro-1,3,5,7,8-pentamethyl-4-bora-3a,4a-diaza-s-indacene] during the swelling/deswelling step. Particles with sizes of 381 nm, 200 nm, and 106 nm were grafted with B-type DNA, and were dyed with Red Bodipy(R) [4,4-Difluoro-5-(2-Thienyl)-4-Bora-3a,4a-Diaza-s-Indacene-3-Dodecanoic Acid]. Bodipy Dyes were obtained from Invitrogen, and were used in confocal imaging of the clusters.

4.3.2 Cluster Formation

The two-component systems were mixed together in a 1.5 mL Eppedorf tube at 1% v/v, with 399 μL of A-type particles and 1 μL of B-type particles. The systems were washed twice in DI water to remove any remaining 1xTE storage buffer. After the last wash, the total volume of the AB system was reduced to 28 μL. The systems were then mixed one last time, and then sedimented to form a close-packed crystal, with A particles comprising the host crystal, and B particles as rare impurities. NaCl was then added in two stages ($1M$ NaCl, 3 μL total) to obtain a concentration of approximately 100 mM. 1 μL of 100 mM linker strand was then added (at high excess), turning on the interactions between A and B particles. 4 μL of 10X Ligase Buffer, obtained from New England Biolabs, was then added. Immediately, 4 μ L of concentrated T4 DNA Ligase is added to the solution. The new mixture then sits at 20 degrees for at least a half hour (if the system is dispersed), but as long as overnight (if the system is in a crystalline pellet), after which it is diluted to a volume of 1.5 mL, and washed up to three times with 1xTE [41].

4.3.3 Purification

Purification was performed in either an 8 mL 3-9% w/w gradient, or in an 8 mL 3-6% w/w of Ficoll 400 (obtained from Sigma) in DI water, made using an Amersham Biosciences SG 15 Gradient Maker. A 10^{-4} volume fraction solution of clusters was made by diluting the ligated system with deionized water. 400 μL of this solution

was then placed atop the density gradient. Centrifugation at 3150 RCF for 25-75 minutes (depending on the size of the clusters) separates clusters into distinct purified bands. [31]. Each band is removed separately, so not only do we get purified resulting clusters, but we can also reuse the single particles from the top band in future cluster assemblies.

4.3.4 Confocal Microscopy

Imaging of glycerol-mounted fluorescently dyed particles was performed on an inverted Leica DM-IRB microscope with a 100x oil immersion lens equipped with a VTEye confocal, by Visitech. Z-stack scans were then taken, averaging 15 frames per slice to reduce noise. The red and green slices were merged to form a single image, after manually correcting for small optical offsets. These corrections were validated by control runs performed with beads dyed with both Bodipy(R) dyes.

4.3.5 SEM Imaging and Cluster Analysis

SEM Images were obtained using a JEOL 7500F HRSEM. Clusters are typically first purified using the above methods, and are then stuck to a positively-charged glass coverslip which has been functionalized with amino-silane. The immobilized samples are then washed with DI water to remove salt and any excess polymer remaining from the separation procedure. The washed samples are then washed with 10 mL of methanol, and dried under a vacuum. After the sample has been

dried, it is then sputter-coated with a 10nm layer of Au-Pd, and copper tape is used to attach the metal coating to an aluminum SEM stub in order to prevent charging issues during imaging. For some samples, a second sputter-coating , with the sample sitting at a 45° angle was necessary. Even with the care taken in preparation, approximately 50% of the clusters imaged were broken in some manner, though in most cases a starting structure could be determined. If a starting structure could not be determined, the cluster was excluded from the analysis.

It is also noted that after imaging methanol-dried samples under SEM, the particles become slightly deformed, and squish together. In order to verify that the slightly squished structures are truly representative, instead of washing in methanol, some samples were set in a film of DI water in the same manner, and then vitrified using liquid ethane. The vitrified glassy water was then sublimated in a freeze-drier, coated with Au-Pd, and imaged in the SEM. The structures were determined to be largely representative. A notable difference is seen by comparing the two bottom images in Figure 4.7b which were prepared using the methanol-drying method, to the top image in Figure 4.7b, which was prepared using vitrification. The methanol-dried samples appear to be more ideally aligned, which we believe is due to the surface forces encountered during the drying process.

4.4 Results and Discussion

We have previously shown [36] that crystal templates can be used to create short-lived and dynamic colloidal clusters, with a single initial symmetry determined by the template lattice. Here, we describe using a single type of colloidal crystal template to produce stable colloidal clusters having a number of distinct symmetries, using a modified process, shown in Figure 4.1, which will be detailed in the following sections. First, to make permanent DNA bridges between the clusters' particles, a new DNA bridge architecture was employed that can be enzymatically ligated. Second, we show that by varying the size ratio of host and impurity particles in the crystal template, five distinct cluster symmetries can be formed at high yield. These clusters can then be purified using density gradient centrifugation. Finally, it will be demonstrated that these clusters exhibit directional binding, effectively behaving as 'patchy particles' which may be suitable for future directed self-assembly experiments.

4.4.1 DNA Design for Ligatable System

A new linker-based DNA system was designed to interact with T4 DNA Ligase, which is a DNA-reactive enzyme that repairs double stranded DNA that contains a 'nick'—a single broken phosphodiester bond in the backbone [42]. It was therefore necessary to design the DNA sequences such that when bridges form between host

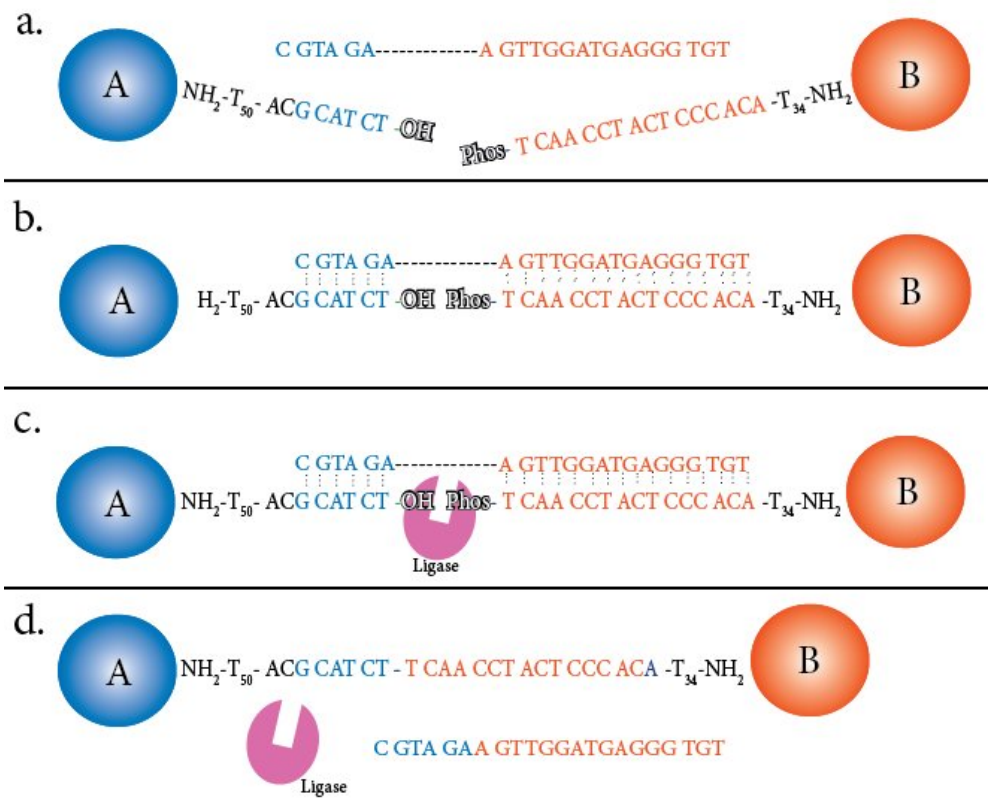

Figure 4.2: A system of two DNAylated particle species (A,B) and a linking strand is sedimented in low salt, with all DNA interactions turned off (a). Salt is then added (b) which links A particles to B *via* the linking strand. A ligase buffer and T4 DNA Ligase is then added to the system (c), which covalently links the 3' hydroxyl group on A-type DNA to the 5' Phosphate group on B-type DNA, forming a permanent bridge between the particles. After diluting the system (d), A and B particles remain held together by single-stranded bridges.

and impurity particles, they contain double-stranded DNA segments that contain such a nick, as shown in Figure 4.2. The design consists of three strands, one type grafted onto each particle type and a *Linker* strand. The strands coupled to the A particles have a terminal hydroxyl group at their free ends, while those on the B particles has a phosphate group at their free end (custom added by the manufacturer). The *Linker* strand hybridizes with the two particle strands, placing the phosphate group from B DNA immediately next to the hydroxyl group from A DNA. The action of T4 DNA Ligase is to form a covalent phosphodiester bond at the nick site, creating a continuous DNA bridge between the particles.

Notably, the nick site alters the thermodynamics of the A-*Linker*-B bridge formation, in ways that need to be accounted for carefully. [43, 44] Specifically, the stacking interactions of the hydrophobic bases adjacent to the nick stabilize the double stranded configuration. To compensate for this additional stability we reduce the $Linker - A$ DNA overlap domain to 5 bases. This reduction allows us to include the *Linker* at a high excess without saturating all tethered DNA strands with *Linker* strands, because at room temperature the *Linker* will only interact with the 5-base long region after first interacting with the 16-base long $Linker - B$ region, such that a nick site is present. This in turn increases the number of $A - B$ bonds formed, and thus increases the number of ligatable bridges.

T4 DNA Ligase with a PEG-free Ligase Buffer was found to be highly effective for the ligation of the DNA bridges. While some ligases can degrade DNA over time,

this system shows no such effects even after 12 hours, providing ample time for the enzyme to diffuse into even large crystals or pellets. Control trials revealed that this enzyme was also highly specific, with ligation only occuring in the presence of nick sites with added phosphate groups. We noted minimal nonspecific binding in the system, and a ligation yield consistent with other groups who have used enzymes in DNA-coated colloid systems [32, 45–48].

4.4.2 Colloidal Crystals as Cluster Templates

After host and impurity particles of a given size ratio have been labeled with the ligatable DNA strands, they are crystallized by simple sedimentation. The formation of DNA bridges is thermodynamically unfavorable at low salt concentration, providing a convenient methods for turning DNA-induced attractive interactions on and off. With no attractions, the particles assemble according to a hard-sphere crystallization process, which is expected to form a random hexagonal close-packed (RHCP) crystal, which has regions of both face-centered cubic (FCC) and hexagonal close-packed (HCP) order. Specifically, a 400 μL solution of A and B particles with a number density ratio of A:B : equal to 400:1 is prepared in deionized water with a volume fraction of 1% solids. The mixture is then sedimented in a bench top centrifuge overnight, which results in a pellet consisting of a close-packed crystal, with the A particles making up the host crystal lattice, and the B particles exist-

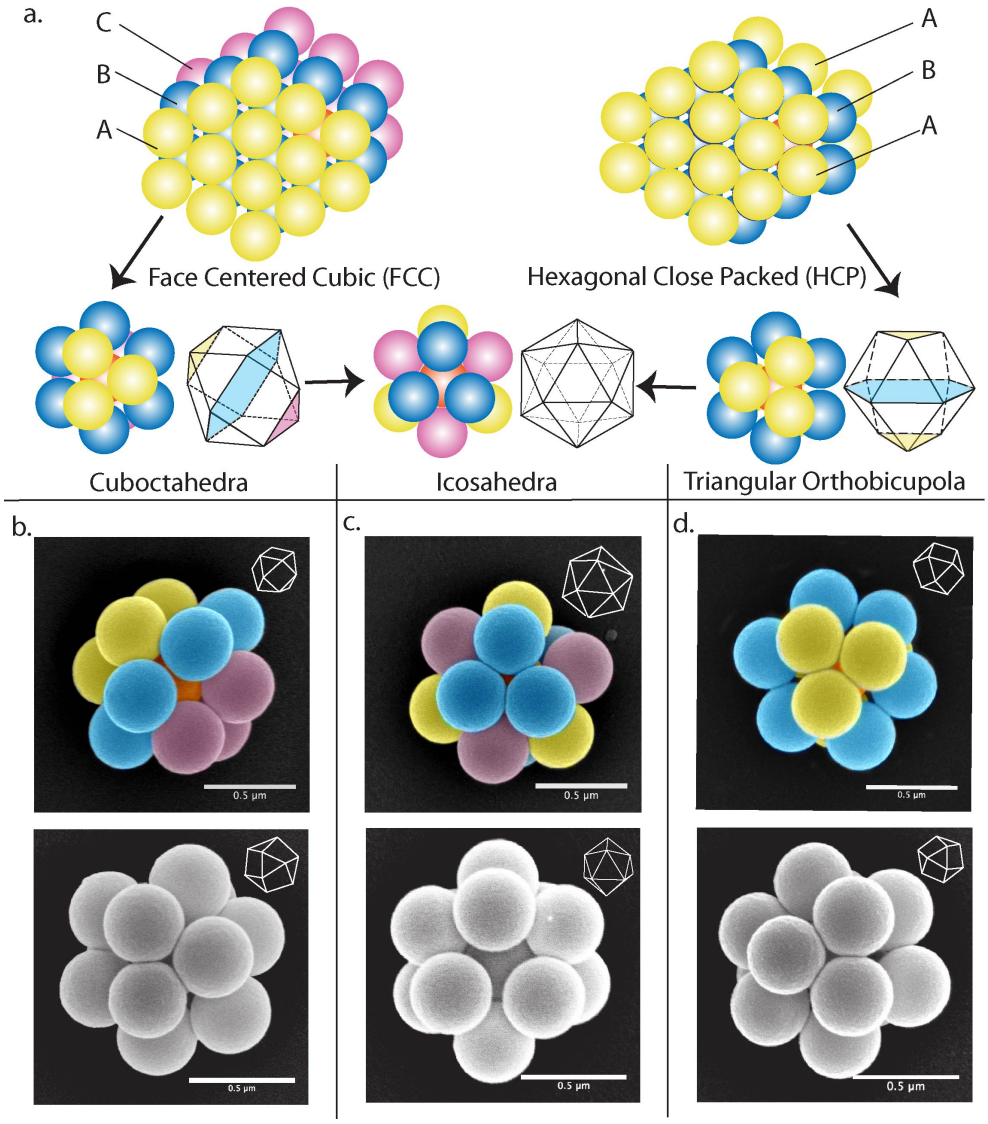

Figure 4.3: From crystals formed by hard-sphere sedimentation, with random hexagonal close-packed structure, we generate three distinct cluster symmetries: Cuboctahedra, Icosahedra, and Triangular Orthobicupola. (a) Cuboctahedra are a product of local face centered cubic (FCC) ordering, triangular orthobicupola are from local hexagonal close packed (HCP) ordering, and icosahedra are the transformed products of the previous two cluster symmetries. (b) A colored SEM image (top), demonstrates the three distinct planes which make up each cuboctahedral cluster, and a non-colored SEM image (bottom) is also provided. (c) A colored SEM image (top), demonstrates the four distinct planes which make up each icosahedral cluster, and a non-colored SEM image (bottom) is also provided. (d) A colored SEM image (top), demonstrates the two distinct planes which make up each cub octahedral cluster, and a non-colored SEM image (bottom) is also provided. Scale bars correspond to $0.5\mu m$.

ing as rare impurities. The size ratio of A particles to B particles determines the location of the impurities in the host lattice.

A particle size ratio of 1:1 leads the impurity particles to substitute randomly into the host lattice and results in 1+12 clusters, as shown in Figure 4.3. Based on an analysis of 27 purified clusters which were ligated while still embedded in the host crystal, a mixture of $\sim 1/2$ cuboctahedra, $\sim 1/6$ triangular orthobicupola, and $\sim 1/3$ icosahedra form. These clusters all contain the same number of particles, and so cannot be easily separated by one another using current separation techniques. The cuboctahedra and triangular orthobicupola correspond to the nearest-neighbor network of FCC and HCP crystals, respectively, shown in Figure 4.3a. Both cuboctahedra, Figure 4.3b, and triangular orthobicupola, Figure 4.3d, are close-packed configurations (the host spheres are all geometrically in contact), and thus have low configurational entropy. As we showed previously [36], the icosahedron is the lowest free energy form for a 1+12 cluster, providing an explanation for their unexpected presence, Figure 4.3c. At the base of the crystal pellet, pressure and particle density are highest due to the weight of the crystal particles above, and the particles are locked into their respective close-packed configurations until ligation takes place. However, nearer the top of the pellet the pressure and particle density are lower, and we suppose that the configurational entropy gained via transformation into icosahedra can outweigh the energetic penalty associated with accommodating the icosahedron into the host crystal.

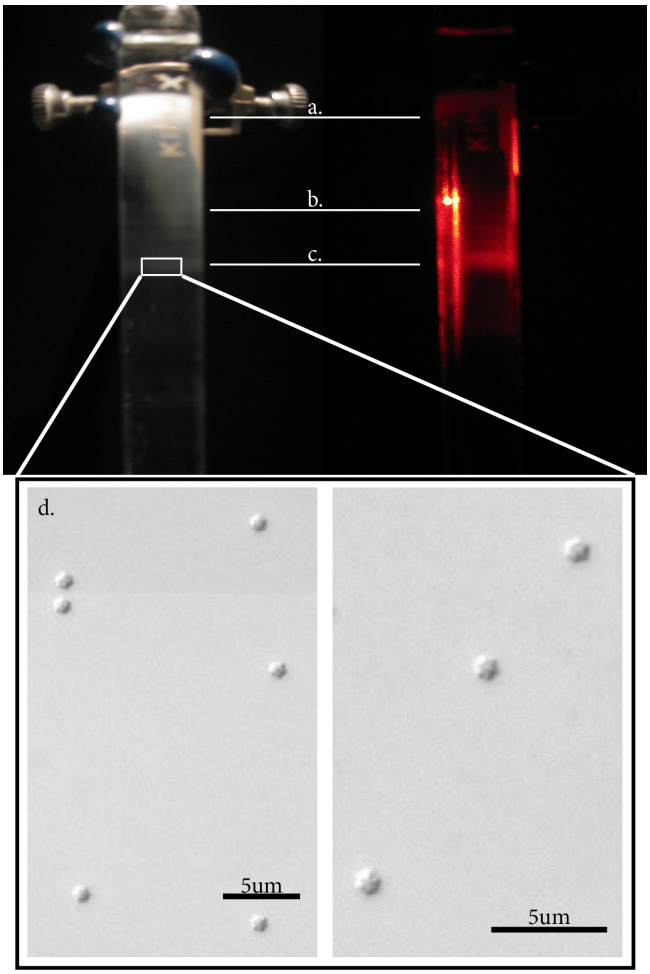

Figure 4.4: Density gradient fractionation of Icosahedral cluster system imaged with white light (left) and laser illumination (right). The single host particles can easily be removed from the top band (a), and a majority of deformed clusters, from '1+1' clusters to '1+11', can be removed from the various middle bands (b). The purified Icosahedral clusters are present with relatively high yield in the lowest band (c,d). Any larger aggregates, such as those with two impurity particles, will fall below this bottom bright band.

Cluster yields in different symmetries having the same 'valence,' where valence is defined as the number of host particles bound to a single impurity particle, were determined by counting in SEM images (after purification by valence using density gradient fractionation). Figure 4.4 illustrates the purification of a 1+12 cluster system. The thick band at the top of the column, Figure 4.4a contains single particles from the host lattice, the thin bands in the center, Figure 4.4b, are defective clusters, and the thick bottom band contains 1+12 clusters. The relative abundance of 1+12 clusters demonstrates that this valence has been effectively templated at high yield. Analysis of the bottom band yielded the aforementioned mixture of $\sim 1/2$ cuboctahedra, $\sim 1/6$ triangular orthobicupola, and $\sim 1/3$ icosahedra in the first case.

Smaller impurity particles can co-crystallize with the host particles by occupying interstitial sites. Because the two such sites within a close-packed lattice are the octahedral and tetrahedral interstitial sites, this results in clusters having octahedral or tetrahedral symmetries, respectively. Specifically, we find that size ratios of ∼5:2 and ∼4:1 lead to high yields of 1+6 (octahedral) and 1+4 (tetrahedral) clusters, respectively, shown in Figure 4.5. The ratios above are flexible, however; we find that size ratios of 2:1 and 3:1 for example, still respectively form 1+6 and 1+4 clusters, but with degraded angular order, presumably due to the lattice distortion from the overly large impurity particle. All resulting clusters, following their formation and ligation, can be stored for months at a time in DI water or 1xTE buffer, and are

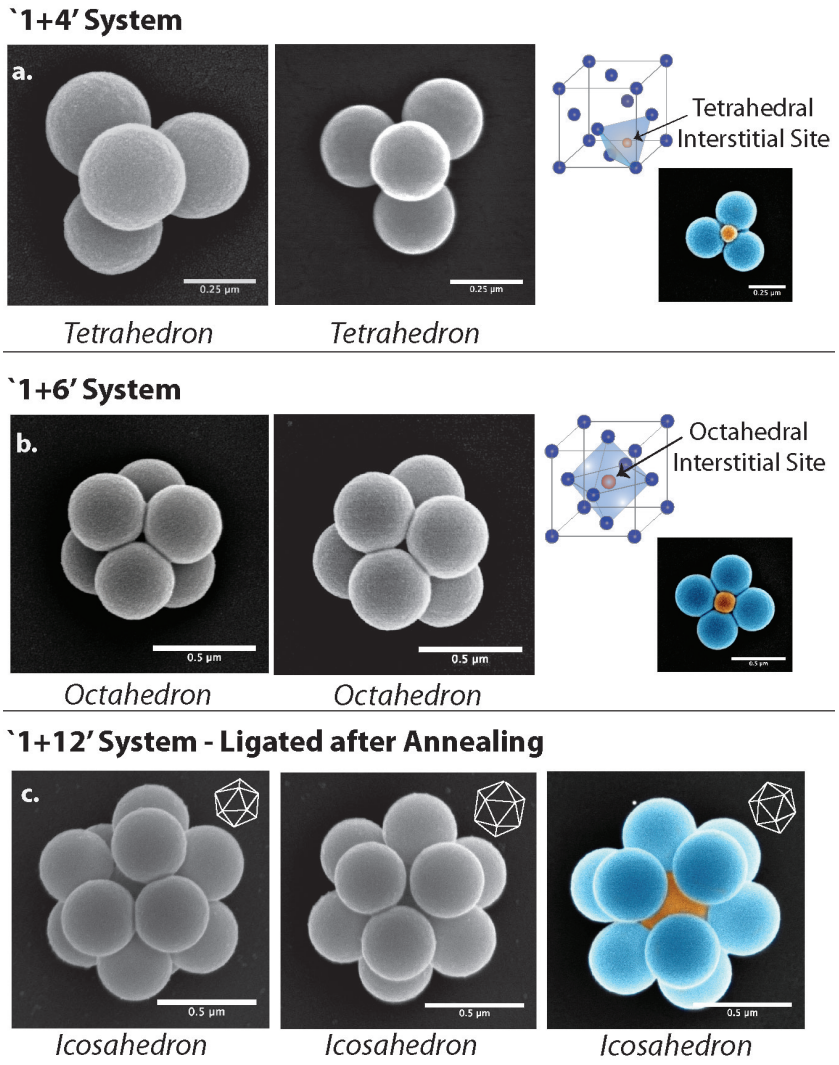

Figure 4.5: SEM images for the three systems which each target one particular cluster formation: Tetrahedral 1+4 System (a), Octahedral 1+6 System, and the Icosahedral 1+12 System (c). (a) Regular tetrahedral clusters (a, left) are generated at a size ratio of 4:1, while a mix of regular and irregular clusters (a, center) are generated at a size ratio of 3:1. The interactions between interstitial and impurity particles for the tetrahedral system are demonstrated by a unit cell rendering and a colored SEM image showing the host particles in blue and the impurity particle in orange(a, right). (c). Slightly irregular octahedral clusters (b, left, center) are generated at a size ratio of 2:1. The interactions between interstitial and impurity particles in the octahedral system are demonstrated by a unit cell rendering and a colored SEM image showing the host particles in blue and the impurity particle in orange (b, right). (c) When the 1:1 ratio system is freed from the pellet after the DNA interactions are turned on, but before ligation occurs, we note a 100% transformation of clusters from those orientations illustrated in Figure 4.3a,c to icosahedra. Scale bars correspond to $0.25\mu m$ for (a,b) and $0.50\mu m$ for (c).

stable enough to be purified and imaged in SEM, as seen in Figures 4.3 and 4.5.

As before, estimation of cluster yield in different symmetries is performed by fractionation in a density gradient. The clusters resulting from the bottommost band with ratios of 4:1 were almost completely regular tetrahedra, as seen in Figure 4.5a(left), and those formed using a ratio of 3:1 were a mix of irregular tetrahedra, Figure 4.5a(middle) (note the differing distances between the three surface-bound particles), and regular tetrahedra (not shown). For the 2:1 system, there were two large bands near the bottom, and analysis of these bands together demonstrated that 2/3 of clusters formed were octahedra, Figure 4.5b, while the remaining clusters were tetrahedra. While impurity particles at this size ratio should not fit into the tetrahedral interstitial sites of a close-packed crystal of spheres, as with the unexpected presence of icosahedra in the 1+12 system above, it appears that the host crystal can readily accommodate the needed lattice distortion.

If a suspension of pure icosahedral building blocks is desired, the process can be readily altered to create them. Our previous work [36] showed that transformation from cuboctahedra and triangular orthobicupola into icosahedra is fast and reproducible once the constraints of the template crystal are removed, and goes essentially to 100% completion. In this process, the pellet is gently resuspended after the salt and liner DNA are added, and the suspended clusters are allowed to anneal for 5 minutes at room temperature before being ligated. After purification and imaging, all 10 clusters observed by SEM were found to have transformed into

regular icosahedra, Figure 4.5c.

4.4.3 Clusters Display Directional Interactions

Non-spherical particles have been shown in simulation to assemble into a wide variety of surprisingly complex structures based solely on their shape. [11] Like hard spheres, in the high particle concentration limit, the densest packing structure results in the highest entropy, and lowest free energy. In contrast, atomic and molecular crystals often form a more open, less dense lattice structure due to the directional interactions afforded by their electronic structure. Recapitulating this physics at the particle level is the domain of 'patchy' particles, that have short-ranged attractive interactions only between small domains on their surfaces. [13–16]

We point out that our sphere clusters, despite being uniformly covered in DNA, also display strongly directional interactions with particles bearing complementary DNA strands. A second sphere bearing complementary DNA can simultaneously bind more than one of the clusters' spheres, with a total binding energy proportional to the number of contacts. As shown in Figure 4.6, the resulting 2-d energy surface contains a small binding site for every three particle 'hollow' on the clusters' surfaces. These are connected to linear two particle troughs that can funnel the spheres to the binding sites [49, 50], provided that the particles have been formulated [40] so as to allow surface rolling or translation [5, 35, 51, 52].

To demonstrate the effectiveness of our clusters' directional binding for forming

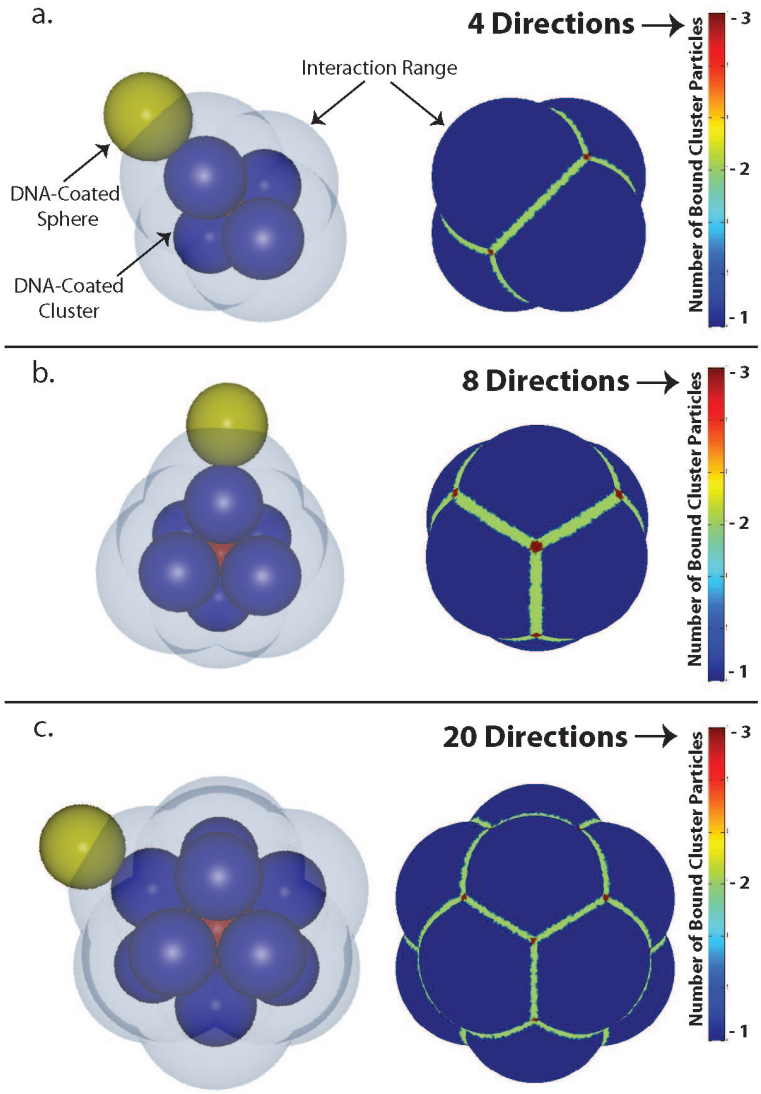

Figure 4.6: Colloidal clusters which are uniformly coated with DNA strands exhibit directional bonding based on the number of cluster particles in contact with a sphere that is uniformly coated with complimentary DNA strands. Here, cluster particles (in blue) bind with a complimentary sphere (in yellow) at a given interaction range (translucent shell). The number of directional bonds that the cluster will preferentially exhibit is given by the number of regions with the most bonds, and thus highest bonding potential, shown here in red. Tetrahedral clusters (a) should exhibit four binding directions, octahedral clusters (b) should exhibit eight binding directions, and icosahedral clusters (c) should exhibit 20 binding directions.

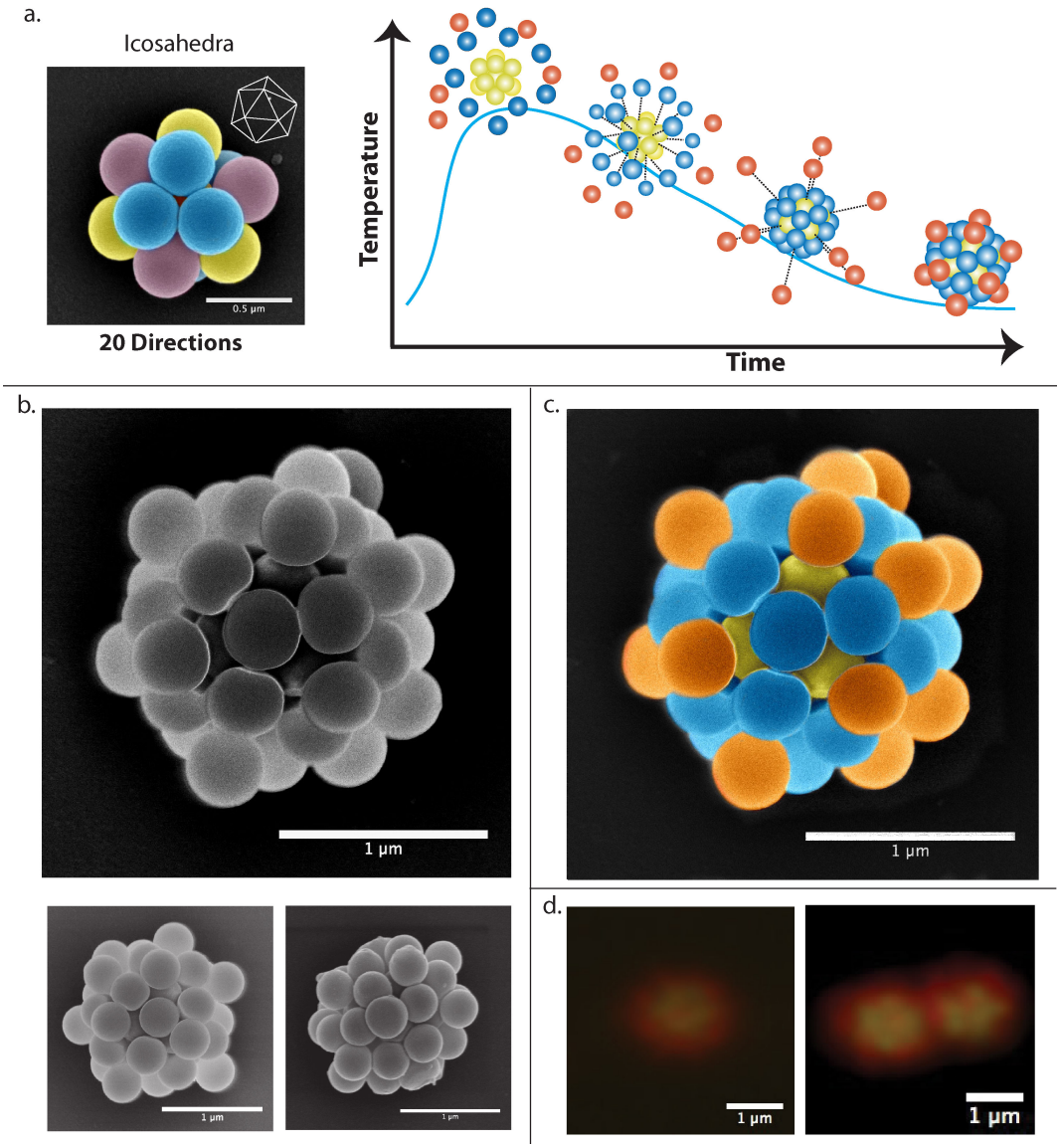

Figure 4.7: Annealing a system of pure icosahedra with an excess of complementary spheres (a), and further analysis using SEM (b,c) and confocal microscopy (d) demonstrates that colloidal clusters exhibit directional bonding. (b) SEM Images of decorated icosahedral clusters prepared using two methods: methanol drying (top) and ethane vitrification followed by sublimation (bottom two). More details of these drying methods can be found in Materials and Methods. (c) A colored SEM image of the methanol-dried cluster illustrates the original icosahedral cluster in yellow, surrounded by face-bound particles with dodecahedral symmetry in blue, and with vertex-bound particles shown in orange. (d) Confocal Images of a decorated Icosahedral cluster on its own as well as of two icosahedral clusters interacting *via* the decoration spheres, with red being the spheres used for decoration and green being the original 1+12 cluster.

ordered structures, we mix our 1+12 clusters with spheres bearing complementary DNA (in practice, they are identical to the original impurity particles). Specifically, we prepare the system with the secondary spheres in a large excess, and slowly reduce the temperature, causing the strength of DNA interactions to rise very gradually over time. This slow annealing should allow the system to reach the lowest energy state: each cluster with a single complementary sphere in each of its binding sites, Figure 4.7a. After reaching room temperature, more linker was added, and the system was ligated as before, in order to make the bonds permanent for SEM visualization. Figure 4.7b shows a high degree of capture efficiency of 381 nm complementary spheres in the clusters' 20 binding sites, shown in blue in Figure 4.7c , as well as the binding of 12 additional singly bound spheres, shown in orange in Figure 4.7c. The small size of the triple-contact binding site gives rise to the strong ordering of the 20 triple-contact spheres. In contrast, the ordering of the single-contact spheres depends on how the sample is prepared for imaging—rapid vitrification reveals the single bound spheres roll around their wide binding sites in equilibrium, while a simple drying preparation centers the particles, perhaps due to capillary forces (both methods are discussed in the Methods section).

Lastly, this work suggests the possibility of forming non-dense, three-dimensional assemblies consisting of clusters, either alone, or in binary combinations with complementary spheres. In the latter case, we envision spheres and clusters bearing complementary DNA occupying alternating sites in a binary lattice, but with a

preference for lattice symmetries compatible with cluster/sphere directional binding. Confocal images of our cluster experiments reveal numerous clusters pairs linked together through such intermediate spheres, Figure 4.7d, demonstrating the feasibility of such cluster-sphere-cluster binding and assembly.

4.5 Conclusions

Our crystal templating approach is scalable in two important ways: both in process scale and the size of the resulting building block clusters. As a three-dimensional method that does not rely upon two-dimensional templates, the process scale should be easy to scale up as needed. The clusters we report here range from ~ 0.6 μm for tetrahedra to ~ 1.1 μm for icosahedra with host spheres of 291 nm and 381 nm, respectively. We have reproduced these results using micron-sized particles and sedimented crystals as well (data not shown). The use of DNA interactions rather than sedimentation, as we previously reported [36], should enable similar templating methods to be applied to still smaller colloids and nanoparticles.

The methods outlined in this paper generate five distinct colloidal clusters from a single RHCP host lattice. More elaborate DNA designs using reprogrammable DNA interactions, such as were used in previous studies [6, 36, 53, 54], can be utilized in conjunction with T4 DNA ligase. In principle, combining ligatable DNA bridge architectures with the wide range of currently reported [2, 35] crystal structures for DNA-grafted particles should result in a significant library of different colloidal

cluster symmetries. In future work, we will use crystal templating methods to augment the library of available building blocks, and explore their utility for forming complex hierarchical assemblies and non-dense crystal lattices.

References

[1] CA Mirkin, RL Letsinger, RC Mucic, and JJ Storhoff. A dna-based method for rationally assembling nanoparticles into macroscopic materials. *Nature*, 382(6592):607–609, August 15 1996.

[2] Robert J. Macfarlane, Byeongdu Lee, Matthew R. Jones, Nadine Harris, George C. Schatz, and Chad A. Mirkin. Nanoparticle superlattice engineering with dna. *Science*, 334(6053):204–208, 2011.

[3] Paul L. Biancaniello, Anthony J. Kim, and John C. Crocker. Colloidal interactions and self-assembly using dna hybridization. *Phys. Rev. Lett.*, 94:058302, Feb 2005.

[4] Marek Grzelczak, Jan Vermant, Eric M. Furst, and Luis M. Liz-Marzán. Directed self-assembly of nanoparticles. *ACS Nano*, 4(7):3591–3605, 2010.

[5] Marie-Pierre Valignat, Olivier Theodoly, John C. Crocker, William B. Russel, and Paul M. Chaikin. Reversible self-assembly and directed assembly of dna-linked micrometer-sized colloids. *Proceedings of the National Academy of Sciences of the United States of America*, 102(12):4225–4229, 2005.

[6] W. Benjamin Rogers and Vinothan N. Manoharan. Programming colloidal phase transitions with DNA strand displacement. *SCIENCE*, 347(6222):639–642, FEB 6 2015.

[7] S. Torquato and Y. Jiao. Dense packings of the platonic and archimedean solids. *Nature*, 460(7257):876–879, 08 2009.

[8] Amir Haji-Akbari, Michael Engel, Aaron S. Keys, Xiaoyu Zheng, Rolfe G. Petschek, Peter Palffy-Muhoray, and Sharon C. Glotzer. Disordered, quasicrystalline and crystalline phases of densely packed tetrahedra. *Nature*, 462(7274):773–777, 12 2009.

[9] Matthew R. Jones, Robert J. Macfarlane, Byeongdu Lee, Jian Zhang, Kaylie L. Young, Andrew J. Senesi, and Chad A. Mirkin. Dna-nanoparticle superlattices formed from anisotropic building blocks. *Nat Mater*, 9(11):913–917, 11 2010.

[10] Sharon C. Glotzer. Nanotechnology: Shape matters. *Nature*, 481(7382):450–452, 01 2012.

[11] Pablo F Damasceno, Michael Engel, and Sharon C Glotzer. Predictive self-assembly of polyhedra into complex structures. *Science*, 337(6093):453–457, Jul 2012.

[12] G. Munao, D. Costa, F. Sciortino, and C. Caccamo. Simulation and theory of a model for tetrahedral colloidal particles. *Journal of Chemical Physics*, 134(19), May 21 2011.

[13] Charles E. Snyder, Allison M. Yake, Jason D. Feick, and Darrell Velegol. Nanoscale functionalization and site-specific assembly of colloids by particle lithography. *Langmuir*, 21(11):4813–4815, 2005. PMID: 15896017.

[14] Huda A. Jerri, Rachel A. Dutter, and Darrell Velegol. Fabrication of stable anisotropic microcapsules. *Soft Matter*, 5:827–834, 2009.

[15] Yufeng Wang, Yu Wang, Dana R. Breed, Vinothan N. Manoharan, Lang Feng, Andrew D. Hollingsworth, Marcus Weck, and David J. Pine. Colloids with valence and specific directional bonding. *Nature*, 491(7422):51–55, 11 2012.

[16] Yufeng Wang, Andrew D. Hollingsworth, Si Kyung Yang, Sonal Patel, David J. Pine, and Marcus Weck. Patchy particle self-assembly via metal coordination. *Journal of the American Chemical Society*, 135(38):14064–14067, 2013.

[17] Zhong Lin Wang and Xiangdong Feng. Polyhedral shapes of ceo2 nanoparticles. *The Journal of Physical Chemistry B*, 107(49):13563–13566, 2003.

[18] Tie Wang, Xirui Wang, Derek LaMontagne, Zhongliang Wang, Zhongwu Wang, and Y. Charles Cao. Shape-controlled synthesis of colloidal superparticles from nanocubes. *Journal of the American Chemical Society*, 134(44):18225–18228, 2012.

[19] Stefano Sacanna, David J. Pine, and Gi-Ra Yi. Engineering shape: the novel geometries of colloidal self-assembly. *Soft Matter*, 9:8096–8106, 2013.

[20] Laura Rossi, Stefano Sacanna, William T. M. Irvine, Paul M. Chaikin, David J. Pine, and Albert P. Philipse. Cubic crystals from cubic colloids. *Soft Matter*, 7:4139–4142, 2011.

[21] S. Sacanna, W. T. M. Irvine, P. M. Chaikin, and D. J. Pine. Lock and key colloids. *Nature*, 464(7288):575–578, 03 2010.

[22] Stefano Sacanna, Mark Korpics, Kelvin Rodriguez, Laura ColÃn-MelÃ©ndez, Seung-Hyun Kim, David J. Pine, and Gi-Ra Yi. Shaping colloids for self-assembly. *Nat Commun*, 4:1688, 04 2013.

[23] Fang Lu, Kevin G. Yager, Yugang Zhang, Huolin Xin, and Oleg Gang. Superlattices assembled through shape-induced directional binding. *Nat Commun*, 6, 04 2015.

[24] Clayton P. Lapointe, Thomas G. Mason, and Ivan I. Smalyukh. Shape-controlled colloidal interactions in nematic liquid crystals. *Science*, 326(5956):1083–1086, 2009.

[25] Vinothan N. Manoharan. Colloidal spheres confined by liquid droplets: Geometry, physics, and physical chemistry. *Solid State Communications*, 139(11-12):557–561, 2006.

[26] Yufeng Wang, Yu Wang, Dana R. Breed, Vinothan N. Manoharan, Lang Feng, Andrew D. Hollingsworth, Marcus Weck, and David J. Pine. Colloids with valence and specific directional bonding. *Nature*, 491(7422):51–U61, NOV 1 2012.

[27] Nicholas A. Licata and Alexei V. Tkachenko. Errorproof programmable self-assembly of dna-nanoparticle clusters. *Phys. Rev. E*, 74:041406, Oct 2006.

[28] Kun-Ta Wu, Lang Feng, Ruojie Sha, Rémi Dreyfus, Alexander Y. Grosberg, Nadrian C. Seeman, and Paul M. Chaikin. Polygamous particles. *Proceedings of the National Academy of Sciences*, 109(46):18731–18736, 2012.

[29] Carolyn L. Phillips, Eric Jankowski, Michelle Marval, and Sharon C. Glotzer. Self-assembled clusters of spheres related to spherical codes. *Physical Review E*, 86(4, 1), OCT 15 2012.

[30] Nicholas B. Schade, Miranda C. Holmes-Cerfon, Elizabeth R. Chen, Dina Aronzon, Jesse W. Collins, Jonathan A. Fan, Federico Capasso, and Vinothan N. Manoharan. Tetrahedral Colloidal Clusters from Random Parking of Bidisperse Spheres. *Physical Review Letters*, 110(14), APR 4 2013.

[31] Guangnan Meng, Natalie Arkus, Michael P. Brenner, and Vinothan N. Manoharan. The Free-Energy Landscape of Clusters of Attractive Hard Spheres. *Science*, 327(5965):560–563, January 29 2010.

[32] Shelley A. Claridge, Alexander J. Mastroianni, Yeung B. Au, Huiyang W. Liang, Christine M. Micheel, Jean M. J. Fréchet, and A. Paul Alivisatos. Enzymatic ligation creates discrete multinanoparticle building blocks for self-assembly. *Journal of the American Chemical Society*, 130(29):9598–9605, 2008. PMID: 18588300.

[33] Shelley A. Claridge, A. W. Castleman, Shiv N. Khanna, Christopher B. Murray, Ayusman Sen, and Paul S. Weiss. Cluster-assembled materials. *ACS Nano*, 3(2):244–255, 2009. PMID: 19236057.

[34] Weigang Lu, Qingsheng Liu, Zhaoyong Sun, Jibao He, Chidi Ezeolu, and Jiye Fang. Super crystal structures of octahedral c-in2o3 nanocrystals. *Journal of the American Chemical Society*, 130(22):6983–6991, 2008.

[35] Marie T. Casey, Raynaldo T. Scarlett, W. Benjamin Rogers, Ian Jenkins, Talid Sinno, and John C. Crocker. Driving diffusionless transformations in colloidal crystals using DNA handshaking. *Nature Communications*, 3, November 2012.

[36] James T. McGinley, Ian Jenkins, Talid Sinno, and John C. Crocker. Assembling colloidal clusters using crystalline templates and reprogrammable DNA interactions. *Soft Matter*, 9(38):9119–9128, 2013.

[37] W. Benjamin Rogers, Talid Sinno, and John C. Crocker. Kinetics and non-exponential binding of DNA-coated colloids. *Soft Matter*, 9(28):6412–6417, 2013.

[38] W. Benjamin Rogers and John C. Crocker. Direct measurements of DNA-mediated colloidal interactions and their quantitative modeling. *Proceedings of the National Academy of Sciences of the United States of America*, 108(38):15687–15692, SEP 20 2011.

[39] A.J. Kim, V.N. Manoharan, and J.C. Crocker. Swelling-based method for preparing stable, functionalized polymer colloids. *Journal of the American Chemical Society*, 127(6):1592–1593, 2005.

[40] Anthony J. Kim, Paul L. Biancaniello, and John C. Crocker. Engineering dna-mediated colloidal crystallization. *Langmuir*, 22(5):1991–2001, 2006.

[41] Xiaoyang Xu, Nathaniel L. Rosi, Yuhuang Wang, Fengwei Huo, and Chad A. Mirkin. Asymmetric functionalization of gold nanoparticles with oligonucleotides. *Journal of the American Chemical Society*, 128(29):9286–9287, JUL 26 2006.

[42] AV Cherepanov and S de Vries. Kinetics and thermodynamics of nick sealing by T4 DNA ligase. *European Journal of Biochemistry*, 270(21):4315–4325, NOV 2003.

[43] MJ Lane, T Paner, I Kashin, BD Faldasz, B Li, FJ Gallo, and AS Benight. The thermodynamic advantage of DNA oligonucleotide ''stacking hybridization' reactions: Energetics of a DNA nick. *Nucleic Acids Research*, 25(3):611–616, February 1 1997.

[44] E Protozanova, P Yakovchuk, and MD Frank-Kamenetskii. Stacked-unstacked equilibrium at the nick site of DNA. *Journal of Molecular Biology*, 342(3):775–785, September 17 2004.

[45] AntoniosG. Kanaras, Zhenxin Wang, Irshad Hussain, Mathias Brust, Richard Cosstick, and Andrew D. Bates. Site-specific ligation of dna-modified gold nanoparticles activated by the restriction enzyme styi. *Small*, 3(1):67–70, 2007.

[46] AntoniosG. Kanaras, Zhenxin Wang, Mathias Brust, Richard Cosstick, and AndrewD. Bates. Enzymatic disassembly of dna–gold nanostructures. *Small*, 3(4):590–594, 2007.

[47] Sheila R. Nicewarner Peña, Surabhi Raina, Glenn P. Goodrich, Nina V. Fedoroff, and Christine D. Keating. Hybridization and enzymatic extension of au nanoparticle-bound oligonucleotides. *Journal of the American Chemical Society*, 124(25):7314–7323, 2002. PMID: 12071740.

[48] Antonios G. Kanaras, Zhenxin Wang, Andrew D. Bates, Richard Cosstick, and Mathias Brust. Towards multistep nanostructure synthesis: Programmed enzymatic self-assembly of dna/gold systems. *Angewandte Chemie International Edition*, 42(2):191–194, 2003.

[49] Raynaldo T. Scarlett, Marie T. Ung, John C. Crocker, and Talid Sinno. A mechanistic view of binary colloidal superlattice formation using dna-directed interactions. *Soft Matter*, 7:1912–1925, 2011.

[50] Anthony J. Kim, Raynaldo Scarlett, Paul L. Biancaniello, Talid Sinno, and John C. Crocker. Probing interfacial equilibration in microsphere crystals formed by dna-directed assembly. *Nat Mater*, 8(1):52–55, 01 2009.

[51] Ian C. Jenkins, Marie T. Casey, James T. McGinley, John C. Crocker, and Talid Sinno. Hydrodynamics selects the pathway for displacive transformations in dna-linked colloidal crystallites. *Proceedings of the National Academy of Sciences*, 111(13):4803–4808, 2014.

[52] Rémi Dreyfus, Mirjam E. Leunissen, Roujie Sha, Alexei Tkachenko, Nadrian C. Seeman, David J. Pine, and Paul M. Chaikin. Aggregation-disaggregation transition of dna-coated colloids: Experiments and theory. *Phys. Rev. E*, 81:041404, Apr 2010.

[53] Christopher K. Tison and Valeria T. Milam. Reversing dna-mediated adhesion at a fixed temperature. *Langmuir*, 23(19):9728–9736, 2007.

[54] Christopher Kirby Tison and Valeria Tohver Milam. Programming the kinetics and extent of colloidal disassembly using a dna trigger. *Soft Matter*, 6:4446–4453, 2010.

Chapter 5

Generation of Patchy Particles *via* Point-of-Contact Templating

5.1 Abstract

Isotropically-interacting DNA-coated colloidal microspheres have been shown to be extremely versatile and highly programmable building blocks in the field of directed self-assembly. Large assemblies using these building blocks are currently limited to close-packed (or near-close-packed) colloidal crystals and amorphous gel structures. Here, we explore a process for the generation of spherical building blocks with anisotropic interactions, which simulations suggest have rich phase diagrams. In the process explained here, homogeneously nucleated colloidal crystals and gels, comprised of two interacting particle species of different sizes, A and B, are used as

template structures for the production of patchy DNA-coated particles. After the template structures are formed, soluble DNA strands are added to the system which interact with the A-type DNA strands, and are then covalently linked *via* ligation to the tail end of the B-type DNA strands *only* at the points of contact between the two species of particles. These DNA extensions, because they only occur at the points of contact between the two species, form well-defined patches on the surface of the colloidal particles. Due to the differing sizes of the particle species, they are effectively separated using a density gradient. These patchy spheres can potentially be used as anisotropic building blocks, with interactions governed by the newly-added DNA extensions.

5.2 Introduction

DNA interactions have been effective drivers of isotropically-interacting colloids, and form a wide variety of colloidal assemblies. Simulations have shown that patchy particles can vastly increase the variety of structures currently generated from colloidal systems with such short-range interactions [1–7]. While many phase diagrams of such systems have been created that highlight the potentially rich phase behavior of patchy particle systems [4, 8–10], no experimental realizations of crystals formed such particles have been published.

Several groups have been working to engineer methods of patchy particle production [11–17]. One method currently in use in the Pine lab uses rigid colloidal clusters

as seeds for patchy particle generation [11, 12, 15–17]. The particles generated using this method are not exceptionally spherical, but the patches on the surface have distinct DNA sequences, and have been shown to drive small assemblies resembling molecules. The Chaikin group has come up with another method, which utilized a gold surface functionalized with double-stranded DNA, and Biotin-Streptavidin interactions between one of those two strands and a colloidal microsphere to template janus-type DNA-patchy particles [14].

Another notable technique for generating patchy particles was developed in the Mirkin Group in 2006 [18], and is similar to the process proposed here. By using T4 DNA Ligase, they were able to extend DNA strands at the points of contact between two particles, though the patchy particles generated using this method did not have ordered patch orientations, and were not shown to be effective building blocks for large, ordered structures.

Here, we present an exceptionally scalable method, illustrated in Figure 5.1, for generating colloids with multiple patches using colloidal crystals and gels as templates. First, a binary colloidal system comprised of two complementary particles, A and B, forms aggregates or crystals, driven by attractive $A - B$ DNA interactions. After the initial aggregation, an *Extension* strand is added to the system, which binds to a recognition domain on Particle A's DNA strands, immediately adjacent to Particle B's DNA strands at all points of $A - B$ contact. An enzyme called T4 DNA Ligase is then added, which covalently links the *Extension* strands

to Particle B's DNA strands at the points-of-contact between A and B particles, thus selectively extending the DNA sequences of Particle B in those domains. After melting the system, the *Patchy B* particles are then easily separated from the *A* particles using a density gradient. Theoretically, we can produce high yields of such purified patchy particles with symmetries that are defined by the host template, which can then be used as anisotropic building blocks in future colloidal assemblies.

5.3 Materials and Methods

5.3.1 Particle Synthesis

Polymer microspheres of varying sizes were functionalized with single stranded DNA molecules using a previously reported technique [19–25]. Carboxylate-modified polystyrene microspheres of varying sizes were obtained from Seradyn Inc. DNA strands, obtained from IDT DNA, were then covalently coupled to Pluronic F108, obtained from BASF. The DNAylated Pluronic was then physically grafted to the surfaces of the microspheres by a swelling/deswelling technique previously developed in this lab [24]. Six types of particles were created for this paper, using four different sizes (381 nm, 424 nm, 531 nm and 1000 nm), and two different DNA strand designs (A-type and B-type). Particles with sizes of $381nm$ and $1000nm$ were grafted with A-type DNA, and were dyed with green Bodipy(R) Dye [4,4-difluoro-1,3,5,7,8-pentamethyl-4-bora-3a,4a-diaza-s-indacene] during the swelling/deswelling step.

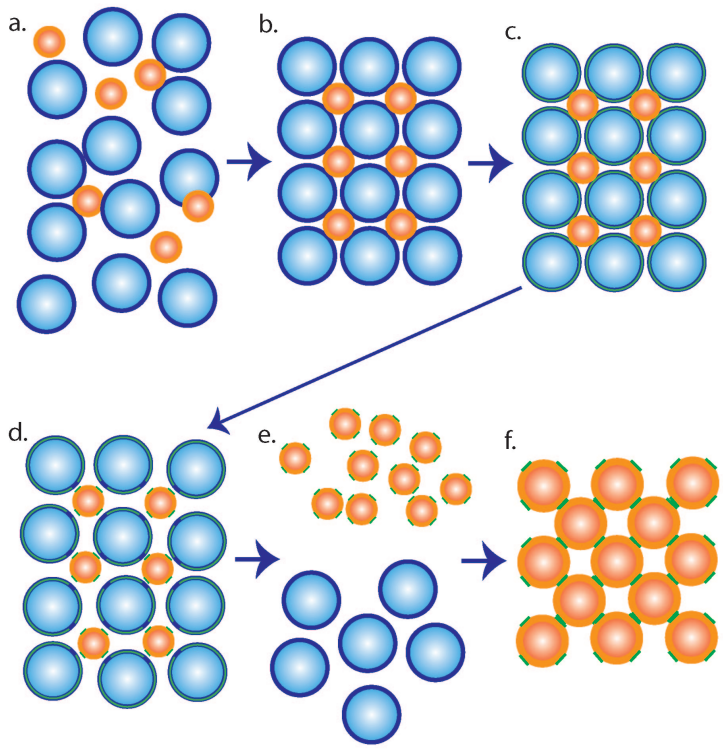

Figure 5.1: Schematic for the generation of patchy particles *via* point-of-contact templating. First, a binary system of DNA-coated A (orange) and B (blue) particles with a size ratio not equal to 1:1 is thermally quenched (a) to form aggregates or crystals (b) due to attractive $A-B$ DNA interactions. After the initial aggregation, a phosphate-group-terminated DNA *Extension* strand (shown in green) is added to the system, which binds to a recognition domain on Particle A's DNA strands, immediately adjacent to Particle B's DNA strands. An enzyme called T4 DNA Ligase is then added, which covalently links the *Extension* strands to Particle B's DNA strands at the points-of-contact between A and B particles, thus selectively extending the DNA sequences of Particle B in those domains (c). The system is then diluted, and a *Kickoff* strand is added which melts the $A-B$ bonds (d). Due to the different-sized particles, separation is easily achieved by sedimentation velocity (e). After purification, the now-patchy B particles can interact with one another *via* their patchy domains (f).

Particles with sizes of 424 nm and 531 nm were grafted with B-type DNA, and were dyed with Red Bodipy(R) [4,4-Difluoro-5-(2-Thienyl)-4-Bora-3a,4a-Diaza-s-Indacene-3-Dodecanoic Acid]. Bodipy Dyes were obtained from Invitrogen, and were used in fluorescence imaging of the clusters.

5.3.2 Homogeneous Colloidal Crystallization

Two component body-centered-cubic (BCC) crystals are formed of A particles that interact selectively with B particles. The B particles were designed to interact with A *via* a 7-base overlap sequence. The melting temperatures of AB aggregates are determined at 100 mM NaCl. BCC crystals of A and B are then formed by homogeneous nucleation at a 20% total particle volume fraction in 100 mM NaCl pH=8 1xTE buffer. 10 μl samples are sealed in 300 μl microcentrifuge tubes and submerged in a water bath in an insulated cooler. The initial temperature of the bath is 55°C and cools to room temperature at a rate of 0.3 degrees per hour.

5.3.3 Extending Bridges using Ligation

After the system of A and B particles are aggregated, or crystallized using the method above, a phosphorylated *Extension* strand is added to the system, which interacts with the A-type DNA, and sits immediately adjacent to the end of the B-type DNA strands. 10x Ligase Buffer and T4DNA Ligase are then added to the system according to the instructions given by the source. The system is allowed

to sit at room temperature for at least 15 minutes, but for as long as 12 hours, during which time the *Extension* strand is covalently attached to any *B*-type DNA strands, see the Results and Discussion for details on the DNA designs. After ligation occurs, a kickoff strand which is complementary to *A*-type DNA is added to the system, and the system is heated to at least 40°C to permanently melt the aggregates or crystals. The system is then washed with DI water 5 times at a 10:1 excess, and is then purified using a density gradient.

5.3.4 Purification by Particle Size *via* Sedimentation Velocity

Purification was performed in either an 8 mL 3-9% w/w gradient, or in an 8 mL 3-6% w/w of Ficoll 400 (obtained from Sigma) in DI water, made using an Amersham Biosciences SG 15 Gradient Maker. A 10^{-4} volume fraction solution of particles was made by diluting the ligated, melted, and washed system with deionized water. 400 μL of this solution was then placed atop the density gradient. Centrifugation at 3150 RCF for 25-99 minutes (depending on the size of the particles) separates particles into distinct purified bands. [26].

5.3.5 Patch Hybridization with Gold Nanoparticles

Gold Nanoparticles functionalized with thiolated single-stranded DNA sequences were prepared using a previously reported technique [27]. The DNA sequences are

designed to be complementary to the interaction domain on the Patchy B particles (fully complimentary to the ligated *Extension* strand). A purified sample of Patchy B particles is prepared using the method above, and a high molar excess of gold nanoparticles is added to the solution at 300 mM NaCl. The solution is brought to 80°C and allowed to slowly quench, letting the gold nanoparticles effectively hybridize.

5.3.6 SEM Sample Preparation

SEM Images were obtained using a JEOL 7500F HRSEM. All gold nanoparticle-hybridized samples were stuck to positively charged glass coverslips. Some samples were first washed with Ethanol to remove salt and residual Ficoll 400, and then by Methanol, followed by drying according to the method outlined in Chapter Two. The ethanol also collapses the DNA bridges between the gold nanoparticles and the polystyrene spheres, locking them in place. Other samples were first washed by 1M Ammonium Acetate (a volatile salt) in water to remove NaCl and residual Ficoll 400, and were then dried by simple evaporation under vacuum. The ammonium acetate salt preserves the DNA bonds during evaporation, and, as a volatile salt, evaporates without leaving residual salt crystals.

5.4 Results and Discussion

The methods outlined in Chapters Three and Four effectively demonstrate that crystal templates and ligation are effective at driving stable targeted assemblies. Here, we describe a modified process which, instead of creating colloidal clusters, creates spheres with patches of distinct DNA strands whose orientations are theoretically determined by the nearest-neighbor contacts within the host template. First, we will describe the new DNA architecture necessary for this modified system, and will demonstrate that this architecture can be effectively used to drive the assembly of crystal templates. Unfortunately, due to insufficient purification, the results from the crystal templating experiments were inconclusive, so we then outline a process of generating patchy particles by using a colloidal gel as a template, and we give this process the more general term: 'point-of-contact templating.' Finally, we describe methods for estimating the size of the resulting patches, and present and analyze SEM images of the resulting patchy particles.

5.4.1 DNA Design and Validation

A new DNA architecture was developed for this system, illustrated in Figure 5.2. The design is a modification of the ligatable system presented in Chapter Four which, instead of forging permanent bonds between neighboring A and B particles *via* Ligation, instead forges permanent bonds between B DNA strands and an adjacent *Extension* strand. The design is composed of three strands (though a fourth

Kickoff strand was implemented in practice), and is accomplished by implementing a multi-step process. First, A and B DNA strands hybridize with one another in the presence of salt with no linker. Then, a phosphorylated *Extension* strand is added to the system, which hybridizes with the A DNA strands, and forms a 'nick' site, described in Chapter Four, with all B strands which are in contact with A strands. T4 DNA Ligase is then added along with a special Ligase Buffer, and it covalently links the phosphate group at the end of the *Extension* strands to the hydroxyl groups on the abutting B strands.

The first step in assessing the viability of this system was to ensure that it effectively generates the proper host templates. Gels were readily generated using a system of 1000 nm A particles and 531 nm B particles, by a fast quench at room temperature (data not shown). Impressively, Figure 5.3 shows that a system of 381 nm A particles and 424 B particles effectively nucleate and grow, forming a body-centered-cubic crystal structure. Furthermore, after adding the *Extension* strands, Ligase Buffer, and T4 DNA Ligase, the structures of both systems are maintained. In both cases, a *Kickoff* strand that is complementary to A-type DNA was added at high excess to lower the system's melting temperature, and the temperatures of the systems were increased above 70°C to melt the respective systems (the presence of the *Kickoff* strands effectively prevents re-aggregation). The systems were immediately washed five times in DI water, and were then purified, as outlined in the Materials and Methods section.

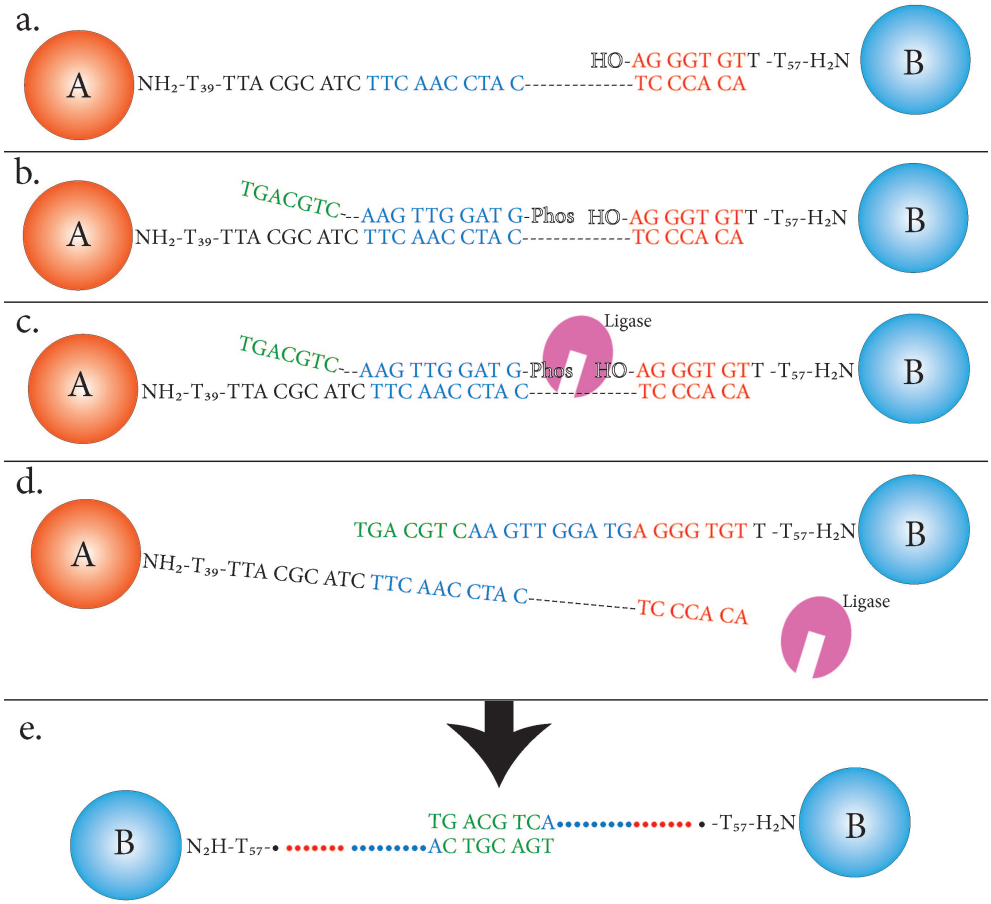

Figure 5.2: A system of two DNAylated particle species (A,B) are allowed to react in the presence of salt such that the two particles are linked by a seven-base DNA interaction (a). Next, a phosphorylated *Extension* strand is then added to the system, which interacts with particle As DNA, and sits immediately adjacent to the tail end of particle B's DNA (b). A ligase buffer and T4 DNA Ligase are then added to the system (c), which covalently link the 3' hydroxyl groups on B-type DNA strands to the 5' Phosphate group on the *Extension* strands, forming a permanent extension to all B DNA strands that are hybridized with A strands. After diluting the system (d), The A particles are left unchanged, while the B particles have well-defined patches of covalently linked *Extension* DNA strands on their surfaces. After purification, B strands can be reacted with one another (e) *via* their patches due to the palindromic domain at the end of the *Extension* strands.

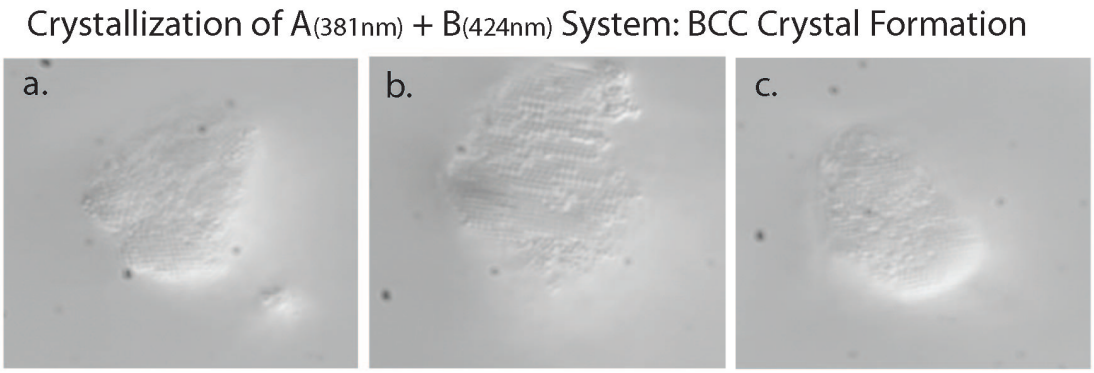

Figure 5.3: Body-centered-cubic colloidal crystals are effectively driven by the A and B DNA strands functionalized to 381 nm and 424 nm spheres, respectively. The white light DIC microscopy images (a-c) clearly show crystalline order. Patchy spheres using these templates are expected to exhibit cubic orientation.

5.4.2 Patchy Particles from Binary Crystals and Gels

Unfortunately, while the binary system presented above crystallizes well, the 10% size difference was not a sufficient enough difference to drive an effective separation *via* sedimentation velocity, as shown in Figure 5.4a, even when centrifuged in the gradient for 99 minutes. There is clearly a small delineation between the upper and lower bands, but because they are so close together, and because *Patchy B* particles were in the band below the A particles, removing the band resulted in significant contamination, as seen in the fluorescent images at the bottom of Figure 5.4.

Therefore, as a proof of concept, the binary gel system comprised of 1000 nm A particles and 531 nm B particles was synthesized. The separation in this case was extremely significant, Figure 5.4b. No contamination was seen, due to the much larger 2:1 size difference and the fact that the *Patchy B* particles are smaller, and

thus are all in the top band. Furthermore, the *Patchy B* particles generated using this system were aggregated in 200 mM NaCl in 1xTE using the palindromic sequence at the tail end of the *Extension*, demonstrating that the ligation was successful, though this data is insufficient to validate the formation of distinct patches.

5.4.3 Patch Size Estimation and Control

Before ascertaining whether the ligated *Extension* strands form the expected patches on the surface of the *Patchy B* particles, a means of estimating an expected patch size is needed. Figure 5.5 illustrates one method for determining the upper bound for patch sizes in a given system. The method makes some large simplifications, such as assuming that the two particles are in direct contact, and assuming that the outer limits of the patch are determined by the total contour length of the hybridized DNA bridges. Due to these simplifications, this analysis overestimates the expected patch size, but it is sufficient enough to use as a means of identifying whether the patches are generated by point-of-contact templates. Furthermore, Figure 5.5 illustrates a convenient means of controlling the patch size by varying the length of the DNA strands. Using this simplified analysis, it appears that doubling the contour length of the DNA strands will generate a larger patch area, so we hypothesize that by increasing or decreasing the length of the DNA strands, we can exercise control over the patch size, which is crucial for controlled self-assembly applications.

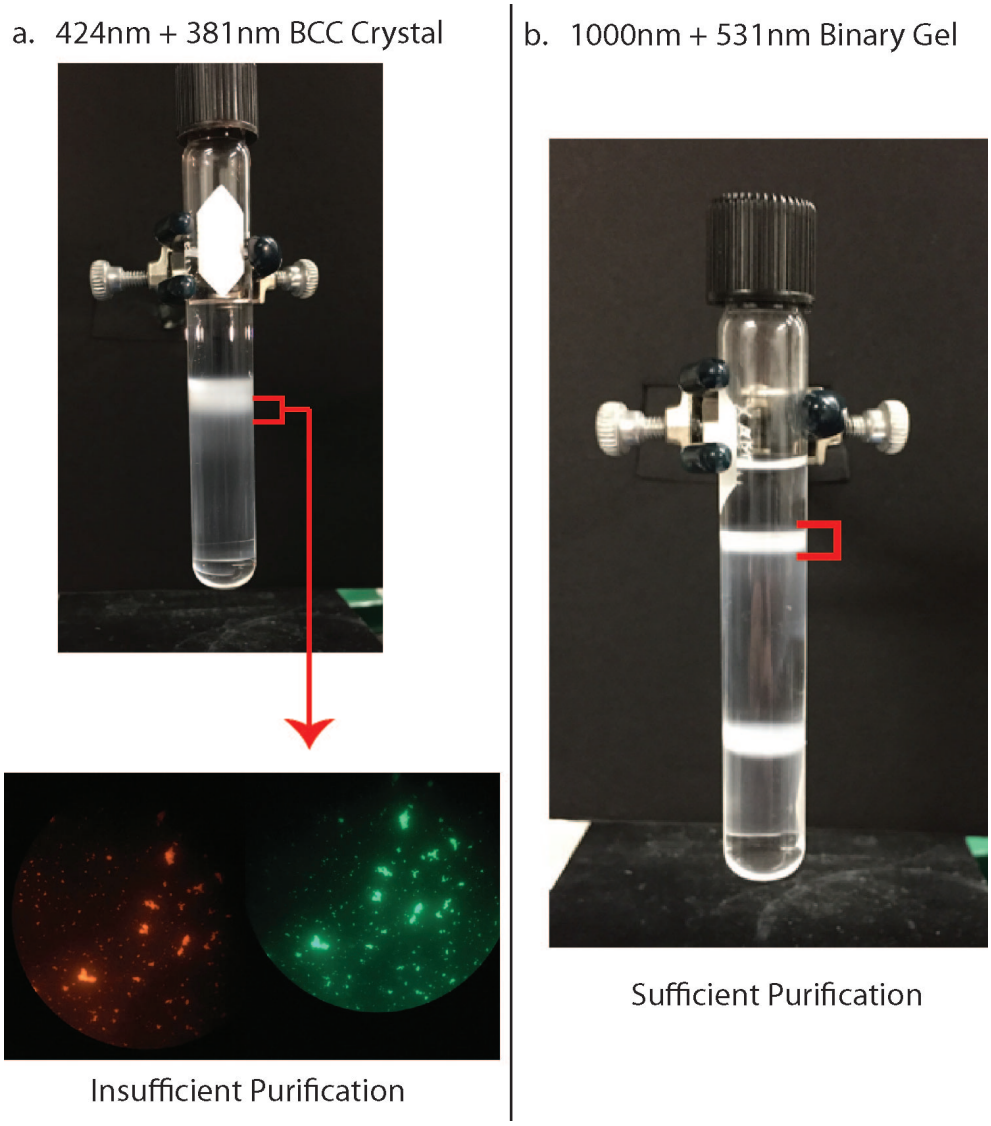

Figure 5.4: Using a 10% difference in particle diameters was not sufficient, and designing the system such that the patchy particles were the bottom band was not ideal for preventing contamination, as seen in the fluorescent images above where A particles have been dyed with a red fluorescent dye, and B particles have been dyed with a green fluorescent dye (a). A 2:1 size ratio system performs much better, especially when the patchy spheres are the top band (b). Contamination was not seen, and the resulting particles were effectively aggregated *via* patch-patch interactions (data not shown).

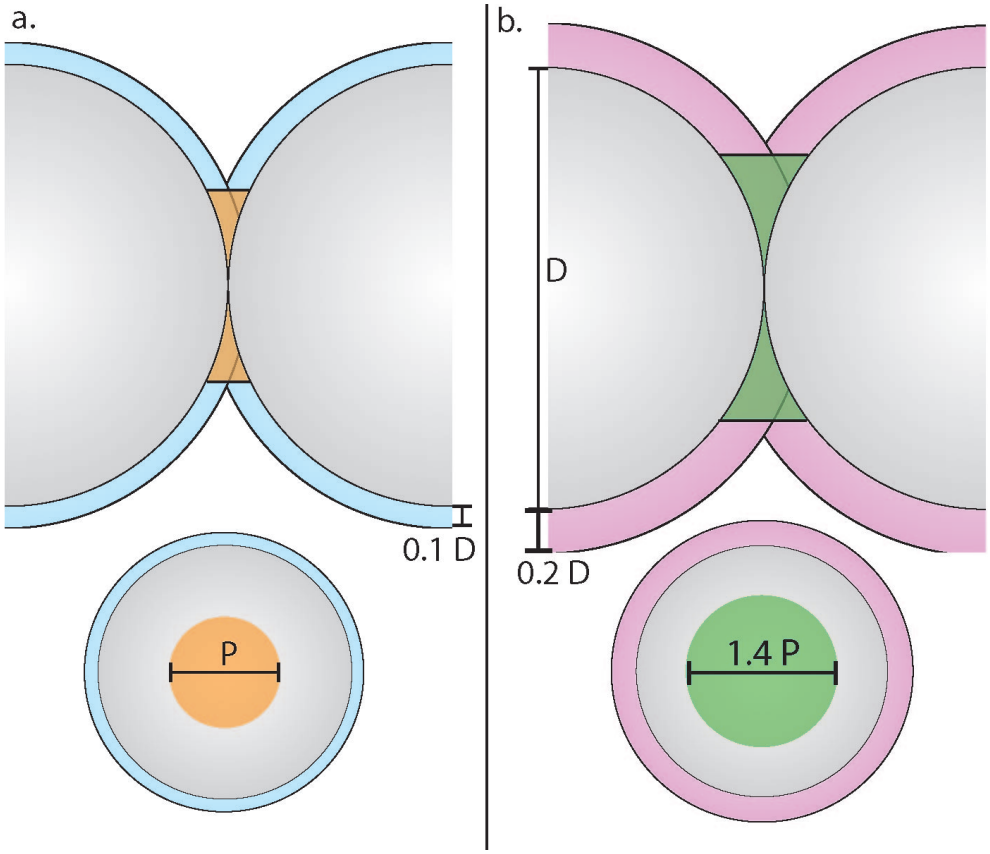

Figure 5.5: A simple schematic for understanding the maximum attainable patch size and control between two particles of the same size. The patch size seems to be somewhat sensitive to the contour length of the DNA strands used in the system. For the case where the DNA contour length is 10% of the particle diameter (a), a patch roughly 44% of the particle's diameter is formed. However, doubling the contour length of the DNA sequences yields a patch with a diameter of roughly 59% of the particle's diameter, which is a sub-linear gain. This depiction is simple, and should only be thought of as a means of estimating an upper bound on the patch size.

After purifying *Patchy B* particles from the binary gel system, the patchy spheres are then incubated with a high excess of functionalized gold nanoparticles whose DNA brushes are complementary to the *Extension* DNA within the patches, according to the protocol outlined in the Materials and Methods section. These *Patchy B*-Gold Nanoparticle aggregates are then prepared for SEM imaging using two methods: a wash with 1M Ammonium Acetate, and sequential washes with Ethanol and Methanol, as outlined above and in Chapter Two. Three of colored SEM Images of the resulting patchy particles are shown in Figure 5.6b-d. Based on an analysis of six such patchy particles, the patch diameters are roughly 230 - 260 nm. This is promising, as using the above method, the upper bound of the resulting patch size for a binary gel system comprised of 1000 nm A particles and 531 nm B particles was determined to be 313nm, Figure 5.6a. While a careful examination of the SEM images shows that the nominally 531 nm spheres are in fact closer to 450 nm, which will change the calculated maximum slightly, it is still clear that the patches seen here are well within the expected range. Furthermore, the circular structure of the patches, and their sizes, demonstrate that these patches were generated at the points of contact between A and B particles.

Notably, The structure of these patches is unexpected - the hybridized gold nanoparticles form a sparsely populated circle, with a well-defined outer ring. We hypothesize that this is because the gold particles were each functionalized with a dense brush of DNA strands, so each gold nanoparticle binds to many *Patchy*

B DNA strands, preventing more gold nanoparticles from binding with the microsphere. There are two methods which could increase the density of hybridized gold nanoparticles, which will be explored in the future. The first, is to shorten the *Patchy B* DNA strands, such that fewer can be physically hybridized with the same nanoparticle's DNA brush. This is not ideal, since we wish to vary the length of the *B* strands so that we can exercise control over the patch size. The second, and most favorable, option is to reduce the density of the DNA-brush on the gold nanoparticles. By reducing the number of complimentary DNA strands from around 70 to around 4, for example, we would be able to reduce the number of *Patchy B* strands each gold nanoparticle could hybridize with, thus significantly driving up gold nanoparticle density within the patches.

5.5 Conclusions

In this chapter we have shown that Point-of-Contact Templating and Reprogrammable DNA Interactions in the form of Ligation can be used to produce colloidal spheres with well-defined patches. These 'patchy particles' have been generated via binary gels and thus the patches on each particle are not ordered. However, promising preliminary results suggest that crystals should be viable templates, which would allow for the development of particles with patches whose orientation are based on contacts within the host crystal.

By incorporating crystal templating, and by expanding the number of crystals

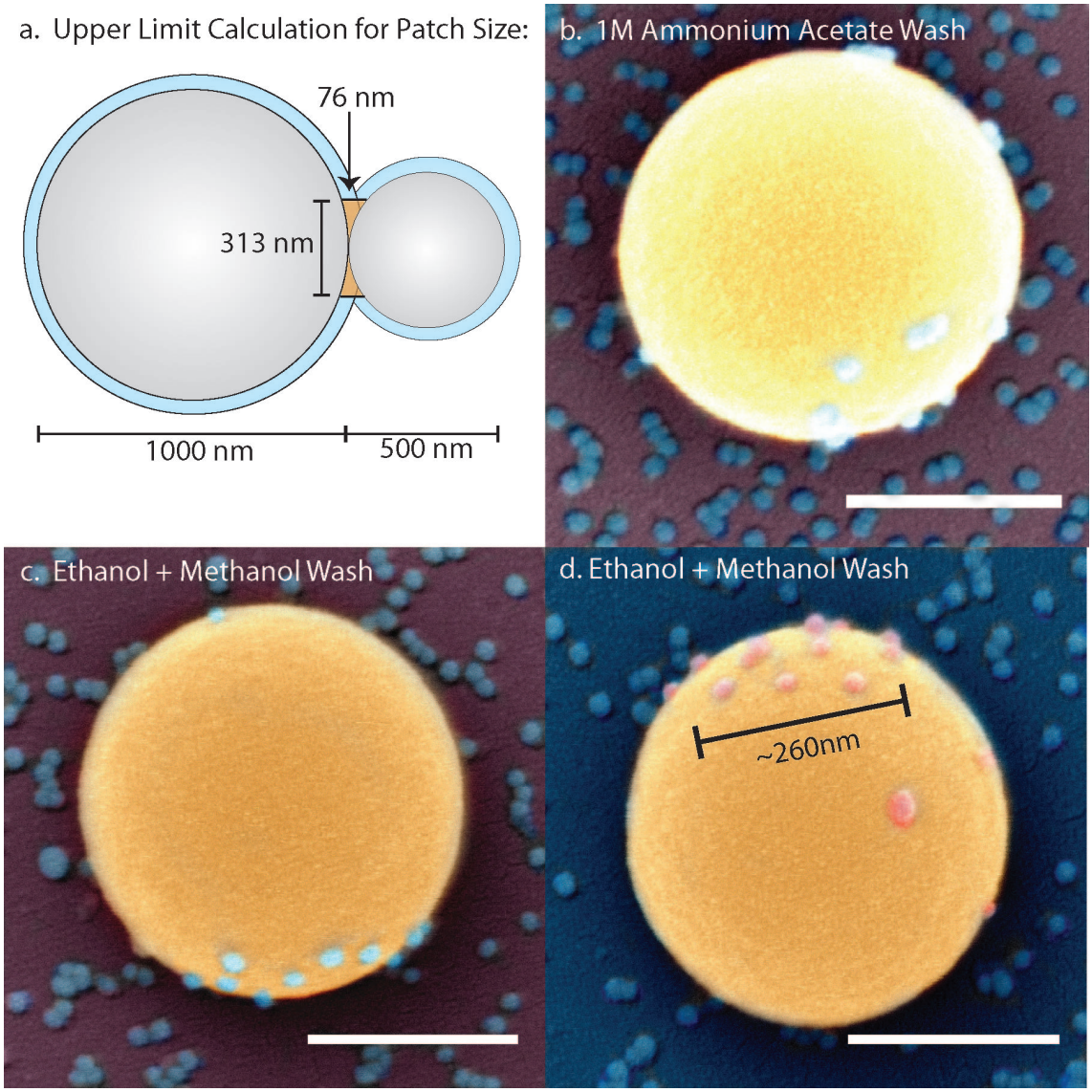

Figure 5.6: Patchy Particles resulting from the 2:1 gel system of binary spheres is shown here. Using the methods explained in Figure 5.5, an upper bound of 313 nm was determined for the diameter of the DNA patches in this system (a). SEM samples of the patchy spheres were prepared using two methods, an Ammonium Acetate Wash (b) and sequential Ethanol and Methanol washes (c,d), outlined in Materials and Methods as well as in Chapter Two. It is noted that the particles imaged here only measure roughly 450 nm across, instead of the nominal value of 531, but nonetheless, the clearly circular patch sizes ranging from 230 to 260 nm (d) are well below the maximum value of 313 nm calculated in (a).

to be used as templates [20, 28], we can generate a library of spheres with distinct patch-patterns and distinct anisotropic interactions. In future work, we will vary the length of the A and B DNA strands to exercise control over the patch sizes, and we will explore their utility as building blocks for further assemblies.

References

[1] Cristiano De Michele, Piero Tartaglia, and Francesco Sciortino. Slow dynamics in a primitive tetrahedral network model. *The Journal of Chemical Physics*, 125(20):–, 2006.

[2] Nicoletta Gnan, Daniel de las Heras, José Maria Tavares, Margarida M. Telo da Gama, and Francesco Sciortino. Properties of patchy colloidal particles close to a surface: A monte carlo and density functional study. *The Journal of Chemical Physics*, 137(8):–, 2012.

[3] Flavio Romano and Francesco Sciortino. Patterning symmetry in the rational design of colloidal crystals. *Nat Commun*, 3:975, 07 2012.

[4] Flavio Romano, Eduardo Sanz, and Francesco Sciortino. Phase diagram of a tetrahedral patchy particle model for different interaction ranges. *The Journal of Chemical Physics*, 132(18):–, 2010.

[5] Lorenzo Rovigatti, Daniel de las Heras, José Maria Tavares, Margarida M. Telo da Gama, and Francesco Sciortino. Computing the phase diagram of binary mixtures: A patchy particle case study. *The Journal of Chemical Physics*, 138(16):–, 2013.

[6] John Russo, Piero Tartaglia, and Francesco Sciortino. Reversible gels of patchy particles: Role of the valence. *The Journal of Chemical Physics*, 131(1):–, 2009.

[7] Frank Smallenburg and Francesco Sciortino. Liquids more stable than crystals in particles with limited valence and flexible bonds. *Nat Phys*, 9(9):554–558, 09 2013.

[8] Oleg A. Vasilyev, Boris A. Klumov, and Alexei V. Tkachenko. Precursors of order in aggregates of patchy particles. *Phys. Rev. E*, 88:012302, Jul 2013.

[9] Eric Jankowski and Sharon C. Glotzer. Calculation of partition functions for the self-assembly of patchy particles. *The Journal of Physical Chemistry B*, 115(48):14321–14326, 2011. PMID: 22004443.

[10] G. Munao, D. Costa, F. Sciortino, and C. Caccamo. Simulation and theory of a model for tetrahedral colloidal particles. *Journal of Chemical Physics*, 134(19), May 21 2011.

[11] Stefano Sacanna, David J. Pine, and Gi-Ra Yi. Engineering shape: the novel geometries of colloidal self-assembly. *Soft Matter*, 9:8096–8106, 2013.

[12] Yufeng Wang, Yu Wang, Dana R. Breed, Vinothan N. Manoharan, Lang Feng, Andrew D. Hollingsworth, Marcus Weck, and David J. Pine. Colloids with valence and specific directional bonding. *Nature*, 491(7422):51–55, 11 2012.

[13] Yufeng Wang, Andrew D. Hollingsworth, Si Kyung Yang, Sonal Patel, David J. Pine, and Marcus Weck. Patchy particle self-assembly via metal coordination. *Journal of the American Chemical Society*, 135(38):14064–14067, 2013.

[14] Lang Feng, Rémi Dreyfus, Ruojie Sha, Nadrian C. Seeman, and Paul M. Chaikin. Dna patchy particles. *Advanced Materials*, 25(20):2779–2783, 2013.

[15] Stefano Sacanna, Mark Korpics, Kelvin Rodriguez, Laura ColÃn-MelÃ©ndez, Seung-Hyun Kim, David J. Pine, and Gi-Ra Yi. Shaping colloids for self-assembly. *Nat Commun*, 4:1688, 04 2013.

[16] Stefano Sacanna and David J. Pine. Shape-anisotropic colloids: Building blocks for complex assemblies. *Current Opinion in Colloid and Interface Science*, 16(2):96 – 105, 2011.

[17] S. Sacanna, W. T. M. Irvine, P. M. Chaikin, and D. J. Pine. Lock and key colloids. *Nature*, 464(7288):575–578, 03 2010.

[18] Xiaoyang Xu, Nathaniel L. Rosi, Yuhuang Wang, Fengwei Huo, and Chad A. Mirkin. Asymmetric functionalization of gold nanoparticles with oligonucleotides. *Journal of the American Chemical Society*, 128(29):9286–9287, JUL 26 2006.

[19] Paul L. Biancaniello, Anthony J. Kim, and John C. Crocker. Colloidal interactions and self-assembly using dna hybridization. *Phys. Rev. Lett.*, 94:058302, Feb 2005.

[20] Marie T. Casey, Raynaldo T. Scarlett, W. Benjamin Rogers, Ian Jenkins, Talid Sinno, and John C. Crocker. Driving diffusionless transformations in colloidal crystals using DNA handshaking. *Nature Communications*, 3, November 2012.

[21] James T. McGinley, Ian Jenkins, Talid Sinno, and John C. Crocker. Assembling colloidal clusters using crystalline templates and reprogrammable DNA interactions. *Soft Matter*, 9(38):9119–9128, 2013.

[22] W. Benjamin Rogers, Talid Sinno, and John C. Crocker. Kinetics and non-exponential binding of DNA-coated colloids. *Soft Matter*, 9(28):6412–6417, 2013.

[23] W. Benjamin Rogers and John C. Crocker. Direct measurements of DNA-mediated colloidal interactions and their quantitative modeling. *Proceedings of the National Academy of Sciences of the United States of America*, 108(38):15687–15692, SEP 20 2011.

[24] A.J. Kim, V.N. Manoharan, and J.C. Crocker. Swelling-based method for preparing stable, functionalized polymer colloids. *Journal of the American Chemical Society*, 127(6):1592–1593, 2005.

[25] Anthony J. Kim, Paul L. Biancaniello, and John C. Crocker. Engineering dna-mediated colloidal crystallization. *Langmuir*, 22(5):1991–2001, 2006.

[26] Guangnan Meng, Natalie Arkus, Michael P. Brenner, and Vinothan N. Manoharan. The Free-Energy Landscape of Clusters of Attractive Hard Spheres. *Science*, 327(5965):560–563, January 29 2010.

[27] Zaki G. Estephan, Zhaoxia Qian, Daeyeon Lee, John C. Crocker, and So-Jung Park. Responsive multidomain free-standing films of gold nanoparticles assembled by dna-directed layer-by-layer approach. *Nano Letters*, 13(9):4449–4455, 2013. PMID: 23930738.

[28] Robert J. Macfarlane, Byeongdu Lee, Matthew R. Jones, Nadine Harris, George C. Schatz, and Chad A. Mirkin. Nanoparticle superlattice engineering with dna. *Science*, 334(6053):204–208, 2011.

Chapter 6

Conclusions and Future Directions

The work presented represents a true expansion of the capabilities of DNA-directed colloidal assemblies. We have developed, in Colloidal Crystal Templating and Reprogrammable DNA Interactions, highly tunable processes for the synthesis of anisotropic building blocks for DNA-directed assembly applications. Notably, these processes are scalable both in batch size and in the size of the resulting building blocks due to the three-dimensional nature of the templates. More notably, these systems are highly tunable and expandable. The templates are only limited by the ever-expanding library of colloidal crystals generated using DNA interactions. The tunability of DNA interactions is virtually unlimited due to DNA's ability to be reprogrammed and edited by enzymes. Finally, the constituent particles are not limited to polystyrene and gold, but can be of any material that can be synthesized into colloids on the micro- and nano-scale and functionalized with DNA.

6.1 Conclusions

By utilizing face-centered cubic (FCC), body-centered cubic (BCC), and random hexagonal close packed (RHCP, *via* sedimentation) crystals as templates, we have produced a large variety of clusters. In Chapter Three, FCC and BCC crystals were reprogrammed using competitive DNA interactions to generate clusters of icosahedra and a wide range of '1+8' symmetries, including cubes, skew cubes, and gyrobifastigium. The clusters generated using this method were unstable at long times, and could not be reliably purified, rendering them useless as building blocks. However, the work done in this system was highly informative; not only did it prove that DNA interactions within colloidal crystals can be reprogrammed at room temperature using competitive strands of DNA, but it also demonstrated that after being freed from a host crystal, the clusters can and do reliably undergo transformations to lower free-energy structures.

In our RHCP system from Chapter Four, we have utilized these structural transformations with our '1+12' cluster systems to attain stable icosahedral clusters not realizable through other means, such as particle confinement in emulsions [1, 2] or through depletion interactions [3]. A surprising variety of clusters can be generated using just sedimented close-packed crystals as templates by utilizing these transformations as well as interstitial sites within the host crystal lattice. By incorporating the DNA-reactive enzyme T4 DNA Ligase, we were able to stabilize the DNA bridges, thus overcoming the stability limitation from the system presented in

Chapter Three. Using this improved system, ordered and stable clusters of cuboctahedra, triangular orthobicupola, icosahedra, octahedra, and tetrahedra can be reliably synthesized, purified, and used in further assemblies. Furthermore, and more significantly, the directional nature of bonds with colloidal clusters was examined and demonstrated, illustrating that such clusters can be used as pseudo-patchy particles with anisotropic interactions.

We have also used binary colloidal gels as templates and a new ligase-reactive DNA design to synthesize DNA-coated Patchy Particles. It has been shown that the DNA patches that were synthesized using the methods presented here were formed at the points of contact between two interacting spheres, and it has been hypothesized that the size and orientation of the patches can be controlled by the length of the DNA strands and the type of template used, respectively. Promising preliminary results show that binary colloidal particles of differing sizes can be crystallized together to form BCC crystals using the DNA architectures presented here, and that their structures are maintained throughout the ligation process. This, coupled with the results from the binary gel experiments, strongly imply that crystals would be a suitable template for the production of patchy particles with targeted patch orientations.

6.2 Future Directions

In the future, by expanding the range of templates to include crystal structures such as those found in the literature [4–6], the list of attainable cluster and patchy particle symmetries can be greatly augmented. While the DNA architecture for ligation presented in Chapter Four was exceptionally simple and straightforward, and might seem to limit the number of crystal structures that can be attained using this method, more elegant DNA designs are definitely possible (and will be necessary in the future). DNA designs which combine the complex competitive DNA interactions presented in Chapter Three with the highly specific and useful ligation interactions presented in Chapters Four and Five are feasible, and should be explored.

In addition to expanding the number of crystal templates and the complexity of DNA interactions, it would be interesting to expand the variety of building blocks by incorporating the production of defective clusters. By designing a system where the host particles are a mix of ligatable and non-ligatable species, after cluster generation, the number of ligated pairings between the impurtiy particle and host particles will be determined by statistics. For example, in the '1+12' system presented in Chapter 4, by creating a 1:1 mix of ligatable:non-ligatable host particles, the resulting '1+12' clusters will be permanently bound to only 6 particles on average, with the other six being transient bonds, like those presented in Chapter Three. After dilution and purification, we should have a system of '1+6' clusters

with a variety of symmetries present. By varying the ratio of ligatable:non-ligatable host particles, we correspondingly vary the targeted cluster valence number. These defective clusters, which will have extremely specific "bonding sites" at the points of the vacancies, could act as model protein building blocks, and can potentially be used in the formation of filaments and non-close-packed structures.

A library of anisotropic building blocks is useless unless it is sufficiently utilized, so in the future, clusters and patchy particles will be used to explore hierarchical assemblies. Specifically, clusters will be used alongside isotropically interacting complementary spheres to yield structures with long-range order. As mentioned in Chapter One, systems which combine DNA interactions with directional interactions are highly useful for generating well ordered structures [7], and we believe that clusters will offer similar specificity and utility. We further propose that the process that has been developed for the generation of these various anisotropic building blocks, due to its scalability and ease of use, presents a path forward for this rich line of research.

References

[1] Vinothan N. Manoharan, Mark T. Elsesser, and David J. Pine. Dense packing and symmetry in small clusters of microspheres. *Science*, 301(5632):483–487, 2003.

[2] Yufeng Wang, Yu Wang, Dana R. Breed, Vinothan N. Manoharan, Lang Feng, Andrew D. Hollingsworth, Marcus Weck, and David J. Pine. Colloids with valence and specific directional bonding. *Nature*, 491(7422):51–U61, NOV 1 2012.

[3] Rebecca W. Perry, Guangnan Meng, Thomas G. Dimiduk, Jerome Fung, and Vinothan N. Manoharan. Real-space studies of the structure and dynamics of self-assembled colloidal clusters. *Faraday Discuss.*, 159:211–234, 2012.

[4] James T. McGinley, Ian Jenkins, Talid Sinno, and John C. Crocker. Assembling colloidal clusters using crystalline templates and reprogrammable DNA interactions. *Soft Matter*, 9(38):9119–9128, 2013.

[5] Marie T. Casey, Raynaldo T. Scarlett, W. Benjamin Rogers, Ian Jenkins, Talid Sinno, and John C. Crocker. Driving diffusionless transformations in colloidal crystals using DNA handshaking. *Nature Communications*, 3, November 2012.

[6] Robert J. Macfarlane, Byeongdu Lee, Matthew R. Jones, Nadine Harris, George C. Schatz, and Chad A. Mirkin. Nanoparticle superlattice engineering with dna. *Science*, 334(6053):204–208, 2011.

[7] Fang Lu, Kevin G. Yager, Yugang Zhang, Huolin Xin, and Oleg Gang. Superlattices assembled through shape-induced directional binding. *Nat Commun*, 6, 04 2015.